LBL-15253

Lawrence Berkeley Laboratory

UNIVERSITY OF CALIFORNIA

Materials & Molecular Research Division

MULTIPLE-QUANTUM NMR IN SOLIDS

Yu-Sze Yen
(Ph.D. Thesis)

November 1982

Prepared for the U.S. Department of Energy under Contract DE-AC03-76SF00098

LEGAL NOTICE

This book was prepared as an account of work sponsored by an agency of the United States Government. Neither the United States Government nor any agency thereof, nor any of their employees, makes any warranty, express or implied, or assumes any legal liability or responsibility for the accuracy, completeness, or usefulness of any information, apparatus, product, or process disclosed, or represents that its use would not infringe privately owned rights. Reference herein to any specific commercial product, process, or service by trade name, trademark, manufacturer, or otherwise, does not necessarily constitute or imply its endorsement, recommendation, or favoring by the United States Government or any agency thereof. The views and opinions of authors expressed herein do not necessarily state or reflect those of the United States Government or any agency thereof.

Lawrence Berkeley Laboratory is an equal opportunity employer.

LBL-15253

MULTIPLE-QUANTUM NMR IN SOLIDS

by

Yu-Sze Yen

Ph.D. Thesis

November 1982

Materials and Molecular Research Division

Lawrence Berkeley Laboratory

University of California

Berkeley, CA 94720

This work was supported by the Director, Office of Energy Research, Office of Basic Energy Sciences, Materials Sciences Division of the U.S. Department of Energy under Contract Number DE-AC03-76SF00098.

This manuscript was printed from originals provided by the author.

MULTIPLE-QUANTUM NMR IN SOLIDS

By

YU-SZE YEN

ABSTRACT

Time domain multiple-quantum (MQ) nuclear magnetic resonance (NMR) spectroscopy is a powerful tool for spectral simplification and for providing new information on molecular dynamics. In this thesis, applications of MQ NMR are presented and show distinctly the advantages of this method over the conventional single-quantum NMR.

Chapter 1 introduces the spin Hamiltonians, the density matrix formalism and some basic concepts of MQ NMR spectroscopy.

In chapter 2, ^{14}N double-quantum coherence is observed with high sensitivity in isotropic solution, using only the magnetization of bound protons. Spin echoes are used to obtain the homogeneous double-quantum spectrum and to suppress a large H_2O solvent signal.

Chapter 3 resolves the main difficulty in observing high MQ transitions in solids. Due to the profusion of spin transitions in a solid, individual lines are unresolved. Excitation and detection of high quantum transitions by normal schemes are thus difficult. To ensure that overlapping lines add

constructively and thereby to enhance sensitivity, time-reversal pulse sequences are used to generate all lines in phase. Up to 22-quantum ^1H absorption in solid adamantane is observed. A time dependence study shows an increase in spin correlations as the excitation time increased.

In chapter 4, a statistical theory of MQ second moments is developed for coupled spins of spin I=1/2. The model reveals that the ratio of the average dipolar coupling to the rms value largely determines the dependence of second moments on the number of quanta. The results of this model are checked against computer-calculated and experimental second moments, and show good agreement.

A simple scheme is proposed in chapter 5 for sensitivity improvement in a MQ experiment. The scheme involves acquiring all of the signal energy available in the detection period by applying pulsed spinlocking and sampling between pulses. Using this technique on polycrystalline adamantane, a large increase in sensitivity is observed.

Correlation of motion of two interacting methyl groups is the subject of chapter 6. This system serves as a model for the study of hindered internal motion. Because the spin system is small and the motions are well-defined, the calculations involved are tractable. Group theory appropriate for nonrigid

molecules is used to treat the change in the Hamiltonian as the methyl groups transit from correlated to uncorrelated motion. Results show that the four-quantum order alone is sufficient to distinguish between the two motions.

ACKNOWLEDGEMENTS

I would like to thank Professor Alex Pines for providing a stimulating environment with which to work in. His insights and his approach to problems from a fundamental point of view have inspired much of the work presented in this document. I have benefited from the many excellent graduate students that he has been able to attract. Special mention goes to Dan Weitekamp and Jau-Huei Tang for collaborative efforts, to Jim Murdoch for computer assistance, and to Gary Drobny and Joel Garbow for their hardware expertise. The other members of the group have been helpful with their suggestions and assistance.

I am also grateful to Dr. Melvin P. Klein and his group for their advice and support, and to Melvin Calvin Laboratory for providing access to the VAX computer system.

Friends outside the Pines group deserve warm thanks for making graduate life enjoyable. To Jim Wong, I owe much for his constant support. Finally, my family have my deepest gratitude for all their encouragement and advice. My parents deserve separate mention for impressing their belief in pursuing higher educaton.

IBM has been generous with providing a two-year predoctoral fellowship. This work has been supported

in part by the Director, Office of Energy Research, Office of Basic Energy Sciences, Materials Sciences Division of the U.S. Department of Energy under Contract No. DE-AC03-76SF00098.

TABLE OF CONTENTS

1. INTRODUCTION TO MULTIPLE-QUANTUM NMR..... 1

1.1 Spin Hamiltonians..... 2

1.1.1 Zeeman Hamiltonian..... 2

1.1.2 Rf Hamiltonian..... 3

1.1.3 Quadrupolar Hamiltonian..... 4

1.1.4 Dipolar Hamiltonian..... 5

1.1.5 Chemical Shift Hamiltonian..... 5

1.1.6 Indirect Spin-Spin Hamiltonian..... 6

1.2 Spin Dynamics..... 7

1.3 Multiple-Quantum Coherence..... 9

1.4 Spectral Simplification..... 12

1.5 Fourier Transform Multiple-Quantum Experiment..... 17

1.6 Even and Odd Selectivity..... 23

1.7 Separation of Orders..... 25

References..... 29

2. INDIRECT DETECTION OF SPIN-1 DOUBLE-QUANTUM COHERENCE IN LIQUIDS..... 30

2.1 Introduction..... 30

2.2 Theory..... 31

2.3 Results and Discussion..... 37

References..... 43

3. TIME-REVERSAL MULTIPLE-QUANTUM NMR IN SOLIDS..... 45

3.1 Introduction..... 45

3.2 Theory..... 48

3.3 Experimental..... 52

3.4 Results and Discussion..... 53

References..... 58

4. SECOND MOMENTS OF MULTIPLE-QUANTUM NMR SPECTRA..... 60

4.1 Introduction..... 60

4.2 Theory..... 61

4.2.1 Exact Dynamics..... 70

4.2.2 Unique Second Moments Value..... 71

4.2.3 Statistical Model..... 72

4.2.3.1 Dipolar Mean and Variance of a Zeeman Manifold..... 74

4.2.3.2 Multiple-Quantum Second Moments... 79

4.3 Comparison of Experiment with Computer Simulations and Statistical Model..... 84

4.4 Conclusions..... 85

Appendix 4.A..... 89

Appendix 4.B..... 91

Appendix 4.C..... 99

References..... 111

5. SENSITIVITY ENHANCEMENT BY SPINLOCKING IN THE DETECTION PERIOD..... 112

5.1 Introduction and Theory..... 112

5.2 Experimental Results and Discussion..... 115

References..... 121

6. CORRELATION OF MOTION OF TWO METHYL GROUPS..... 122

6.1 Introduction..... 122

6.2 Definition of Correlated and Uncorrelated Motion.. 123

6.3 Determination of the Spin Hamiltonian..... 123

6.3.1 Intramethyl Couplings..... 127

6.3.2 Intermethyl Couplings..... 127

6.3.2.1 Uncorrelated Motion..... 128

6.3.2.2 Correlated Motion..... 128

(i) Equivalent Methyl Groups.... 130

(ii) H_o and the Methyl C_3 Axes Are Contained in a Plane.... 131

(iii) Arbitrary Orientation..... 131

6.4 NMR Permutation Group of Non-Rigid Molecules..... 132

6.5 Determination of the Hamiltonian Symmetry Group... 138

6.5.1 Uncorrelated Equivalent Methyl Groups..... 138

6.5.2 Uncorrelated Inequivalent Methyl Groups.... 140

6.5.3 Correlated Equivalent Methyl Groups..... 141

6.5.4 Correlated Inequivalent Methyl Groups in a "Planar" Orientation..... 141

6.5.5 Correlated Inequivalent Methyl Groups at an Arbitrary Orientation..... 142

6.6 Effect of Spinning or Molecular Reorientation About a Fixed Axis..... 142

6.7 Energy Level Diagrams..... 147

6.8 Multiple-Quantum Spectra..... 154

6.9 Intermediate Region - Exchange Theory..... 163

6.9.1 Exchange Operators..... 163

6.9.2 Master Equation With Exchange..... 165

6.10 1,8-Dimethylnaphthalene..... 168

6.11 Computer Simulation of Exchange Prcoess..... 171

6.11.1 Secular Determinants for m=±2 to m=∓2 Manifolds..... 172

6.11.2 Secular Determinant for m=±1 to m=∓3 Manifolds..... 173

6.12 1,8-Dimethylnaphthalene-d_6 in a Nematic Liquid Crystal..... 177

6.13 1,8-Dimethylnaphthalene-d_{10}..... 183

6.13.1 Single-Quantum Spectrum..... 186

6.13.2 Impurity Content..... 190

6.13.3 Conclusion..... 196

Appendix 6.A..... 197

Appendix 6.B..... 201

References..... 203

CHAPTER 1

INTRODUCTION TO MULTIPLE-QUANTUM NMR

Multiple-quantum (MQ) spectroscopy has proven to be a practical tool in the simplication of spectral analysis[1] as well as providing new information in molecular spin dynamics.[2] Diverse in its applications, MQ NMR has been applied to heteronuclear as well as homonuclear coupled spin systems, and to systems with J coupling, dipolar and quadrupolar interactions. Multiple-quantum transitions have been observed in liquids, solids and liquid crystals. Excellent reviews on this widely useful topic have been available in the last couple of years.[3-6]

This chapter presents some of the basic concepts of Fourier transform MQ NMR spectroscopy. The succeeding chapters will extend on particular aspects relevant to the subject of discussion.

Before we enter into the realm of MQ NMR, the matter of spin Hamiltonians and spin dynamics as described in the density operator formalism will be first discussed. Then we will proceed with a definition of MQ coherence, discuss the information content of MQ spectroscopy, describe a Fourier transform MQ experiment, and present some properties of MQ coherences.

1.1 SPIN HAMILTONIANS

The interaction of nuclear spins with their surrounding can be divided into two parts:

$$H = H_{ext} + H_{int}.$$

The external Hamiltonian H_{ext} is an interaction of the spins with applied magnetic fields, whether they be static or oscillating, and is subject to the experimentalist's choice. The internal Hamiltonian H_{int} is inherent to the spin system; it is composed of the interaction of nuclear spins with the local surroundings.

In the class of substances that we will be dealing with, the following interactions are of interest:

$$H = H_{Z} + H_{rf} + H_Q + H_D + H_{cs} + H_J.$$

The Zeeman term H_Z and the applied rf term H_{rf} are grouped as external Hamiltonians. The remainder are internal Hamiltonians. These terms will be discussed separately.

1.1.1 Zeeman Hamiltonian

In typical laboratory magnets, by far the largest term is the Zeeman Hamiltonian. Nuclei with dipole moments $\vec{\mu} = \gamma\hbar\vec{I}$, where γ is the magnetogyric ratio,

will interact with the large applied static magnetic field $\vec{H}_o$. Expressed in units of $\hbar$, this interaction is described by

$$H_Z = -\vec{H}_o \cdot \sum_i \vec{\mu}_i / \hbar = -H_o \sum_i \gamma_i I_{zi}$$

where z is chosen to be in the direction of $\vec{H}_o$ and the summation runs through all nuclei in the sample.

As a result of this interaction, the spins experience a torque in the direction defined by

$$\frac{d\vec{\mu}_i}{dt} = \gamma_i \vec{\mu}_i \times \vec{H}_o$$

and will precess at a rate $\gamma_i H_o$. This constant $\omega_{o,i} = \gamma_i H_o$ is referred to as the Larmor precession frequency.

1.1.2 Rf Hamiltonian

For spin excitation, an oscillating field in the radiofrequency range can be applied. To avoid coupling with the static field, it is applied in the xy-plane. Choosing the rf field to be in the x-direction, the rf Hamiltonian is expressed as:

$$H_{rf} = 2H_1 \cos(\omega t + \phi) \sum \gamma_i I_{xi}$$

where H_1 is the amplitude of the rf field rotating at a frequency ω with an initial phase ϕ.

1.1.3 Quadrupolar Hamiltonian

Nuclei with $I>1$ possess an electric quadrupole moment due to the nonspherical distribution of nuclear charge. The nuclear quadrupole moment can interact with the local electric field gradient generated by the spacial anisotropy in the distribution of the valence electrons. The quadrupolar Hamiltonian is given by:[7]

$$H_Q = \sum_i \frac{eQ_i}{2I_i(2I_i-1)} \vec{I}_i \cdot \underset{\sim}{V}_i \cdot \vec{I}_i$$

$$= \sum_i \frac{eQ_i V_{zz,i}}{4I_i(2I_i-1)} [3I_{zi}^2 - I_i(I_i+1) + \tfrac{1}{2}\eta_i(I_{+i}^2 + I_{-i}^2)]$$

where Q_i is the quadrupole moment and $\underset{\sim}{V}_i$ is a second rank tensor describing the electric field gradient. The asymmetry parameter η_i is defined as:

$$\eta_i = \frac{(V_{xx,i} - V_{yy,i})}{V_{zz,i}} ,$$

and $V_{xx,i}$, $V_{yy,i}$, and $V_{zz,i}$ are the electric field gradient tensor components expressed in the principle axis frame. For axially symmetric gradients, $\eta=0$.

In the presence of a large magnetic field, only the secular part (i.e. the part that commutes with H_Z) is retained:

$$H_Q = \sum_i \frac{eQ_i V_{zz,i}}{4I_i(2I_i-1)} [3I_{zi}^2 - I_i(I_i+1)] .$$

1.1.4 Dipolar Hamiltonian

The direct interaction between magnetic dipoles is given by:

$$H_D = \sum_{i<j} \vec{I}_i \cdot \underset{\sim}{D}_{ij} \cdot \vec{I}_j$$

$$= \sum_{i<j} \frac{\gamma_i \gamma_j \hbar}{r_{ij}^3} \left[\frac{3(\vec{I}_i \cdot \vec{r}_{ij})(\vec{I}_j \cdot \vec{r}_{ij})}{r_{ij}^2} - \vec{I}_i \cdot \vec{I}_j \right]$$

where $\underset{\sim}{D}_{ij}$ is a traceless second rank tensor and $\vec{r}_{ij}$ is the vector connecting nuclei i and j. In high fields, only the secular part of H_D is retained:

$$H_D = \sum_{i<j} \frac{\gamma_i \gamma_j \hbar}{r_{ij}^3} (3\cos^2\theta_{ij} - 1)[I_{zi} I_{zj} - \tfrac{1}{4}(I_{+i} I_{-j} + I_{-i} I_{+j})] \ .$$

This is referred to as the "truncated" dipolar Hamiltonian.

For nuclei of different γ_i, γ_j and spins I, S the Hamiltonian is further truncated to:

$$H_D = \sum_{i<j} \frac{\gamma_i \gamma_j \hbar}{r_{ij}^3} (3\cos^2\theta_{ij} - 1) I_{zi} S_{zj} .$$

1.1.5 Chemical Shift Hamiltonian

The electron cloud surrounding a nucleus is polarized by the applied magnetic field and effectively

shields the nucleus. As a result, nuclei in different chemical surrounding do not experience the same local field. In general, the shielding is expressed in tensor form:

$$H_{cs} = \sum_i \gamma_i \vec{I}_i \cdot \underset{\sim}{\sigma}_i \cdot H_o$$

where $\underset{\sim}{\sigma}_i$ is a second rank tensor. In isotropic solution, it is reduced to a scalar interaction:

$$H_{cs} = \sigma_i I_{zi}$$

where only $\sigma_i = \frac{1}{3}\mathrm{Tr}(\underset{\sim}{\sigma}_i)$ is retained.

1.1.6 Indirect Spin-Spin Hamiltonian

The interaction between nuclei via electron clouds in general is given by:

$$H_J = \sum_{i<j} \vec{I}_i \cdot \underset{\sim}{J}_{ij} \cdot \vec{I}_j$$

where $\underset{\sim}{J}_{ij}$ is a second rank tensor. In high fields, only the secular parts remain:

$$H_J = \sum_{i<j} [J_{ij} \vec{I}_i \cdot \vec{I}_j + J_{ij}^{aniso}(3I_{zi}I_{zj} - \vec{I}_i \cdot \vec{I}_j)] \ .$$

Since the anisotropic part of H_J has the same form as H_D, it is sometimes called the pseudo-dipolar

coupling. In isotropic solution, the anisotropic term is averaged to zero, resulting in a purely scalar coupling:

$$H_J = \sum_{i<j} J_{ij} \vec{I}_i \cdot \vec{I}_j \ .$$

As in H_D, the interaction between unlike nuclei I and S is truncated to give:

$$H_J = \sum_{i<j} J_{ij} I_{zi} S_{zj} .$$

1.2 SPIN DYNAMICS

The state of a coupled spin system is conveniently described by the density operator ρ. At thermal equilibrium, the state of maximum entropy dictates that the density operator takes the following form:

$$\rho_o = \frac{\exp(-\beta H)}{\mathrm{Tr}\{\exp(-\beta H)\}}$$

[illegible] $= \hbar/k_B T$ and k_B is the Boltzmann constant. At [illegible]mperatures $\beta H < 1$, the density operator can be expanded in a Taylor's series. Keeping only up to the first order term,

$$\rho_o \simeq Z^{-1}(1 - \beta H)$$

where $Z = Tr\{\exp(-\beta H)\}$. Since the first term is proportional to identity and can never have an effect on the spin dynamics, it is usually dropped, yielding what is called the reduced density operator:

$$\rho = bI_z.$$

In all our discussions, the constant $b = -\beta\omega_o Z^{-1}$ will be suppressed.

The equation of motion for ρ under the influence of an explicitly time-independent Hamiltonian H is given by:

$$\frac{d\rho}{dt} = -i[H, \rho].$$

The formal solution to this first order differential equation is:

$$\rho(t) = \exp(-iHt)\rho(0)\exp(iHt)$$

where $\rho(0)$ is the initial density operator. If the Hamiltonain changes discretely from one time-independent Hamiltonian to another, successive applications of the above equation yields:

$$\rho(t) = \ldots\exp(-iH_2t_2)\exp(-iH_1t_1)\rho_o\exp(iH_1t_1)\exp(iH_2t_2)\ldots$$

The precession at the Larmor frequency is common to all like spins. To remove this uninteresting term, it is common to transform the equation of motion into the rotating frame in which the rf Hamiltonian is stationary:

$$\frac{d\rho^*}{dt} = -i[H^*, \rho^*].$$

In the rotating frame,

$$\rho^* = \exp(-i\omega t I_z)\rho\exp(i\omega t I_z)$$
$$H^* = \exp(-i\omega t I_z)H\exp(i\omega t I_z)$$

are the effective operators. In this representation, the Hamiltonian for like spins is,

$$H^* = -\Delta\omega I_z + \omega_1 I_x + H_Q^* + H_D^* + H_{cs}^* + H_J^*$$

where $-\Delta\omega = (\omega - \omega_o)$ is the resonance offset and the internal Hamiltonians retain only the secular parts.

In all our discussions, the rotating frame is the relevant one and the notation * will be suppressed.

1.3 MQ COHERENCE

Formally, MQ coherences are related to the off-diagonal elements of the density matrix ρ, with the n-quantum coherences associated with the elements n off

the diagonal of ρ. A MQ coherence describes the transition between two eigenstates where the well-known selection rule $\Delta m = \pm 1$ is violated. Consider the energy level diagram for N coupled spin-1/2 system of Fig.1.1. An "allowed" transition is one in which the quantum number changes by ± 1. A MQ transition has no such restriction; it can be n-quantum or even zero-quantum. In single-quantum spectroscopy, effectively only one spin flips. In a n-quantum transition multiple spins flip. This multiple flip involves a simultaneous absorption or emission of n photons. The process is a coherent one and should be contrasted to a sequential, and hence incoherent, process.

Because a MQ coherence is a many-body correlation phenomenon, it requires a Hamiltonian that couples spins. More precisely, the criterion for whether a Hamiltonian term will excite MQ coherences is that it must be a bilinear operator. Such bilinear operators are the dipolar, the J coupling and the quadrupolar Hamiltonians.

In the nonlinear regime where H_{rf} is no longer a weak perturbation, a nonselective excitation of MQ coherences can be accomplished by either a long weak pulse[8] ($|H_{rf}| \approx |H_{int}|$), or short intense pulses ($|H_{rf}| > |H_{int}|$) sandwiching time delays in which a bilinear operator is operative. Our focus will be on using short intense pulses to excite MQ coherences. In

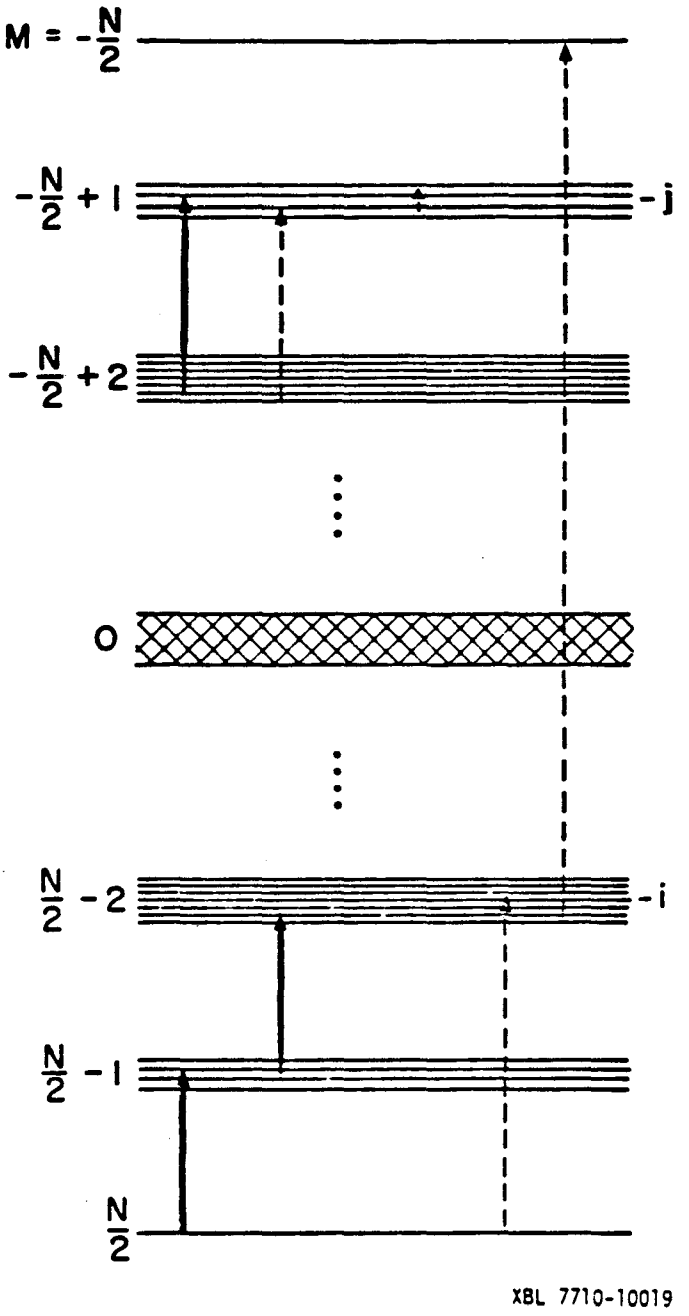

Figure 1.1 Generalized energy level diagram of N coupled spin-1/2's. The dashed arrows indicate "forbidden" MQ transitions, the solid arrows are "allowed" single-quantum transitions. The $\Delta m = -1$ dashed arrow indicate a transition forbidden by symmetry.

this limit, H_{int} can neglected in the duration of the pulses.

1.4 SPECTRAL SIMPLIFICATION

The problem with single-quantum (SQ) spectroscopy is apparent from the SQ spectra of oriented systems shown in Fig. 1.2. In Fig. 1.2, the number of coupled protons increases monotonically down the page. One observes that the spectral complexity increases with the number of spins. For a two or three spin system, the spectrum is still fairly simple. But one notices that for, say, a six spin system, already the lines are beginning to overlap. The situation for a sixteen spin system is intractable - one only gets a broad featureless lineshape.

Three methods to reduce spectral complexity are proposed and can be used in combination. The first two methods involve reducing the number of coupled spins. When reduction of system size is no longer feasible, MQ spectroscopy offers a viable alternative.

The first method is to simulate isolated molecular systems, thereby removing intermolecular dipolar couplings.

In solids, extensive dipolar couplings can exist and because of the rigid lattice structure, the full effect of H_D is achievable. In order to simulate isolated molecules and maintain the crystal structure,

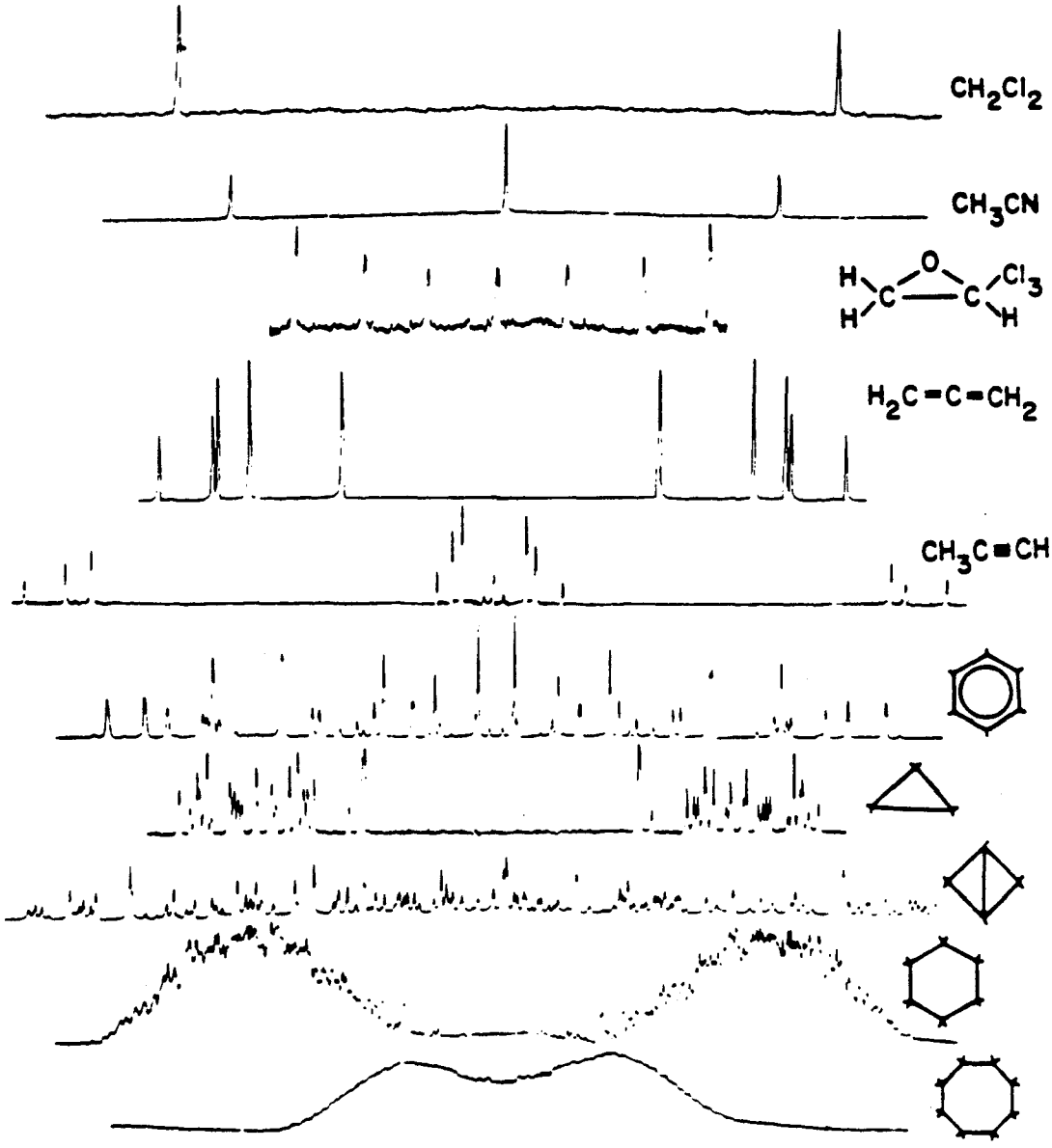

Figure 1.2 High resolution proton single-quantum spectra of solutes oriented in liquid crystal solvents.

the desired compound can be diluted into a matrix of the isotopic counterpart. Oftentimes, the nuclei of interest are in low natural abundance, as in the case of ^{13}C, and thus the isotopic dilution is already provided.

Solutes dissolved in a liquid crystal solvent are particularly convenient systems for studying intramolecular dipolar couplings. The translational diffusion of the liquid crystal molecules averages to zero the intermolecular couplings. However, because the liquid crystal molecules are restricted in their molecular reorientation, the intramolecular couplings remain but are scaled by order parameters.(9) The same situation occurs for solutes dissolved in a liquid crystal solvent. Thus we have a convenient method for isolating molecules, provided the molecule is soluble in some liquid crystal or is in liquid crystalline form.

Another alternative is to reduce the number of coupled spins per molecule with selective isotopic labeling. This can often be expensive or synthetically difficult, and sometimes infeasible.

To see what spectral simplication can be found from MQ spectroscopy, we refer again to Fig. 1.1. We notice that there is only one N-quantum transition, where N is the maximum quantum possible. The number of (N-1) quantum is at most N, and so on. One can show

through a combinatorial argument that statistically the number of transitions falls off with the number of quanta in a Gaussian manner.[3] In fact, even for a small spin system such as benzene, this statistical argument holds well at least qualitatively (Fig. 1.3). Thus, it would be advantageous to observe the higher quantum orders where the density of lines are much lower, provided they contain the same amount of information. This leads us to the problem of determining the information content of MQ orders.

We compare the number of unknown physical constants with the number of measurables, based on a statistical argument. The claim is that it is usually enough to consider only the (N-1) and (N-2) quantum transitions, provided that all the lines in these orders are resolvable.

In oriented systems, typically one has as unknowns the chemical shifts, J couplings, and dipolar couplings. The number of dipolar couplings is equal to the number of pairs of spins. Likewise for the number of J couplings. The number of chemical shift differences is equal to the number of spins minus one. Thus, the total number of unknowns is $N^2 - 1$.

The (N-1) quantum order has 2N lines, and the (N-2) quantum order has N(N-1) lines. The accumulative amount of information available thusfar is already $N^2 - 1$. Therefore, indeed the (N-1) and (N-2)

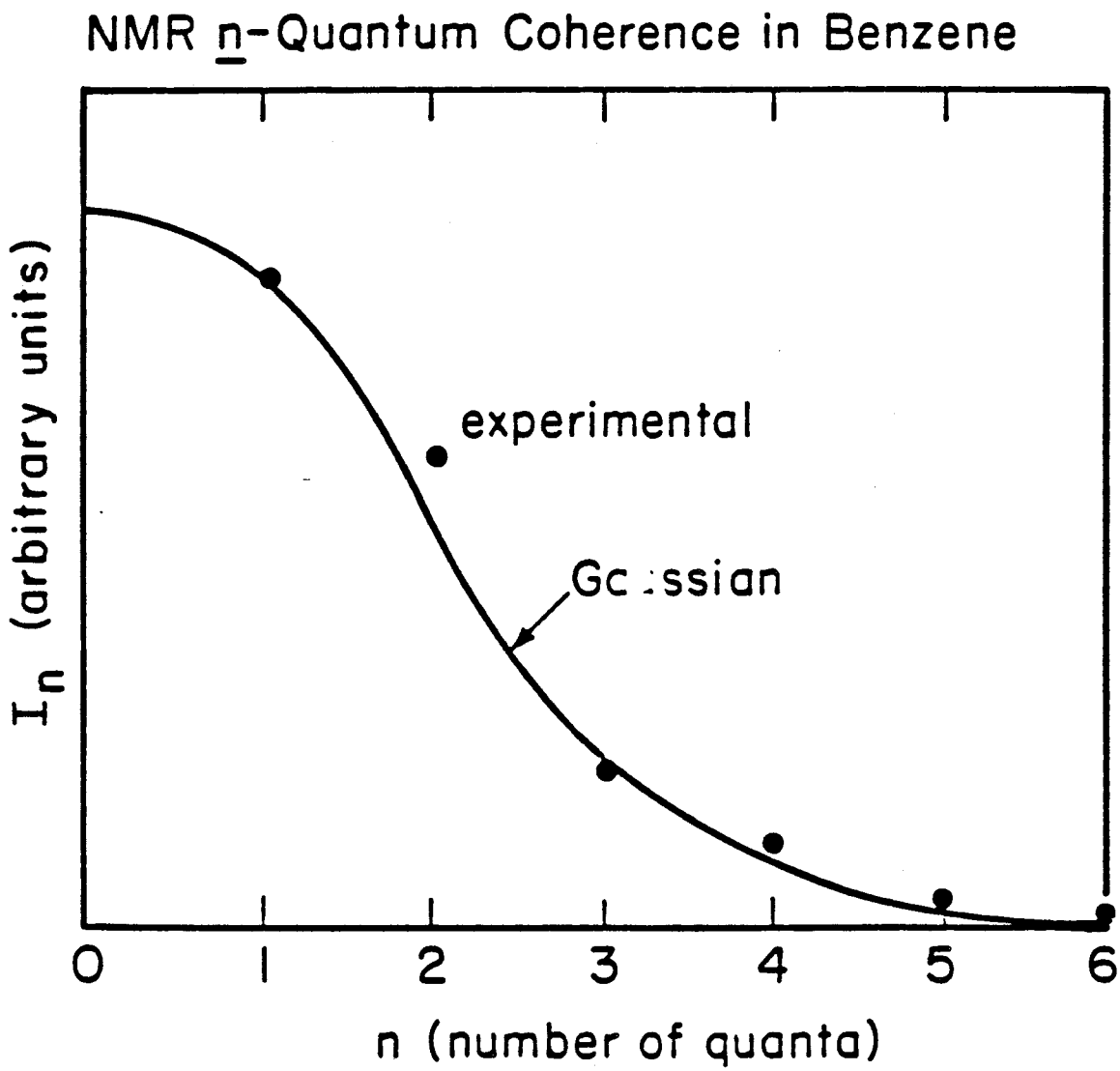

XBL 781-6894

Figure 1.3 Integrated intensity versus the number of quanta n. The measured benzene values (solid dots) are compared against a gaussian curve based on a statistical counting argument (solid line).

quantum orders offer enough information for a complete determination of the physical constants.

1.5 FOURIER TRANSFORM MQ EXPERIMENT

A multiple-quantum experiment can be separated into four time domains: preparation, evolution, mixing and detection (Fig. 1.4). Separation of time domains allows the experimentalist to create the effective Hamiltonian of interest in each time period. This offers great flexibiltiy for the experimentalist on what he chooses to observe, depending on his ingenuity.

In the preparation period, the coherences of interests are created, let evolve in t_1 under some Hamiltonian H_1. A direct detection of MQ coherences would require multipole detectors. Since our coil is capable of detecting only oscillating dipoles, a mixing period is required to convert the MQ coherences into single quantum coherences, which are detected in time t_2. This is repeated for many values of t_1 until a MQ interferogram in t_1 is obtained. The MQ evolution in t_1 is detected as a modulation of the single-quantum amplitude. The signal is given as the trace of the observable $I_+ = I_x + iI_y$ with the density matrix at the time of observation:

$$\begin{aligned} S(\tau,t_1,\tau',t_2) &= \mathrm{Tr}\{I_+^\dagger \rho(\tau,t_1,\tau',t_2)\} \\ &= \mathrm{Tr}\{I_- \exp(-iH_2t_2)V^\dagger(\tau')\exp(-iH_1t_1)U^\dagger(\tau) \\ &\qquad \times \rho_o U(\tau)\exp(iH_1t_1)V(\tau')\exp(iH_2t_2)\} \end{aligned}$$

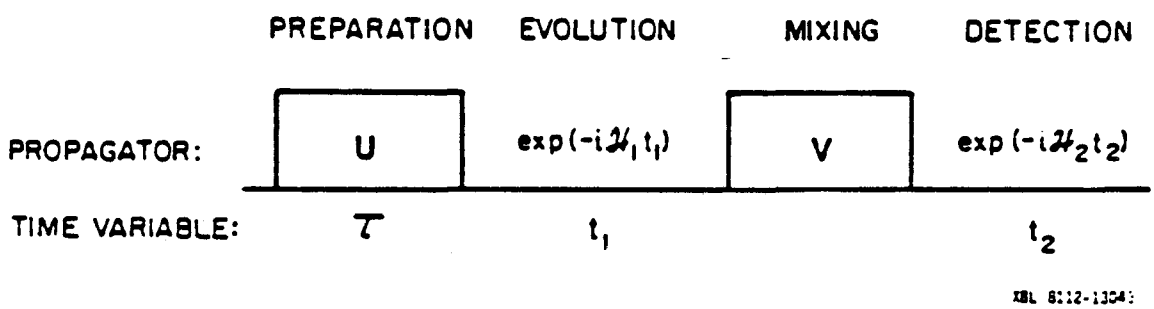

Figure 1.4 A block diagram of MQ pulse sequence, indicating the separation of time domains.

Shown in Fig. 1.5 are two simple MQ pulse sequences. The first two pulses separated by a time delay suffice to prepare MQ coherences.

The amount of coherence prepared depends on the time delay between the pulses. To demonstrate, exact dynamics calculation have been performed on benzene, a 6-spin system.(5) Figure 1.6 shows the dependence of the average integrated intensity of n-quantum coherence on the preparation time. Basically, after an incubation period time on the order of the inverse of the couplings, this dependence is roughly constant for the lower orders. For the 6-quantum transition, since there is no averaging with other transitions, the oscillation is pronounced and continues for all times.

For small pumping times τ, the power of the rate of growth of n-quantum integrated intensity varies with n (Fig. 1.7). For the two-pulse preparation sequence, the power is $2n-1$ $(n>1)$.(3) This power dependence clearly indicates that it takes more time to build up an n-body correlation. In chapter 4, preliminary experiments in solid adamantane verify that excitation of the higher quantum coherences do require longer preparation times.

Transition phase and intensity depend on the preparation and mixing times for general MQ pulse sequences. The transition phase can be independent of preparation time only if the mixing propagator is the

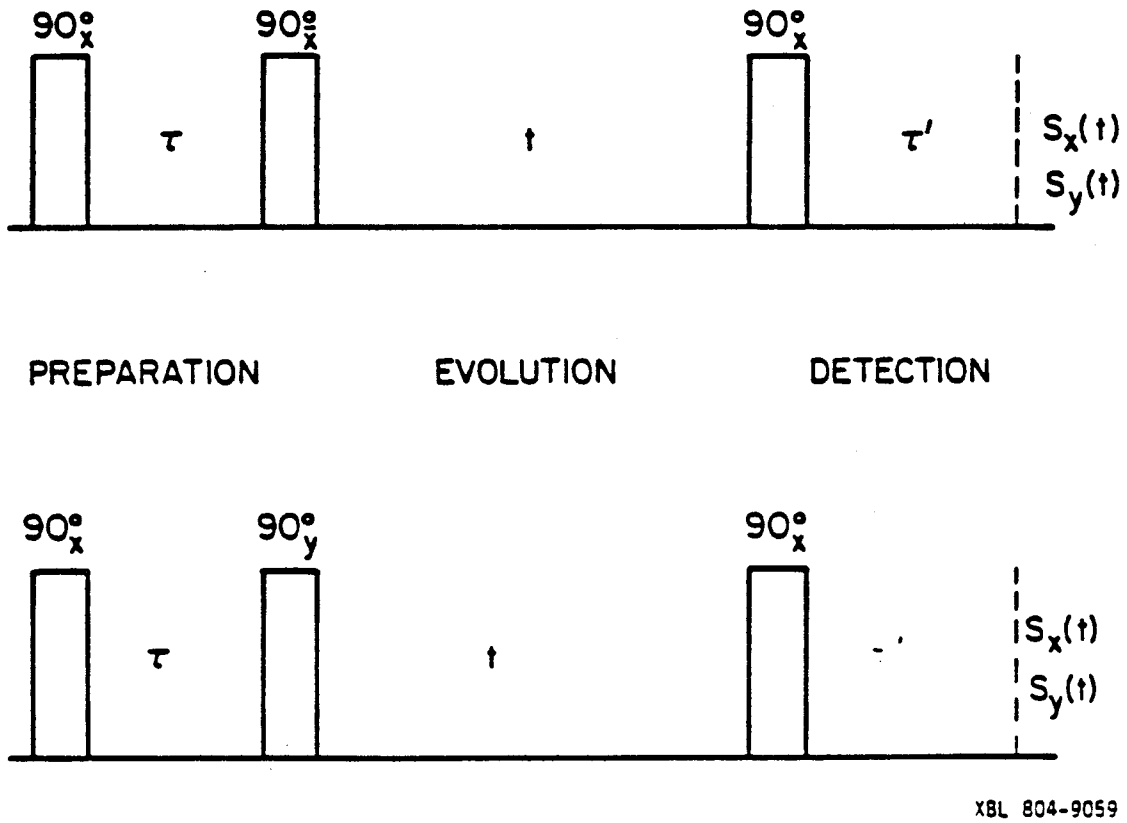

Fig. 1.5 Two simple three-pulse sequences for exciting and detecting MQ coherences in both channels. If there is no offset, then the upper pulse sequence is even-selective, and the lower sequence is odd-selective.

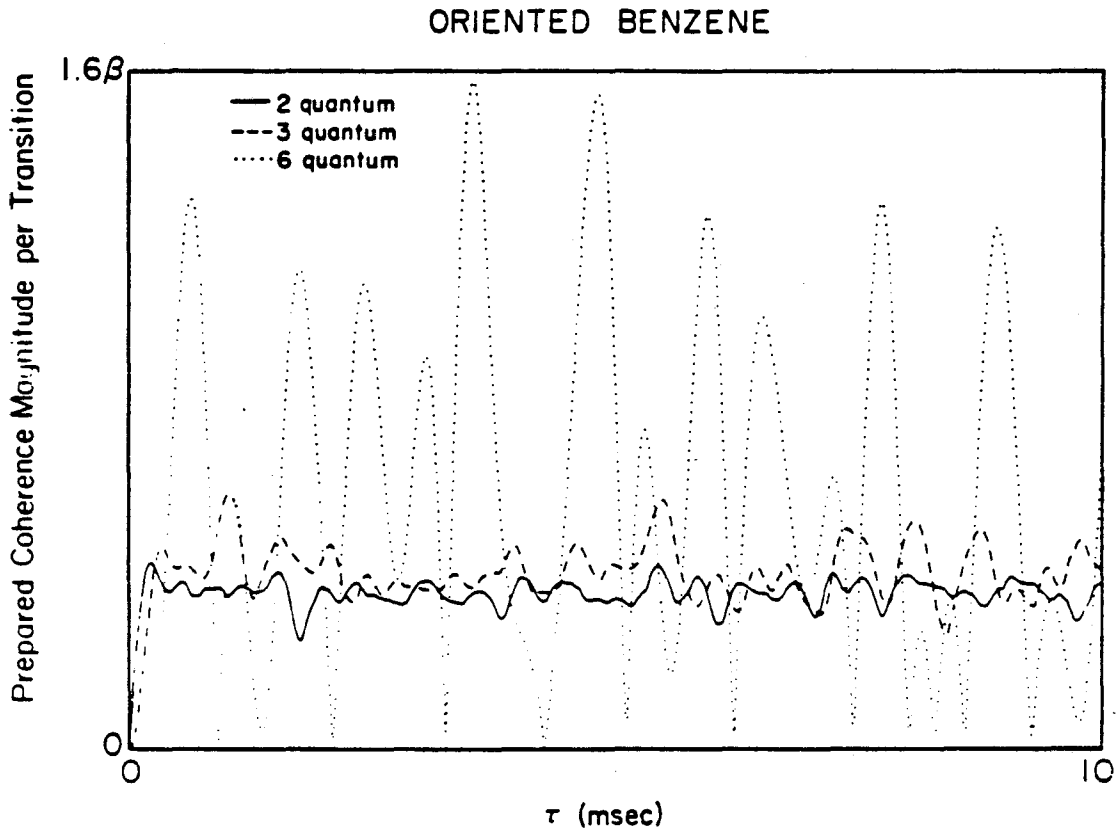

Figure 1.6 Exact dynamics calculations of average integrated intensity versus the preparation time for the oriented benzene molecule. Only the 2-, 3-, 6-quantum orders are shown. The dependence is roughly constant for all but the six-quantum order.

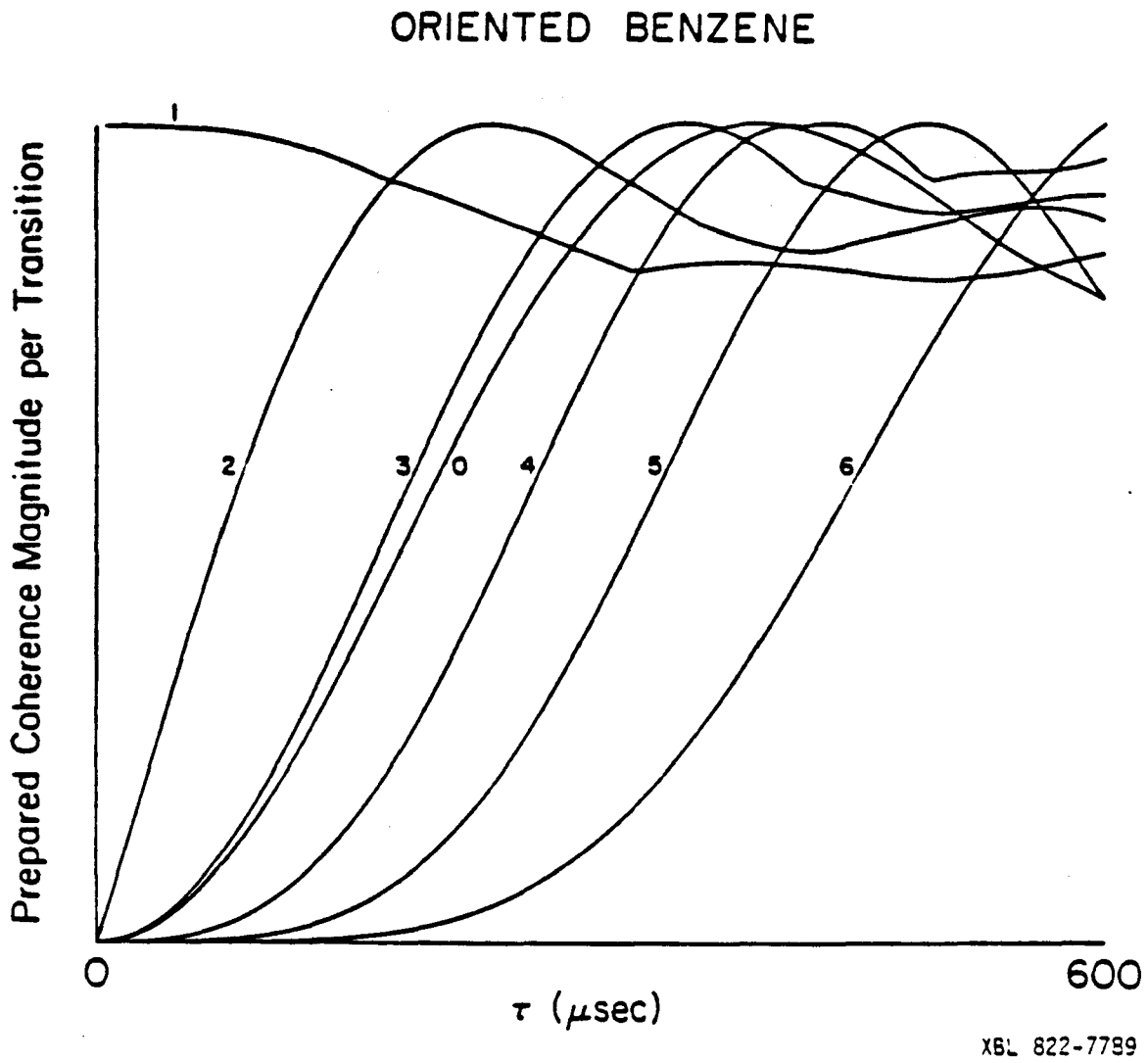

Figure 1.7 An expansion of the smaller preparation times of the previous figure, showing the rate of growth of coherences varies monotically with n (n>1).

time-reversal of the preparation propagator. This can be important since overlapping lines that are out of phase destructively interfere. To avoid missing lines that happen to have a small intensity at some poorly chosen preparation time, it becomes necessary to do the same experiment with enough different preparation times and take an average.

1.6 EVEN AND ODD SELECTIVITY

Consider the sequence $\frac{\pi}{2}I_x - \tau - \frac{\pi}{2}I_{-x}$ for preparation (Fig. 1.5). The "prepared" density operator for this sequence is

$$\bar{\ }(\tau) = \exp(i\tfrac{\pi}{2}I_x)\exp(-iH\tau)\exp(-i\tfrac{\pi}{2}I_x)I_z \times\exp(i\tfrac{\pi}{2}I_x)\exp(iH\tau)\exp(-i\tfrac{\pi}{2}I_x). \qquad (1)$$

A useful concept is to let the rotations operate on H, thereby defining an effective preparation Hamiltonian. We separate the linear terms from the bilinear terms in H:

$$H = -\Delta\omega I_z + H_{zz}$$

where H_{zz} is bilinear. The effect of the rotation on H is:

$$\exp(i\tfrac{\pi}{2}I_x)H\exp(-i\tfrac{\pi}{2}I_x) = \Delta\omega I_y + H_{yy}$$

where $H_{yy} = \exp(i\frac{\pi}{2}I_x)H_{zz}\exp(-i\frac{\pi}{2}I_x)$.

With this, Eq. (1) becomes:

$$\rho^{x\bar{x}}(\tau) = \exp(-iH_{yy}\tau)(I_z\cos\Delta\omega\tau + I_x\sin\Delta\omega\tau)\exp(iH_{yy}\tau)$$

$$\equiv U_{yy}[I_z]\cos\Delta\omega\tau + U_{yy}[I_x]\sin\Delta\omega\tau,$$

where $U_{yy}[I_\alpha] \equiv \exp(-iH_{yy}\tau)I_\alpha\exp(iH_{yy}\tau)$. The operator $U_{yy}[I_z]$ is composed of even-quantum operators, and $U_{yy}[I_x]$ of odd-quantum operators. In the limit $\Delta\omega=0$,

$$\rho^{x\bar{x}}(\tau) = U_{yy}[I_z]$$

is purely even-quantum.

For the sequence $\frac{\pi}{2}I_y - \tau - \frac{\pi}{2}I_x$, the prepared density operator is:

$$\rho^{yx}(\tau) = \exp(-i\frac{\pi}{2}I_x)\exp(-iH\tau)\exp(i\frac{\pi}{2}I_y)I_z$$
$$\times\exp(i\frac{\pi}{2}I_y)\exp(iH\tau)\exp(i\frac{\pi}{2}I_x) .$$

$$= U_{yy}[I_x]\cos\Delta\omega\tau + U_{yy}[I_z]\sin\Delta\omega\tau.$$

In the limit $\Delta\omega=0$,

$$\rho^{yx}(\tau) = U_{yy}[I_x]$$

is purely odd-quantum.

By inserting a π pulse in the middle of τ to remove all resonance offsets, selective preparation sequences can be created. Thus, an even-selective preparation sequence is $\frac{\pi}{2}I_x - \frac{\tau}{2} - \pi - \frac{\tau}{2} - \frac{\pi}{2}I_{-x}$ and an odd-selective one is $\frac{\pi}{2}I_x - \frac{\tau}{2} - \pi - \frac{\tau}{2} - \frac{\pi}{2}I_y$.

1.6 SEPARATION OF ORDERS

A highly useful property is that the offset experienced by MQ coherences scales with n. By going off-resonance by an amount $\Delta\omega$ greater than the largest MQ second moments, the orders can be separated. To see how this comes about, we expand the density operator in the irreducible spherical tensor operator basis:[10]

$$\rho(t) = \sum_{k,n} a_{k,n}(t) T_{k,n}$$

where $T_{k,n}$ is the nth-component of a k-rank tensor ($n \leq k$). The tensor components $T_{k,n}$ are related to n-quantum operators. It is convenient to group the n-quantum operators:

$$\rho(t) = \sum_{n} \rho_n(t)$$

where $\rho_n(t) = \sum_k a_{k,n}(t) T_{k,n}$.

As a result of the commutation rule:[10]

$$[I_z, T_{k,n}] = nT_{k,n}$$

and the following property of exponential operators[10]

$$e^{A}Be^{-A} = B + [A,B] + \frac{1}{2!}[A,[A,B]] + \frac{1}{3!}[A,[A,[A,B]]]+...$$

the effect of a rotation about I_z on ρ is:

$$\exp(-i\phi I_z)\rho_n(t)\exp(i\phi I_z) = \rho_n(t)\exp(-in\phi).$$

This implies that the existence of an offset term in H_1 will cause n-quantum coherences to oscillate as $n\Delta\omega$:

$$\exp(i\Delta\omega t_1 I_z)\rho_n(\tau)\exp(-i\Delta\omega t_1 I_z) = \rho_n(\tau)\exp(in\Delta\omega t_1).$$

If the offset $\Delta\omega$ is greater than the largest MQ second moments, this will result in separation of the orders in the Fourier spectrum.

As a corollary, the inhomogeneity is also scaled by n. For high resolution work, it would be desirable to remove the inhomogeneity by applying a π pulse in the middle of the evolution period. But by doing so, the centers of orders will coincide.

The method of time proportional phase incrementation[1,11] (TPPI) allows sorting of orders meanwhile removing inhomogeneous line broadening. It can accomplish separation regardless of whether there is a real resonance offset.

As is evident from its name, the method involves

incrementing the phase of the preparation pulses for each increment in t_1, and keeping the mixing pulses at a fixed phase.

Suppose we phase shift the preparation propagator by an amount ϕ:

$$U_\phi(\tau) = \exp(-i\phi I_z)U(\tau)\exp(i\phi I_z)$$

where $U(\tau)$ is at an arbitrary fixed phase. Applying the propagator on the initial density operator gives:

$$\rho(\tau) = U_\phi^\dagger(\tau)I_z U_\phi(\tau)$$

$$= \exp(-i\phi I_z)U^\dagger(\tau)I_z U(\tau)\exp(i\phi I_z)$$

Consider incrementing the phase of the preparation pulses by an amount $\Delta\phi$ proportional to t_1. We can express the phase as

$$\phi = \Delta\omega t_1$$

where $\Delta\omega = \frac{\Delta\phi}{\Delta t_1}$.

The fictitious offset $\Delta\omega$ is a parameter that can be varied by changing the phase increment $\Delta\phi$. To observe up to a maximum order M, the bandwidth $1/\Delta t_1$ must encompass up to $2M\Delta\omega/2\pi$. That is, the minimum increment in t_1 must satisfy:

$$\frac{1}{\Delta t_1} > \frac{2M\Delta\omega}{2\pi}$$

The corresponding condition on $\Delta\phi$ given Δt_1 is:

$$\Delta\phi < \frac{2\pi}{2M}.$$

Keeping the mixing propagator $V(\tau')$ at a fixed phase, the expression for the signal is then:

$$S(\tau,t_1,\tau') = Tr\{V(\tau')I_-V^\dagger(\tau')\exp(-iH_1t_1) \times U_\phi^\dagger(\tau)I_zU_\phi(\tau)\exp(-iH_1t_1)\}$$

$$= Tr\{V(\tau')I_-V^\dagger(\tau')\exp(-iH_1t_1)\exp(-i\Delta\omega t_1) \times U^\dagger(\tau)I_zU(\tau)\exp(i\Delta\omega t_1)\exp(iH_1t_1).$$

Thus the signal experiences an additional, although artificial, offset.

By inserting a π pulse in the middle of t_1, the effective H_1 is free of all real offset terms. With this and TPPI, we can obtain separation of orders without losing high resolution.

In chapter 2, the scaling of inhomogeneity with n is put to use to obtain separation of MQ spin echoes and to allow selective detection.

CHAPTER 1 REFERENCES

1. G. Drobny, A. Pines, S. Sinton, D.P. Weitekamp, and D. Wemmer, Faraday Symp. Chem. Soc. 13, 49 (1979).
2. A. Wokaun and R.R. Ernst, Molec. Phys. 36, 317 (1978).
3. W.S. Warren, Ph.D. thesis, University of California, Berkeley, 1980.
4. G. Bodenhausen, Progr. NMR Spectrosc. 14, 137 (1981).
5. J.B. Murdoch, Ph.D. thesis, University of California, Berkeley, 1982.
6. D.P. Weitekamp, Advan. Magn. Reson., submitted for publication.
7. A. Abragam, Principles of Nuclear Magnetism, (Oxford, London, 1961).
8. S. Yatsiv, Phys. Rev. 113, 1522 (1959).
9. J.W. Emsley and J.C. Lindon, NMR Spectroscopy Using Liquid Crystal Solvents, (Pergamon Press, New York, 1975).
10. E. Merzbacher, Quantum Mechanics, (John-Wiley & Sons, New York, 1961), 2nd ed.
11. G. Bodenhausen, R.L. Vold, and R.R. Vold, J. Magn. Reson. 37, 93 (1980).

CHAPTER 2

INDIRECT DETECTION OF SPIN-1 DOUBLE-QUANTUM COHERENCE IN LIQUIDS

2.1 INTRODUCTION

Time domain multiple-quantum (MQ) NMR has been demonstrated in a variety of systems[1] to offer higher resolution and more information on relaxation dynamics than single-quantum (SQ) methods. Although S = 1 nuclei in anisotropic systems were among the early applications of time domain double-quantum (DQ) NMR,[2,3,4] it is only recently that the interesting problem has been raised of observing these transitions in isotropic solution where the quadrupole coupling vanishes. Prestegard and Miner[5] recognized that the usual preparation sequence using two $\pi/2$ pulses[6,7] on the S spins (^{14}N) does not excite DQ coherence, even when the spectrum shows resolved J coupling to neighboring heteronuclei. They demonstrated that augmentation of this sequence by spin tickling of bound protons (I = 1/2) did allow S spin DQ coherence to be prepared from and mixed to S spin magnetization.

In this work we demonstrate that the S DQ coherence can be excited and detected by using only the I spin magnetization and applying simple hard pulses at both I and S frequencies. This is an example of heteronuclear coherence transfer[8,9] and is an

extension of heteronuclear MQ techniques already demonstrated for I = S = 1/2 in liquids[10] and in liquid crystals[11], and for I = 1/2, S = 1 in liquid crystals[12] and solids.[13,14,15]

This indirect method of observation of S = 1 DQ coherence benefits from the signal enhancement[10,12] which comes from using only proton magnetization as the initial and final conditions. In addition, we employ spin echoes and time proportional phase incrementation (TPPI)[7,16] to separate orders and a form of coherence transfer echo[9,17] to suppress large zero-quantum interference.

In discussing the various coherences possible in a heteronuclear system, it is useful to label them with a pair of quantum numbers (n^I, n^S) which are conserved under free evolution. For any coherent superposition $|i\rangle\langle j|$ of two eigenstates these are defined by the relations

$$[I_z, |i\rangle\langle j|] = n^I_{ij}|i\rangle\langle j|, \tag{1a}$$

$$[S_z, |i\rangle\langle j|] = n^S_{ij}|i\rangle\langle j|. \tag{1b}$$

These are just the differences in Zeeman quantum numbers for the states connected: $n^I_{ij} = m^I_i - m^I_j$, $n^S_{ij} = m^S_i - m^S_j$.

2.2 THEORY

Shown in Fig. 2.1 are two pulse sequence

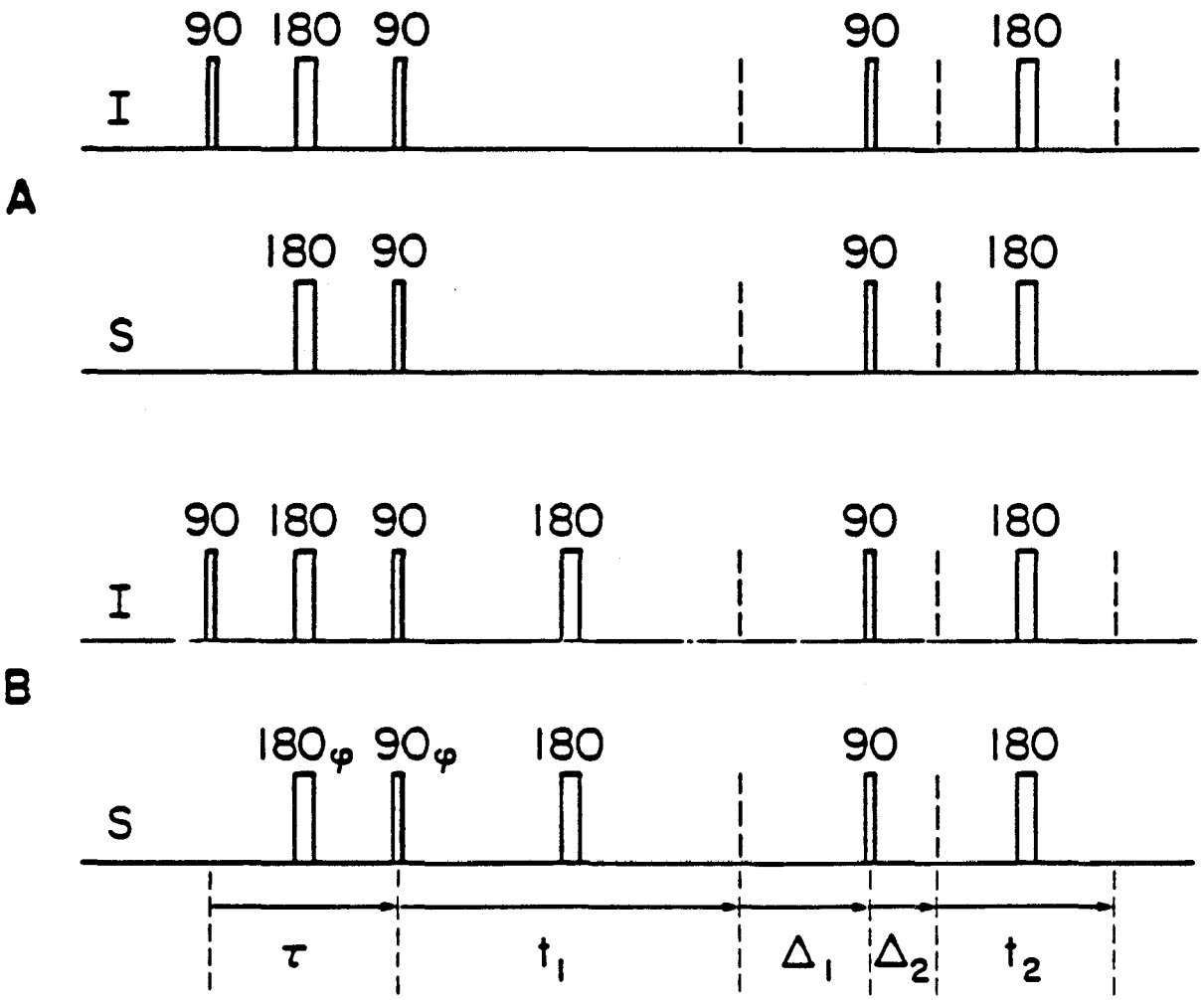

XBL 819-4952

Fig. 2.1 Pulse sequences used for observing heteronuclear MQ coherence. The I spin FID is monitored at $t_2 = \tau$. Pulse sequence B has the first two S spin rf pulses phase shifted by $\phi = \Delta\omega t_1$ (TPPI). All other rf pulses of a given frequency may be of the same phase. The delays Δ_1 and Δ_2 allow suppression of the signal from all but one order of coherence.

variations for observation of various orders of coherence (n^I_{ij}, n^S_{ij}) using only I spin magnetization. Perfect rf pulses of negligible duration are assumed. We consider here the case of a group of equivalent I spins identically coupled to a single S =1 spin. The unperturbed rotating frame Hamiltonian is

$$H = -\Delta\omega_I I_z - \Delta\omega_S S_z + J' I_z S_z, \tag{2}$$

where $J' = 2\pi J$ is the scalar heteronuclear coupling (in rad/sec) and $I_z = \sum_i I_{zi}$. For the preparation sequence $(\pi/2)_x - \tau/2 - (\pi)_x(I,S) - \tau/2 - (\pi/2)_x(I,S)$ the propagator is

$$\begin{aligned} U(\tau) &= \exp[i(\pi/2)(I_x + S_x)]\exp(-iH\tau/2)\exp[i\pi(I_x + S_x)] \\ &\quad \times \exp(-iH\tau/2)\exp[i(\pi/2)I_x] \\ &= \exp(-i\tau J' I_y S_y)\exp[-i(\pi/2)S_x]. \end{aligned} \tag{3}$$

The simultaneous π pulses remove the dependence on the offset terms in the Hamiltonian of Eq. (2) making the propagator even-quantum selective[4,10,18] and dependent only on the variable $J'\tau$.

The density operator at the end of the preparation period is $\rho(\tau) = U(\tau)\rho(0)U^{-1}(\tau)$. Neglecting the term proportional to the identity this is given by

$$\begin{aligned} \rho(\tau) &= \exp(-i\tau J' I_y S_y)(bI_z)\exp(i\tau J' I_y S_y) \\ &= b[I_z\cos(J'\tau S_y) + I_x\sin(J'\tau S_y)] \end{aligned}$$

$$= b\{I_z[1 + S_y^2(\cos J'\tau - 1)] + I_x S_y \sin J'\tau\}. \quad (4)$$

In the last step, the identities

$$\cos(\theta S_y) = 1 + S_y^2(\cos\theta - 1), \quad (5a)$$

$$\sin(\theta S_y) = S_y \sin\theta \quad (5b)$$

appropriate to S = 1 have been used. The initial equilibrium spin density operator proportional to S_z is not included in the expression, since it does not yield DQ coherence nor does it lead to an eventual signal in the proton channel. Equation (4) can be written using the fictitious spin-1/2 operators[19,20] for the S operators:

$$\rho(\tau) = b\{I_z[1 + (2/3 - S_x^{1-3} - 1/3(S_z^{1-2} - S_z^{2-3}))(\cos J'\tau - 1)] + 2^{1/2} I_x (S_y^{1-2} + S_y^{2-3}) \sin J'\tau\}. \quad (6)$$

This expansion shows that S_y^2 consists of zero-quantum and DQ operators. The coefficient of the operator $I_z S_y^2$, and thus of the ($n^I = 0$, $n^S = \pm 2$) coherence $I_z S_x^{1-3}$, is maximized by setting $\tau = 1/2J$ sec, where J is in hertz.

The prepared coherences evolve during t_1. Since only ($n^I = \pm 1$, $n^S = 0$) coherences can freely evolve

into proton transverse magnetization, the $\pi/2$ pulses at the end of t_1 are needed to convert MQ coherence into such SQ coherence. For each increment in t_1, only the peak of the MQ spin echo at $t_2 = \tau$ is sampled in the proton channel. The resulting heteronuclear MQ interferogram as a function of the evolution time t_1 is the autocorrelation function of $\rho(\tau) = \rho(\tau, t_1 = 0)$. Neglecting relaxation and with $\Delta_1 = \Delta_2 = 0$ (Fig. 2.1), this is

$$\begin{aligned} S(t_1) &= \mathrm{Tr}\{\rho(\tau,0)\rho(\tau,t_1)\} \\ &= \mathrm{Tr}\{\rho(\tau,0)\exp(-it_1 J' I_z S_z)\rho(\tau,0)\exp(it_1 J' I_z S_z)\} \\ &= \sum_{i,j} |\rho(\tau,0)|^2_{i,j} \exp(-i\omega_{ij} t_1), \end{aligned} \tag{7}$$

where $\omega_{ij} = \omega_i - \omega_j$ and $\omega_i = \langle i | J' I_z S_z | i \rangle$.

Evaluation of the matrix elements of $I_z S_x$[1-3] [Eq. (6)] for the case of four equivalent $I_i = 1/2$ spins shows that the DQ spectrum is a quintet with line separation of 2J and line amplitude of

$$\begin{aligned} A(m^I) &= (1/4)(\cos J'\tau - 1)(\cos J' t_2 - 1)(m^I)^2 g(m^I) \\ &= (\cos J'\tau - 1)(\cos J' t_2 - 1), && m^I = \pm 2 \\ &= (\cos J'\tau - 1)(\cos J' t_2 - 1), && m^I = \pm 1 \\ &= 0, && m^I = 0. \end{aligned}$$

Note that the central line of the quintet has zero amplitude. The degeneracies $g(m^I)$ are 1,4,6 for $m^I =$

±2, ±1, 0, respectively.

The fixed time delays Δ_1 and Δ_2 are included to selectively echo the desired order for detection. The scheme is similar to pulsed field gradient methods[17], except that here the static field inhomogeneity and a longer time delay are used for the dephasing and selective rephasing. Advantage is taken of the proportionality of the dephasing rate to $n^I\gamma_I + n^S\gamma_S$, thereby allowing separation of various MQ echoes. Sampling at the peak of the desired MQ echo results in detection of the selected order and suppression of the other orders. In our experiments, the ^{14}N DQ coherence dephases at a rate proportional to $2\gamma_S$ in Δ_1 and rephases as proton SQ coherence at a rate proportional to γ_I in Δ_2. To observe the ^{14}N DQ coherence echo as proton transverse magnetization, Δ_2 must be set at

$$\Delta_2 = \frac{2\gamma_S}{\gamma_I}\Delta_1 \qquad (9)$$

This scheme can be viewed as a coherence transfer echo filterng (CTEF) process. The desired DQ signal is a small oscillation on top of a large signal originating from coherences not of DQ nature, the largest being from the H_2O solvent. Fluctuations in the large signal resulting from instrumental instability appear in the Fourier transform as noise at all values of ω_1. Because this t_1 noise can be

comparable to the DQ signal, it is desirable to eliminate it by "filtering" out the large signal. In addition, the dynamic range requirements of the spectrometer are reduced, since the largest signals never reach the receiver.

Pulse sequence B differs from A only in the way the separation of MQ orders is accomplished. Because of the tensorial properties of MQ operators expressed in Eq. (1), the center of the order (n^I, n^S) is at $n^I \Delta\omega_I + n^S \Delta\omega_S$. Pulse sequence A requires a real resonance offset, whereas pulse sequence B creates an artificial offset by TPPI.[7,16] The π pulses in t_1 remove all real resonance offset terms and thus field inhomogeneity. The phase incrementation of the S rf pulses in the preparation period for each incrementation in t_1 effects an apparent S frequency offset in the observing frame. TPPI yields a spectrum that is free of inhomogeneous broadening and yet retains separation of the MQ orders.

2.3 RESULTS AND DISCUSSION

Spectra were obtained at 27°C of an 8 molar NH_4NO_3 aqueous solution acidified to pH 1 to slow down proton exchange with the solvent. The spectrum in Fig. 2.2 was obtained using pulse sequence A with the ^{14}N carrier frequency offset by 0.85 kHz from NH_4^+ resonance and the proton carrier frequency on resonance

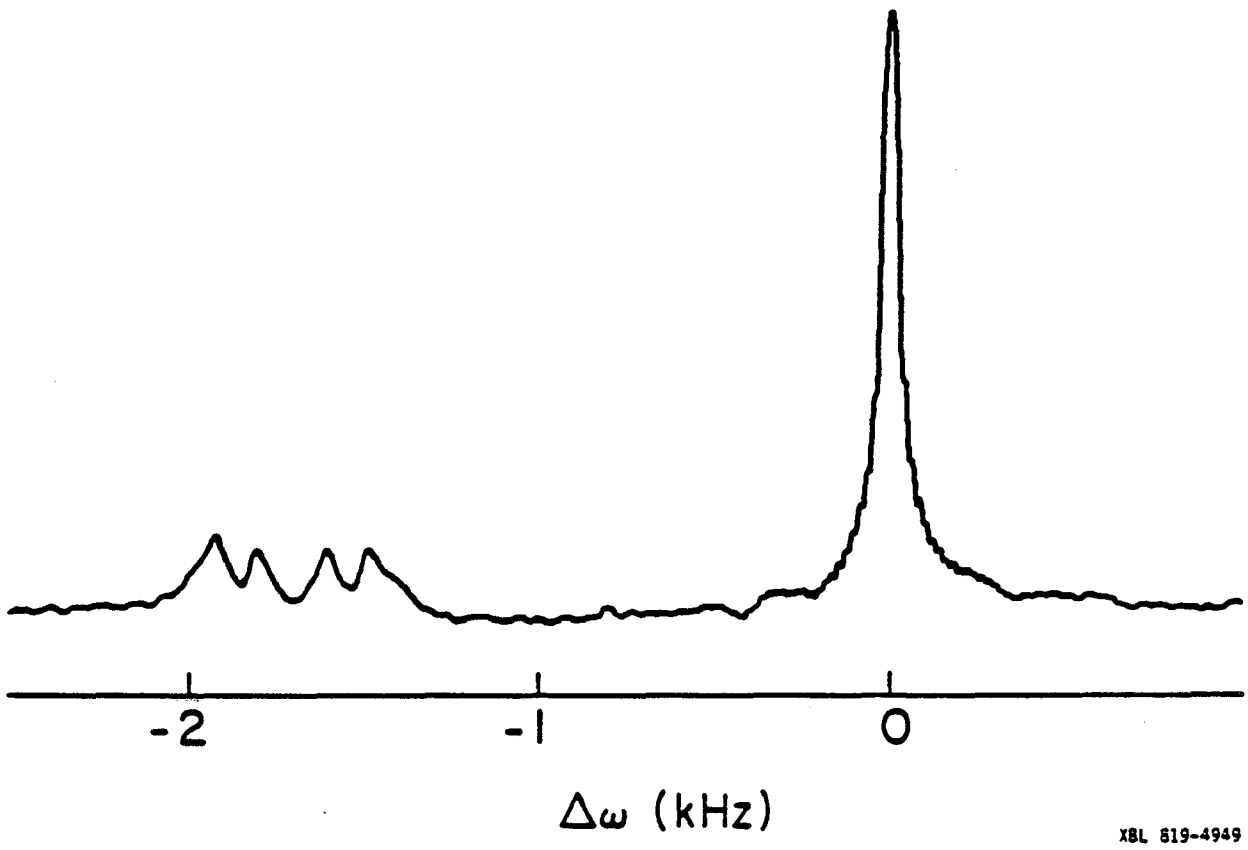

Fig. 2.2 Proton-detected heteronuclear MQ magnitude spectrum of acidified 8 molar NH_4NO_3 aqueous solution observed at 185 MHz. The spectrum is obtained using pulse sequence A in Fig. 2.1 with ^{14}N carrier frequency offset from NH_4^+ resonance by $\Delta\omega_S$ = 0.85 kHz, $\tau = t_2$ = 9.6 msec, t_1 increment = 200 μsec, Δ_1 = 11.327 msec, and Δ_2 = 1.618 msec. The incompletely suppressed on-resonance line arises predominantly from longitudinal H_2O magnetization present during t_1. The multiplet with the center offset by 1.70 kHz is the ^{14}N DQ spectrum.

at 185 MHz. The time delays Δ_1 and Δ_2 were set according to Eq. (9). The central peak at $\Delta\omega = 0$ arises predominantly from imperfect CTEF of the longitudinal proton magnetization of the solvent H_2O present during evolution. Other contributions are from the zero-quantum portion of $I_z S_y^2$ and from I_z of the ammonium protons, both of which are present in $\rho(\tau)$ even when DQ coherence is maximized [Eqs. (4) to (6)]. The multiplet corresponds to the DQ coherence transfer spectrum of ^{14}N. Its center is offset by 1.70 kHz, which is twice the carrier frequency offset, the splitting is 2J, and the linewidth is twice that of ^{14}N SQ inhomogeneous linewidth - all of which are indicative of ^{14}N DQ transitions.

Figure 2.3 shows the improvement in resolution of the multiplet using pulse sequence B with the same parameter settings. The spectrum is a quintet with relative amplitudes of 1:1:0:1:1 and splittings of 2J, in agreement with the calculations [Eq. (8)]. The splitting is 105 ± 1 Hz; the homogeneous absorption linewidth (full width at half maximum) is 7 ± 1 Hz as compared with the inhomogeneous linewidth of 70 to 80 Hz in Fig. 2.2.

Also of importance is the comparison of the homogeneous ^{14}N DQ and SQ linewidths. Through a conventional ^{14}N detected spin echo sequence, with a simultaneous π pulse applied to the protons to preserve

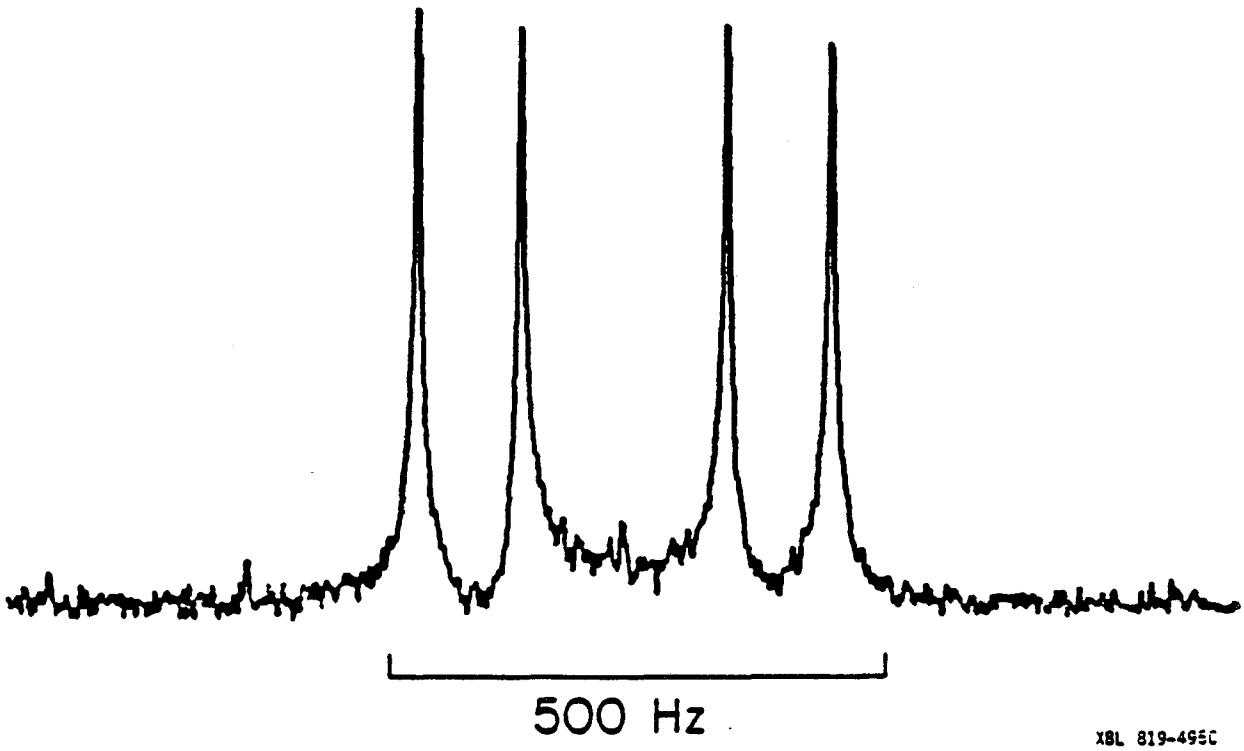

Fig. 2.3 Proton-detected ^{14}N DQ magnitude spectrum using pulse sequence B in Fig. 2.1 with ^{1}H and ^{14}N carrier frequencies on resonance. $\tau = t_2 = 10$ msec; all other parameter settings are the same as in Fig. 2.2. The spectrum is a quintet with 1:1:0:1:1 amplitude ratio and 105 Hz peak separation.

the J coupling, the absorption linewidth of ^{14}N DQ and SQ homogeneous linewidths are the same.

In both Figs. 2.2 and 2.3, the magnitude spectra are displayed. The lines of the quintet can in principle be observed in phase [Eq. (7)], but were not because of the use of CTEF. The insertion of the time delay Δ_1 in t_1 necessitates that the heteronuclear MQ interferogram is first sampled not at $t_1 = 0$ but at $t_1 = \Delta_1$. During the extra time Δ_1, the lines accumulate phase at different rates resulting in a large phase shift linear in ω_1.

To demonstrate the sinusoidal dependence of the $I_z S_x{}^{1-3}$ operator on preparaton time [Eq. (6)], pulse sequence B was employed with t_2 held constant for different values of τ. With t_2 fixed, the line amplitude varies with τ as $(\cos J'\tau - 1)\exp(-\tau/T_2)$, where now T_2 refers to the $n^I = 1$ homogeneous decay time. Figure 2.4 shows the integrated line amplitude of the quintet as a function of τ. A least squares analysis gave $T_2 = 80 \pm 11$ msec.

In summary, DQ transitions in ^{14}N, a quadrupolar n[illegible]us of spin S = 1, is made possible through the J coupling to the protons. Sensitivity is greatly improved by indirectly detecting the quadrupolar nuclei through the protons. Using TPPI and a spin echo in the evolution period, the inherently higher resolution of the DQ spectrum is realized.

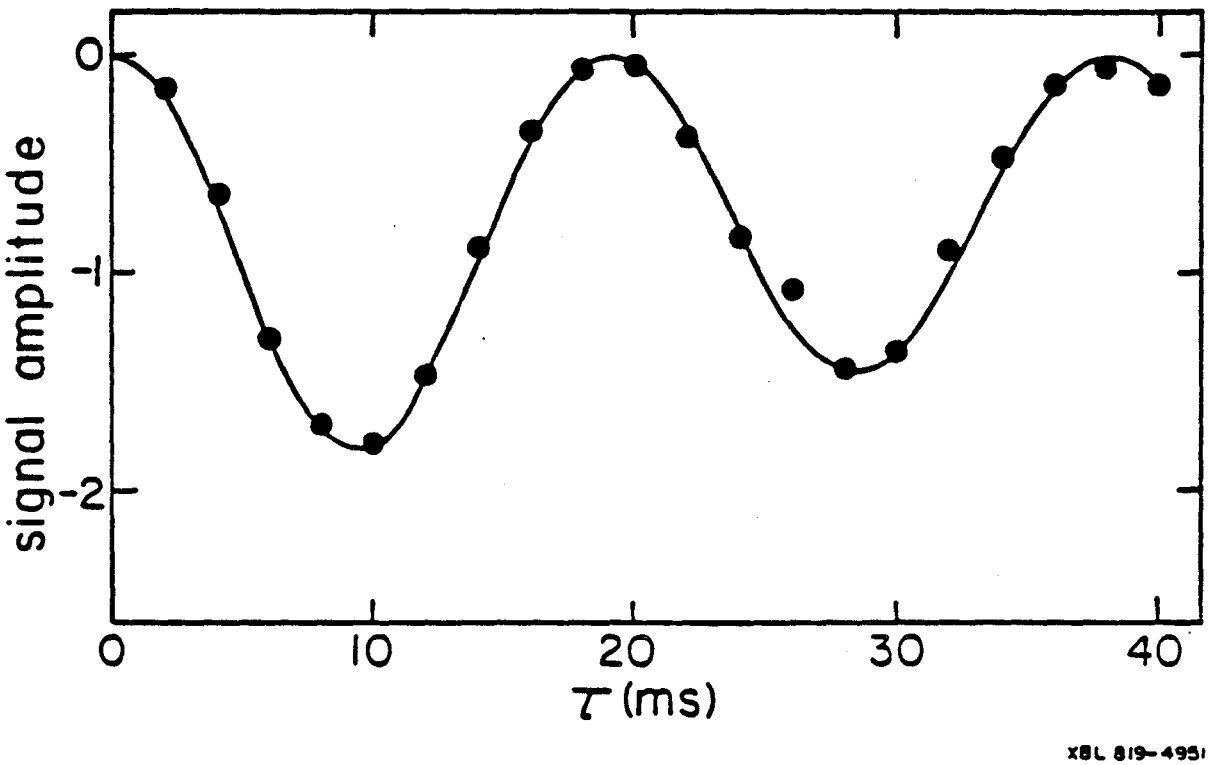

Fig. 2.4 Normalized ^{14}N DQ line amplitude as a function of the preparation time τ. The experimental points are compared with the solid theoretical curve of $(\cos J'\tau - 1)\exp(-\tau/T_2)$.

CHAPTER 2 REFERENCES

1. G. Bodenhausen, Progr. NMR Spectrosc. 14, 137 (1981).
2. S. Vega and A. Pines, J. Chem. Phys. 66, 5624 (1977).
3. S. Hsi, H. Zimmerman, and Z. Luz, J. Chem. Phys, 69, 4126 (1978).
4. D.E. Wemmer, Ph.D. thesis, University of California, Berkeley, 1978.
5. J.H. Prestegard and V.W. Miner, 22nd Experimental NMR Conference, 1981; V.W. Miner and J.H. Prestegard, J. Am. Chem. Soc. 108, 5979 (1981).
6. W.P. Aue, E. Bartholdi, and R.R. Ernst, J. Chem. Phys. 64, 2229 (1976).
7. G. Drobny, A. Pines, S. Sinton, D.P. Weitekamp, and D. Wemmer, Faraday Symp. Chem. Soc. 13, 49 (1979).
8. A.A. Maudsley and R.R. Ernst, Chem. Phys. Lett. 50, 368 (1977).
9. A.A. Maudsley, A. Wokaun, and R.R. Ernst, Chem. Phys. Lett. 55, 9 (1978).
10. L. Müller, J. Am. Chem. Soc. 101, 4481 (1979).
11. D.P. Weitekamp, J.R. Garbow, and A. Pines, submitted for publcation.
12. A. Minoretti, W.P. Aue, M. Rheinhold, and R.R. Ernst, J. Magn. Reson. 40, 175 (1980).
13. S. Vega, T.W. Shattuck, and A. Pines, Phys. Rev A

22, 638 (1980).

14. P. Brunner, M. Rheinhold, and R.R. Ernst, J. Chem. Phys. 73, 1086 (1980).

15. M. Rheinhold, P. Brunner, and R.R. Ernst, J. Chem. Phys. 74, 184 (1980).

16. G. Bodenhausen, R.L. Vold, and R.R. Vold, J. Magn. Reson. 37, 93 (1980).

17. A. Bax, P.G. de Jong, A.F. Mehlkopf, and J. Smidt, Chem. Phys. Lett. 69, 567 (1980).

18. W.S. Warren, D.P. Weitekamp, and A. Pines, J. Chem. Phys. 73, 2084 (1980).

19. A. Wokaun and R.R. Ernst, J. Chem. Phys. 67, 1752 (1977).

20. S. Vega, J. Chem. Phys. 68, 5518 (1978).

CHAPTER 3

TIME-REVERSAL MULTIPLE-QUANTUM NMR IN SOLIDS

3.1 INTRODUCTION

Multiple-quantum (MQ) NMR spectroscopy has generally been applied to systems of isolated molecules with a small number of spins.[1,2] The small system size limits the complexity of the spectrum as well as the number of rf quanta that can be absorbed or emitted. One difficulty in studying large spin systems is that the average intensity per transition decreases rapidly with the number of spins. As a result, selective excitation schemes[3] may be necessary to channel intensity into the desired n-quantum order. Thus, comparatively few applications have been performed in solids,[4,5] where extensive dipolar coupling makes the coupled spin system essentially infinite in size.

In this chapter, we present the utilization of time reversal[3,6] to enhance overall signal intensity so that very high quantum absorption can be observed in solids. In Fig. 3.1, we show a ^1H MQ spectrum of solid adamantane $C_{10}H_{16}$ obtained by such a time-reversal excitation-detection scheme, where up to 22-quantum absorption is observed. Adamantane is a plastic crystal; the molecule is nearly spherical and as such can tumble isotropically in the solid phase. At room

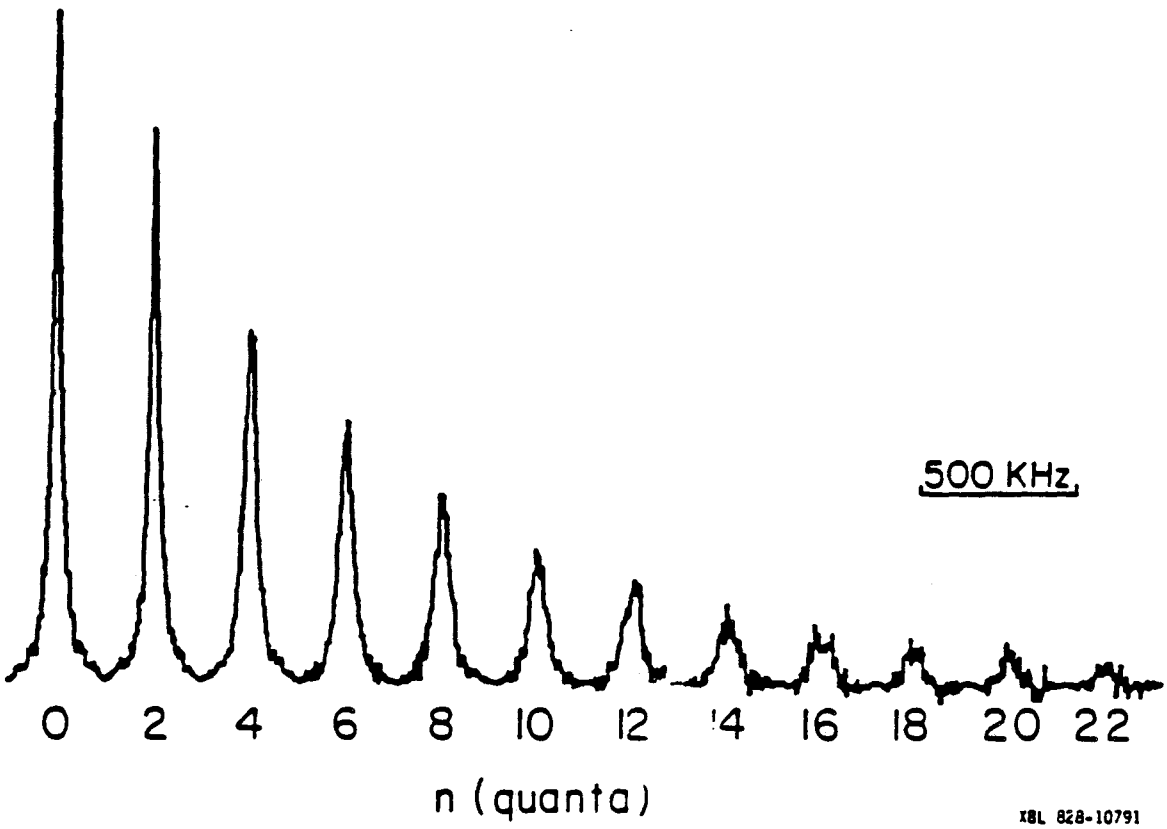

Figure 3.1 ^{1}H multiple-quantum NMR spectrum of solid adamantane at room temperature, obtained with time-reversal sequence of Fig. 3.2(d) and excitation time of 480 μsec.

temperature, this motion averages to zero all intramolecular couplings but retains the intermolecular terms. Our system is thus not an isolated molecule but rather a network of molecules. Very high quantum transitions might thereby be excited.

One of the main features of solids is the high density of spin states. Due to the continuum of transitions, individual lines within each n-quantum order are unresolved. Since both the intensity and phase of individual MQ coherences depend uniquely on the excitation time, there may occur destructive interference between overlapping lines. The integrated intensity of the MQ spectrum is decreased and the signal-to-noise ratio suffers. This problem becomes more severe as the excitation time is increased, as is observed experimentally. Very quickly, typically within 10^{-4} sec, the signal-to-noise ratio is dominated by instrumental noise. It eventually becomes very difficult to observe high quantum absorption, where long excitation times are required.

What is desired then is the generation of all lines in phase at the point of detection, that is, in some manner to reverse the dephasing that occurred in the excitation period. In solids, the dominant dephasing mechanism is the dipole-dipole interaction, which is homogeneous in nature. If one is able to produce a homogeneous spin echo,[6] the peak of the

echo is free of the dipolar Hamiltonian. This in fact can be accomplished by applying a series of intense rf pulses to the spin system to effect what is in essence time reversal. With the method of time reversal, we were able to regain the intensity lost due to fast homogeneous dephasing of spins in solids.

3.2 THEORY

For the following discussions, it is convenient to introduce the time-domain MQ NMR experiment, described schematically in Fig. 3.2(a). The sequence can be partitioned into four time domains:[7] preparation (τ), evolution (t_1), mixing (τ'), and detection (t_2) periods. As a specific example, consider the simple three-pulse sequence in Fig. 3.2(b). The first two pulses separated by an excitation delay τ prepare MQ coherences, which then evolve freely for a time t_1. Because MQ coherences do not correspond to magnetization, they are not directly observable with our detection coil. A third pulse is needed to convert them into single-quantum coherences, which are detected in time t_2. For our experiments, only the point at $t_2 = \tau$ is sampled.[8] The sequence is repeated for many values of t_1 until one maps out an interferogram. Fourier transformation with respect to t_1 of this interferogram yields the MQ spectrum.

The equation of motion of a coupled spin system is

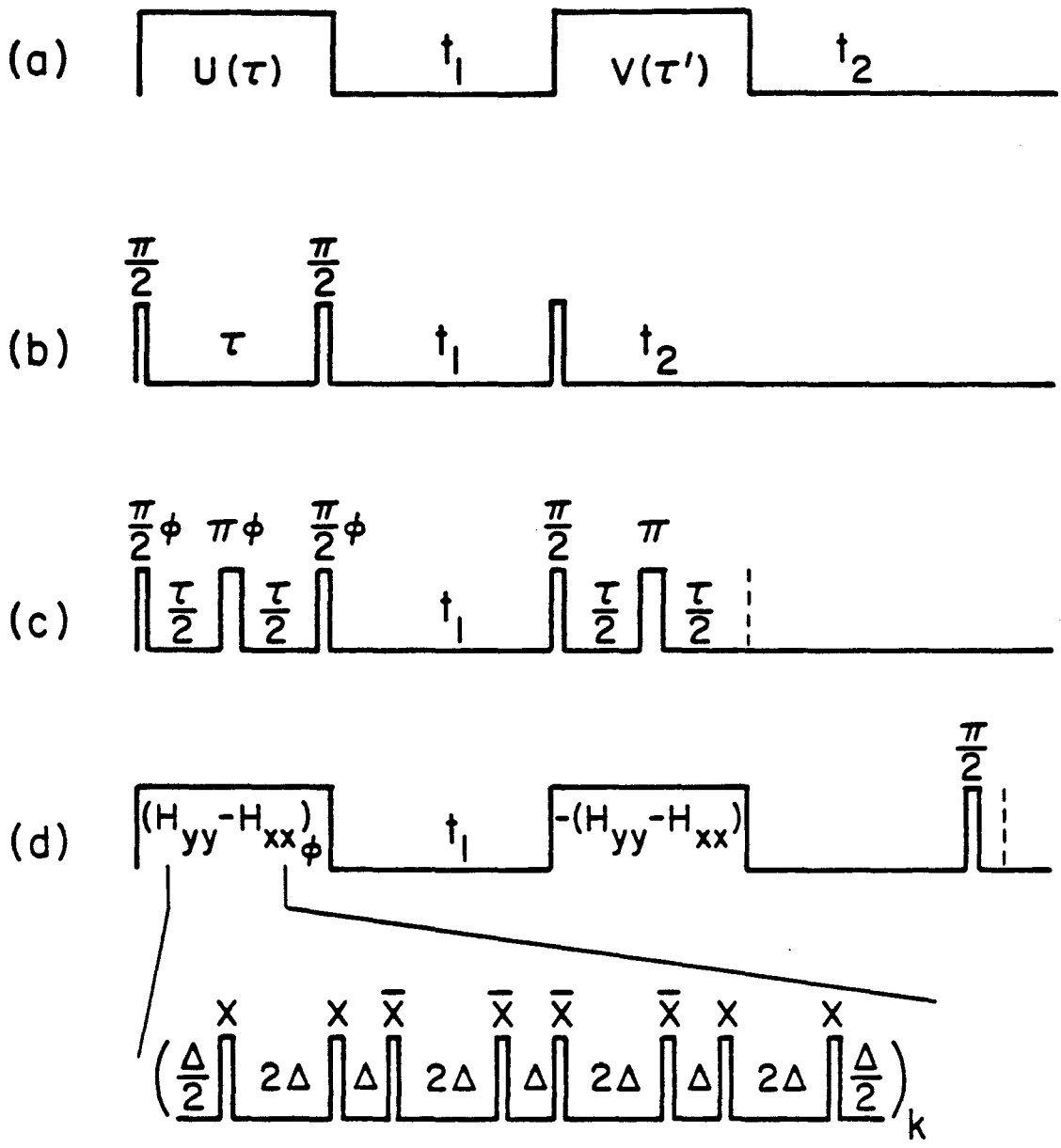

XBL 828-10792

Figure 3.2 Multiple-quantum pulse sequences: (a) Schematic pulse sequence showing relevant periods. (b) Nonselective three-pulse experiment. (c) Even-selective sequence with preparation pulses phase shifted by an amount $\phi = \Delta\omega t_1$ (TPPI) to separate n-quantum orders. (d) Time-reversed preparation and mixing periods with the preparation $\pi/2$ pulses phase shifted by an amount ϕ (TPPI). The preparation and mixing periods are composed of cycles of the 8-pulse $(H_{xx}-H_{yy})$ sequence shown below. A delay of 1.6 msec separates the mixing period from the final detecting pulse to allow

transients to decay away. 30 μsec is allowed for receiver deadtime before sampling is taken at the dotted line.

conveniently described in the density matrix formalism. In this formalism, neglecting relaxation, the signal in the time domain is given by the trace of the product of the observable and the reduced density matrix:

$$\begin{aligned} S(\tau,t_1,\tau') &= \mathrm{Tr}\{I_z\rho(\tau,t_1,\tau')\} \\ &= \mathrm{Tr}\{VI_zV^\dagger\exp(-iH_1t_1)U^\dagger I_zU\exp(iH_1t_1)\} \\ &= \mathrm{Tr}\{Q(\tau')\exp(-iH_1t_1)P(\tau)\exp(iH_1t_1)\} \\ &= \sum_{j,k} P_{jk}(\tau)Q_{kj}(\tau')\exp(-i\omega_{jk}t_1). \qquad (1) \end{aligned}$$

Here $U = \exp(iH\tau)$ is the preparation propagator, $V = \exp(iH'\tau')$ is the mixing propagator, $P = U^\dagger I_z U$ is the preparation density operator, $Q = VI_zV^\dagger$ is the mixing density operator, $|j\rangle$'s are eigenstates of the Hamiltonian H_1, and $\omega_{jk} = \omega_j - \omega_k$ is the transition frequency. In the above equation, the invariance of the trace to cyclic permutation is used. The spin system is assumed to be initially at equilibrium. For notational convenience, a virtual $\pi/2$ pulse is applied at end of τ' so that I_z rather than $I_+ = I_x + iI_y$ is our observable.

To see how phase terms can arise in a MQ NMR experiment, let us consider the situation $V = U$, which is the case for the commonly-used pulse sequences in Figs. 3.2(b) and 3.2(c). The transition between states $|j\rangle$ and $|k\rangle$ is then described by a complex vector

$(P_{jk})^2$, where the intensity is given by $|P_{jk}|^2$ and the phase is a complicated function of the preparation period:

$$\theta_{jk}(\tau) = \tan^{-1}\{\frac{\mathrm{Im}[P_{jk}{}^2(\tau)]}{\mathrm{Re}[P_{jk}{}^2(\tau)]}\}. \qquad (2)$$

The preparation density operator P and hence the phase of a transition vary with the excitation time τ.[9]

If we now look at the case $V = U^\dagger$, then $Q = P = P^\dagger$, and the signal can be written as an autocorrelation function of the preparation density operator $P(\tau)$:

$$S(\tau,t_1) = \mathrm{Tr}\{P^\dagger(\tau)\exp(-iH_1t_1)P(\tau)\exp(iH_1t_1)\}$$
$$= \sum_{j,k} |P_{jk}(\tau)|^2\exp(-i\omega_{jk}t_1). \qquad (3)$$

Note that here the signal contains no phase factor for <u>all</u> lines. Suppose further that V differs from $U^\dagger$ only in phase by an amount χ, i.e.,

$$V = \exp(-i\chi I_z)U^\dagger\exp(i\chi I_z). \qquad (4)$$

Then $Q = \exp(-i\chi I_z)P\exp(i\chi I_z)$, and the signal is given by:

$$S(\tau,t_1) = \sum_n \sum_{j,k} |P_{jk}|^2\exp(in\chi)\exp(-i\omega_{jk}t_1). \quad (5)$$

This states that all lines within order $n = m_j - m_k$, where the m_j's are Zeeman magnetic quantum numbers, have the same phase, and lines between neighboring

orders differ in phase by $\pm\chi$. Thus, if orders are well-separated, the condition in Eq. (4) is sufficient to ensure no phase cancellation. In practice, Hermitian conjugation of U or V is achieved by negating the Hamiltonian, which has the same effect as reversing time, hence the term time reversal.

3.3 EXPERIMENTAL

The actual pulse sequence used to generate the time-reversed spectra is shown in Fig. 3.2(d). The eight-pulse cycle preparation sequence creates an average Hamiltonian[10] ($H_{xx} - H_{yy}$), which is a pure double-quantum operator[3] and can excite only even-quantum transitions. The excitation time is increased by adding more cycles. To account for finite rf pulsewidths, $2\Delta + t_p$ is used in place of 2Δ, where t_p is the pulse duration. The experiment was performed on resonance, causing all MQ orders to overlap. To create the large artificial offset required for separation of orders, the method of time proportional phase incrementation (TPPI)[11] is used. For each incrementation in t_1, the phase of the preparation pulses is incremented by the amount:

$$\Delta\phi = \frac{2\pi}{2M} \tag{6}$$

where M is the maximum MQ order to be observed.

In principle, detection can be made immediately after the mixing pulses with a final detecting pulse.

In practice, however, due to pulse imperfections and relaxation, a delay of 1.6 msec is introduced after the mixing pulses, allowing transients to decay before applying a detecting pulse. These transients should decay on the order of T_2, the spin-spin relaxation time,[12] which is typically 10^{-4} sec for solids. The desired signal, after mixing, is in the form of populations. It decays as T_1, the spin-lattice relaxation time,[12] which is on the order of seconds, and should essentially be preserved during the 1.6 msec delay. The final $\pi/2$ pulse rotates it into the transverse plane for detection. The detecting pulse can be of arbitrary phase, as long as it remains fixed from point to point in t_1. A delay of 30 μsec is inserted before sampling to allow for receiver deadtime.

3.4 RESULTS AND DISCUSSION

To demonstrate the severity of intensity loss due to phase cancellation in the normal nontime-reversal approach to MQ NMR, in Fig. 3.3 we compare ^1H MQ magnitude spectra of adamantane obtained with and without time reversal, using pulse sequences of Figs. 3.2(d) and 3.2(c), respectively. The π pulses in Fig. 3.2(c) remove all resonance-offset terms, rendering this sequence even-selective,[13] as is the sequence of Fig. 3.2(d). Both spectra were obtained at 35°C with a

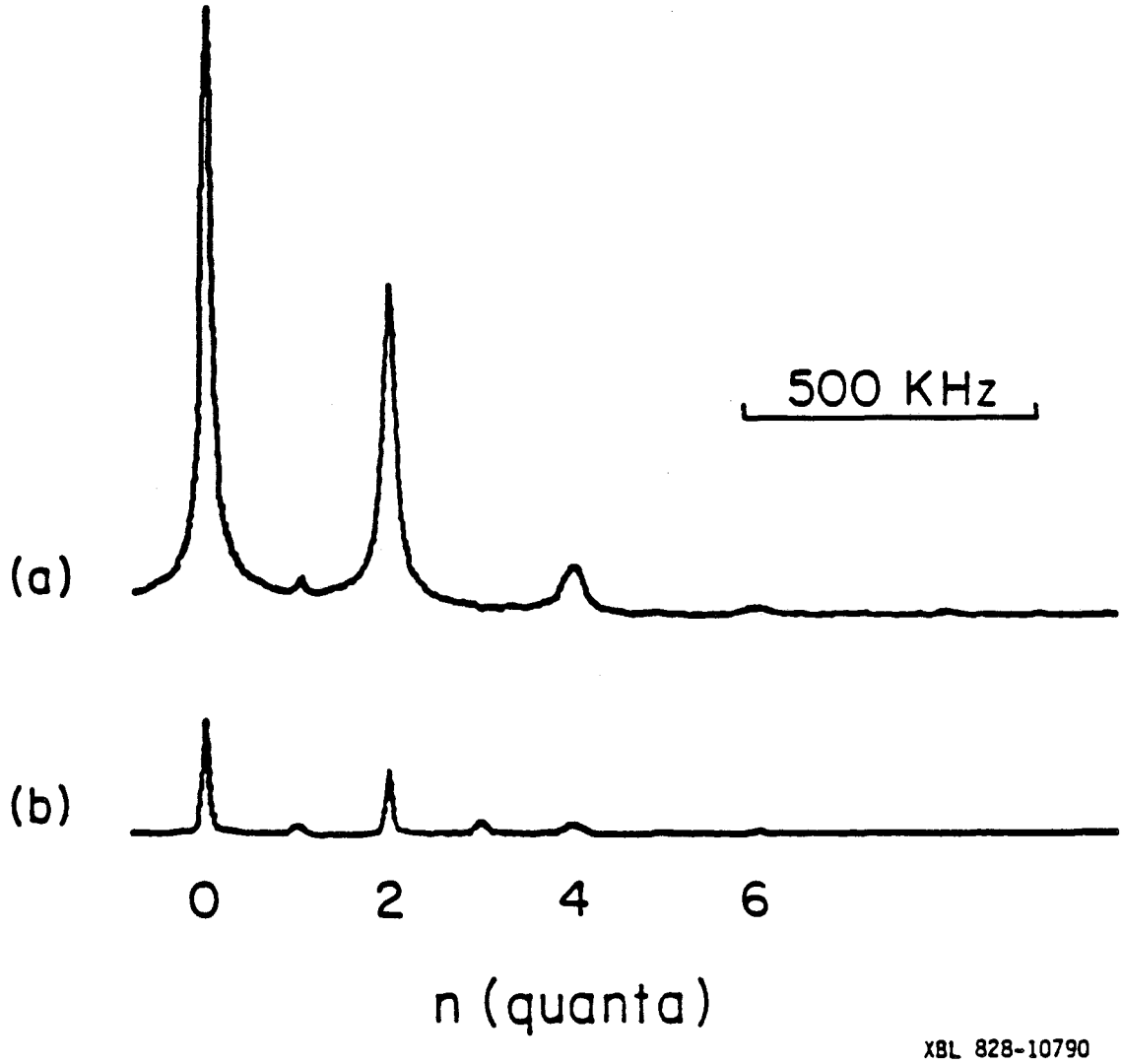

Figure 3.3 Comparison of adamantane ^1H multiple-quantum NMR spectra obtained with 144 μsec excitation time and using (a) time-reversal pulse sequence of Fig. 3.2(d) with Δ=0.8 μsec and t_p=3.2 μsec, and (b) nontime-reversal pulse sequence of Fig. 3.2(c).

preparation time of 144 μsec. Without time reversal, phase cancellation results in a significant reduction of absolute integrated intensity. This difference in intensity becomes more pronounced as the excitation time increases. We emphasize here that without time reversal, we were not able to increase the excitation time long enough to observe high quantum absorption. Comparison of lineshapes, in particular second moments, with and without incorporation of time reversal will be discussed elsewhere.[14]

An interesting result of these experiments is the initial time dependence of MQ intensities on n, the number of quanta. The short time behavior can be obtained from a power expansion in τ of the preparation density operator:[1]

$$\begin{aligned} P(\tau) &= \exp(-iH\tau)P(0)\exp(iH\tau) \\ &= P(0) - i\tau[H,P(0)] - \frac{\tau^2}{2}[H,[H,P(0)]] + \ldots \end{aligned} \tag{7}$$

For the $(H_{xx} - H_{yy})$ pulse sequence in Fig. 3.2(d) assuming perfect δ-function pulses, evaluation of the commutators for $P(0) = I_z$ reveals that the integrated intensity of a given order (n=0,4,6,8,...) grows in as:

$$\sum_{j,k} |P_{jk}|^2 \propto \tau^{n+4} \tag{8}$$

where the summation runs through all j,k such that m_j -

$m_k = n$. The intensity of the double-quantum order grows in as τ^2. Thus, in the short τ limit, the higher quantum operators appear at a later excitation time than the lower quantum operators. This behavior is illustrated in experimental results for adamantane in Fig. 3.4. We observe that indeed the coherences "diffuse" outward toward higher n as the excitation time is increased. A physical interpretation for this behavior can be obtained by realizing that MQ coherence is a many-spin correlation phenomenon - at least n spins are interacting concertedly to absorb n photons. The higher the number of quanta, the more spins involved, and hence the longer it takes for correlations to occur. A random walk picture connecting spin diffusion with evolution of multiple spin correlations and MQ coherences is appealing.

In summary, the difficulty in applying normal MQ NMR methods to solids can be attributed to the fast homogeneous dephasing of spins. The incorporation of time reversal enables all transition lines to be phased with respect to each other, thereby enhancing the signal-to-noise ratio. Using time-reversal pulse sequences, we were able to obtain very high quantum absorption spectra of solid adamantane. From a time-dependence study, we observed an increase in spin correlations as the excitation time increased.

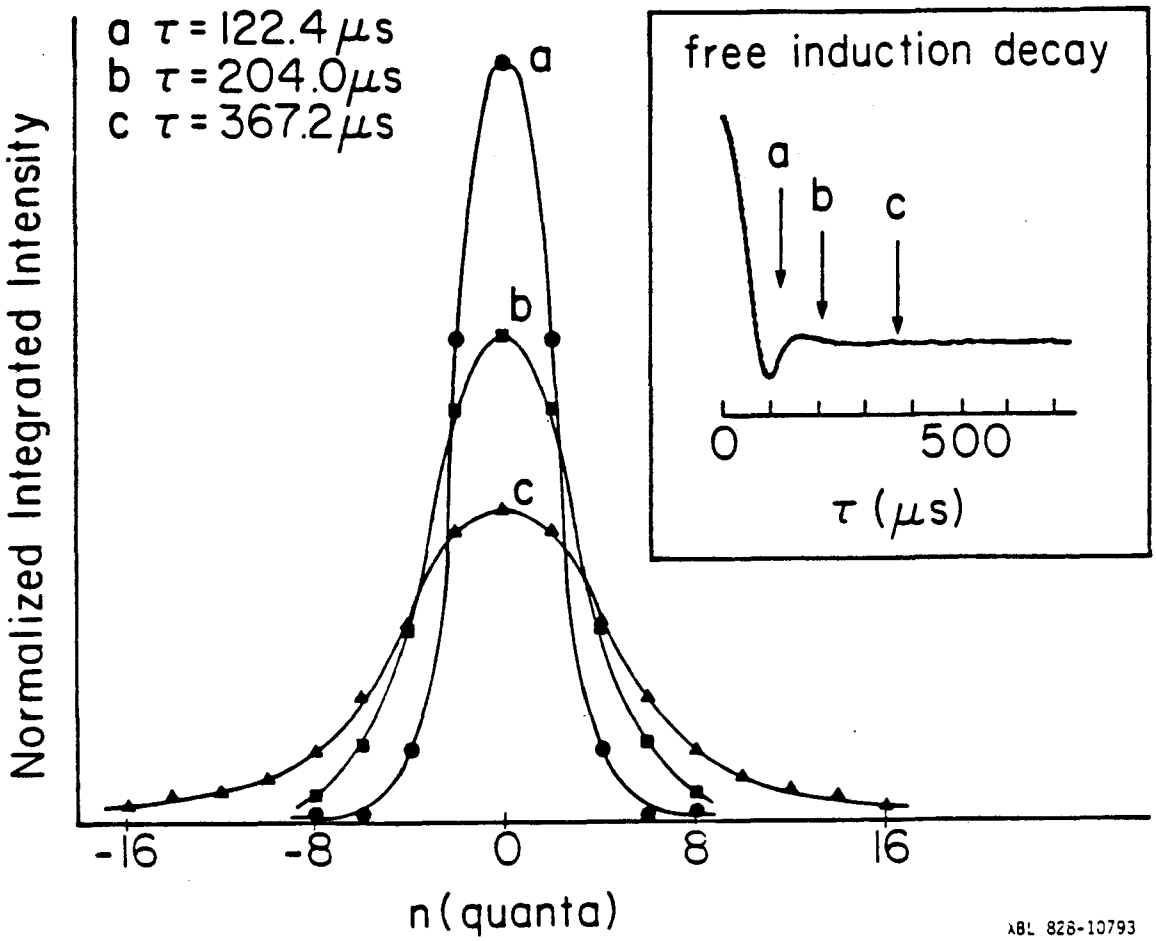

Figure 3.4 Normalized integrated intensity of n-quantum order for various excitation times extracted from adamantane time-reversal spectra, showing how the spin correlations "diffuse" out to higher n. These intensities are normalized so that the total integrated intensity for each excitation time is unity. The corresponding excitation times on the single-quantum free induction decay are indicated in the insert.

CHAPTER 3 REFERENCES

1. W.S. Warren, Ph.D. thesis, University of California, Berkeley, 1980.
2. G. Bodenhausen, Progr. NMR Spectrosc. 14, 137 (1981) and references therein.
3. W.S. Warren, D.P. Weitekamp, and A. Pines, J. Chem. Phys. 73, 2084 (1980).
4. S. Emid, A. Bax, J. Konijnendijk, J. Smidt, and A. Pines, Physica 96B, 333 (1979).
5. S. Emid, J. Smidt, and A. Pines, Chem. Phys. Lett. 73, 496 (1980).
6. W.-K. Rhim, A. Pines, and J.S. Waugh, Phys. Rev. B 3, 684 (1971).
7. W.P. Aue, E. Bartholdi, and R.R. Ernst, J. Chem. Phys. 64, 2229 (1976).
8. a) J.B. Murdoch, W.S. Warren, D.P. Weitekamp, and A. Pines, submitted to J. Magn. Reson.;
   b) D.P. Weitekamp, Adv. Magn. Resonance, submitted for publication.
9. With one exception: when $\tau = \tau'$, transitions between spin inversion states produce lines in phase, as described in detail in reference 8.
10. U. Haeberlen, High Resolution NMR in Solids, Selective Averaging, (Academic, New York, 1976).
11. a) G. Drobny, A. Pines, S. Sinton, D.P. Weitekamp, and D. Wemmer, Faraday Symp. Chem. Soc. 13, 49 (1979);

b) G. Bodenhausen, R.L. Vold, and R.R. Vold, J. Magn. Reson. 37, 93 (1980).

12. A. Abragam, Principles of Nuclear Magnetism, (Oxford, London, 1961).

13. D. Wemmer, Ph.D. thesis, University of California, Berkeley, 1978.

14. Y.S. Yen, J.B. Murdoch, J. Tang, and A. Pines, in preparation.

CHAPTER 4

SECOND MOMENTS OF MULTIPLE-QUANTUM NMR SPECTRA

4.1 INTRODUCTION

Recent years have shown much experimental and theoretical progress on multiple-quantum (MQ) NMR studies of dipolar systems.[1,2,3] Most of these studies depend on the high resolution available in the spin systems for dynamical and structural information. In studies where resolution is poor, particularly in solids, lineshape analysis provides the only practical means of extracting information. Thus, it would be of interest to explore the behavior of MQ lineshapes as a function of the number of rf quanta absorbed or emitted.

For a system containing nuclei of spin I=1/2, the second moments (M_2) of the dipolar structure of MQ spectra can be rigorously calculated by assuming a statistical model. With this assumption, only sums and products of the dipolar coupling constants are needed to determine the second moments. No diagonalization of the Hamiltonian is necessary. Results reveal that the ratio r of the average dipolar coupling constant to the rms value:

$$r = \frac{\bar{d}}{\overline{d^2}^{\,1/2}}$$

determines to a large extent the second moments behavior. The two extreme cases:

(1) r=1, all the couplings are the same,

(2) r=0, couplings of both signs occur in such a way that the average coupling is zero,

show distinctively different behavior.

One may inquire here whether a statistical model contains enough information to describe lineshape behavior as a function of n. A statistical assumption implies no symmetry in the spin system. What are the implications of neglecting symmetry, or conversely, what role does spin symmetry play in M_2 behavior? Also, how large does the system have to be in order for the statistical assumption to hold? These are the questions that we explore in our experiments.

In section 4.2, we will proceed first with a brief description of a Fourier transform MQ experiment and some terminologies. A formulation for the MQ signal and its moments is given, the need for an unique M_2 definition is recognized, and the statistical model for MQ moments is introduced. In section 4.3, a comparison of experiment with theory is made.

4.2 THEORY

In a Fourier transform MQ experiment (Fig. 4.1), MQ coherences are created by applying a series of intense rf pulses to the spin system. The preparation

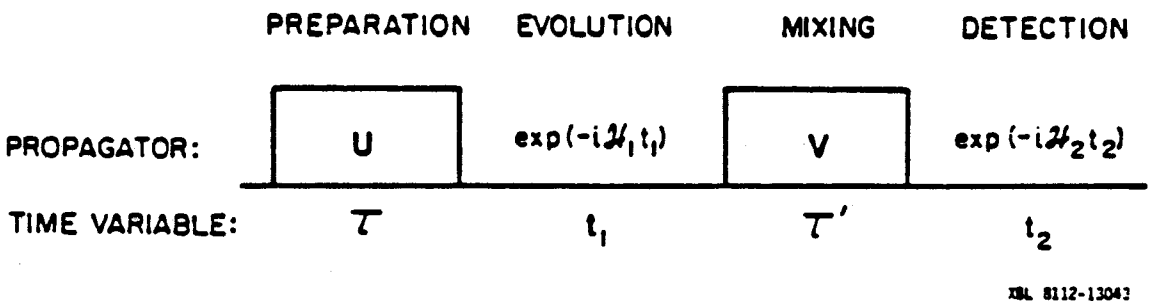

Figure 4.1 Schematic pulse sequence showing the relevant periods in a Fourier transform multiple-quantum NMR experiment.

sequence may be described by a preparation propagator $U(\tau)$. The density operator at the end of the preparation pulse sequence is given by $U^{\dagger}\rho_o U$, where ρ_o is the initial density operator, and contains MQ coherences. The system evolves in t_1 under the effect of the Hamiltonian H_1. To detect MQ coherences, a mixing period described by the operator $V(\tau')$ is required to convert MQ coherences into detectable single-quantum coherence. Typically, one point at $t_2=0$ is sampled for each incrementation in t_1, keeping (τ,τ') fixed. The resultant MQ interferogram in t_1 is given by:[3]

$$S(t_1) = \langle I_+(t_1)\rangle \tag{1}$$
$$= \mathrm{Tr}\{Q(-\tau')\exp(-iH_1t_1)P(\tau)\exp(iH_1t_1)\}$$

where

$$Q(-\tau') = V(\tau')I_-V^{\dagger}(\tau'),$$
$$P(\tau) = U^{\dagger}(\tau)\rho_o U(\tau).$$

Fourier transforming Eq. (1) with respect to t_1 yields the conjugate frequency spectrum in ω_1, the frequency spectrum of interest (as opposed to ω_2, the conjugate of t_2, if the entire free induction decay in t_2 is sampled). Henceforth, the subscript 1 will be dropped.

If the signal $S(t)$ is separable into components of order n, labeled $S_n(t)$, such as by selective excitation or detection schemes,[1,3] the n-quantum moments can be

obtained from the time-domain signal S(t) with the following well-known relation:[4]

$$M_k(n) = \frac{(-i)^k}{S_n(0)} \frac{d^k S_n(t)}{dt^k}\bigg|_{t=0}.$$

By differentiating Eq. (1), the analogous n-quantum k^{th}-moment expression to Van Vleck's single-quantum moments formula[6] is:

$$M_k(n) = \frac{\mathrm{Tr}\{Q_n(-\tau')\overbrace{[\ldots\ldots[H,[H}^{k\ \text{times}},P_n(\tau)]]\ldots\ldots]}{\mathrm{Tr}\{Q_n(-\tau')P_n(\tau)\}}.$$

Specifically, the second moments M_2 expression is:[7]

$$M_2(n) = \frac{\mathrm{Tr}\{[H,\ Q_n(-\tau')][H,\ P_n(\tau)]\}}{\mathrm{Tr}\{Q_n(-\tau')P_n(\tau)\}}.$$

Finding expressions for P_n and Q_n, which depend on the pulse sequence used, and performing the commutations are nontrivial tasks. Instead of evaluating the commutators directly, an alternative is to examine the density of states distributed by the dipolar Hamiltonian and see what information can be inferred.

A schematic energy level diagram of an N spin-1/2 system with random coupling constants is depicted in Fig. 4.2. The spin states are most strongly split by the Zeeman interaction of spin dipoles with the large external static magnetic field. Each Zeeman manifold

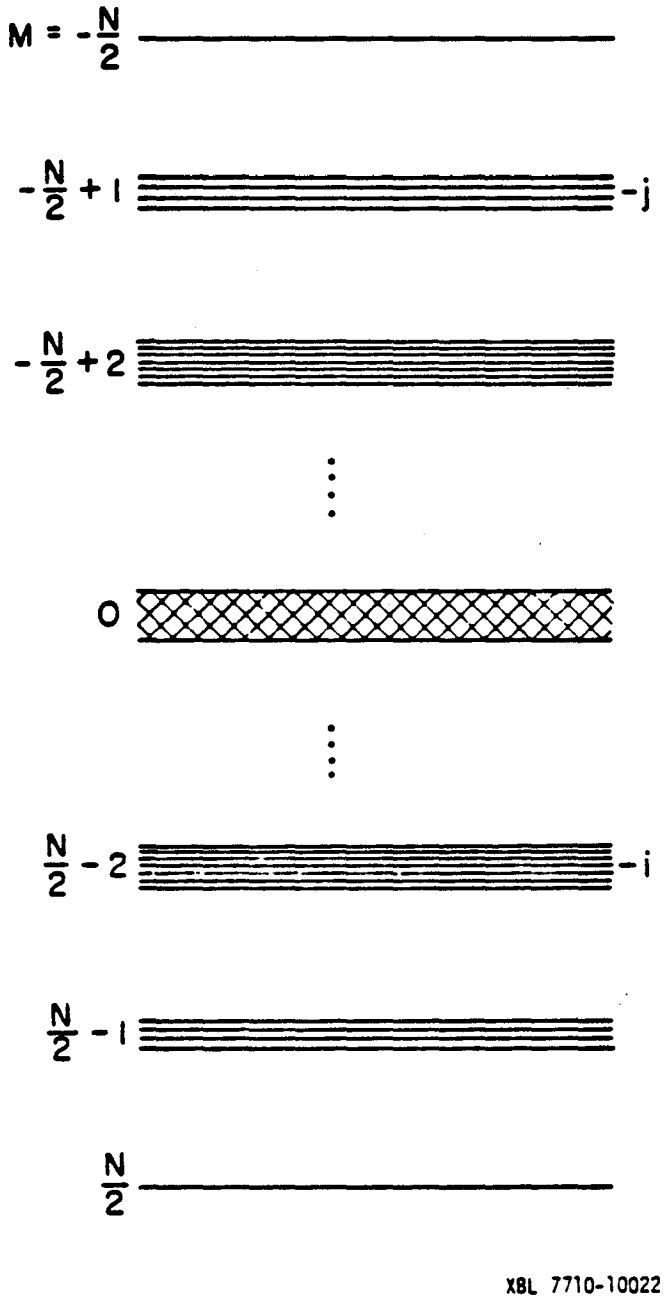

Figure 4.2 Schematic energy level diagram for an arbitrary spin system of N spin-1/2's. The states, split by the Zeeman interaction, are grouped according to their Zeeman quantum numbers. Within each Zeeman manifold, the states are further split by the dipolar Hamiltonian.

of magnetic quantum number m is further split by dipole-dipole interactions among spins to form a distribution of states. An n-quantum order is composed of the sets of transitions between states of m_1 and m_2 that satisfy the condition $n = m_1 - m_2$. There may be more than one pair (m_1, m_2) that satisfies this condition.

Each Zeeman manifold can be labeled by either m, the magnetic quantum number, or p, the number of spins aligned parallel to the static external magnetic field. The relationship between m and p is:

$$p = \frac{N}{2} - m,$$

where N is the total number of spins in the system. We find the label p more convenient for the following discussions.

Let $G_1(\omega)$ and $G_2(\omega)$ be the distribution functions for the density of states of manifolds labeled by p_1 and p_2. The statistical lineshape of the set of transitions between two manifolds is described by the cross-correlation of the two distribution functions:

$$I(\omega, p_1, p_2) = G_1(\omega) * G_2(\omega) \qquad (2)$$

where * denotes a cross-correlation integral (Fig. 4.3). Explicitly, this is:[8]

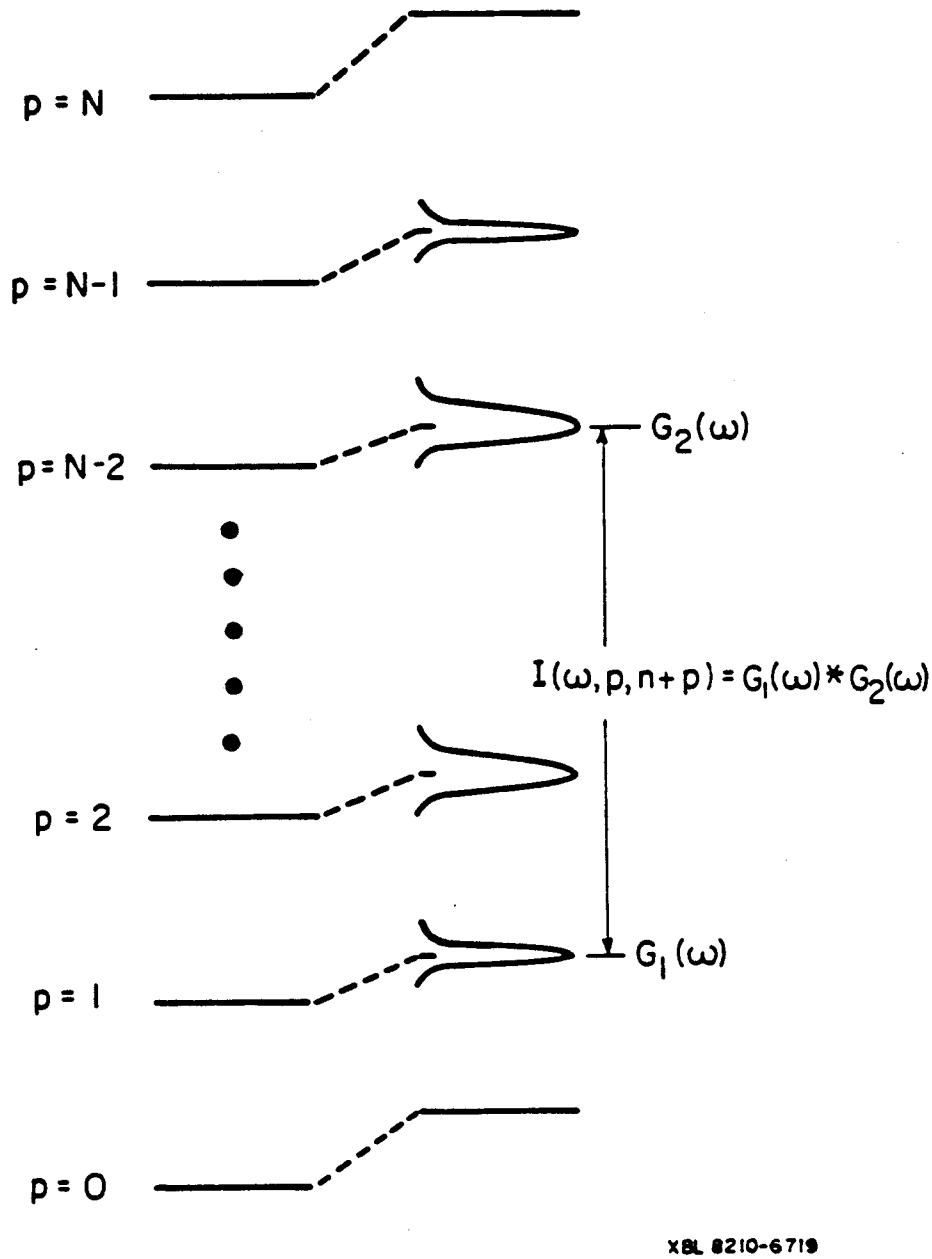

Figure 4.3 Each Zeeman manifold can be described by a characteristic distribution of states with a mean dipolar energy shift and a dipolar width. The statistical lineshape function for a set of transitions between two Zeeman manifolds is a cross-correlation between the two distributions.

$$G_1(\omega)*G_2(\omega) = \int G_1(u)G_2(u-\omega)du. \tag{3}$$

The n-quantum spectrum is the superposition of all cross-correlations between manifolds that satisfy the condition $n=p_2-p_1$:

$$I(\omega,n) = \sum_{p_1=0}^{N-n} I(\omega,p_1,p_2=p_1+n). \tag{4}$$

The kth-moment of the lineshape function $I(\omega,n)$ is:

$$M_k(n) = \frac{\int \omega^k I(\omega,n)d\omega}{\int I(\omega,n)d\omega}. \tag{5}$$

We shall show that the MQ moments can be related to the moments of the distributions $G_i(\omega)$. To do so, we list the following properties of cross-correlation integrals.

Let $G_1(\omega)$ and $G_2(\omega)$ be two distribution functions with normalization constants N_1 and N_2, centroids at Δ_1 and Δ_2, and variances σ_1^2 and σ_2^2, i.e.:

$$\int G_i(\omega)d\omega = N_i,$$

$$\frac{\int \omega G_i(\omega)d\omega}{\int G_i(\omega)d\omega} = \Delta_i,$$

$$\frac{\int (\omega-\Delta_i)^2 G_i(\omega)d\omega}{\int G_i(\omega)d\omega} = \sigma_i^2.$$

Let $h = G_1 * G_2$ be the cross-correlation of G_1 with G_2. The corresponding properties of h are:

$$N \equiv \int h(\omega)d\omega = -N_1 N_2,$$

$$\Delta \equiv \frac{\int \omega h(\omega)d\omega}{\int h(\omega)d\omega} = \Delta_1 - \Delta_2,$$

$$\sigma^2 \equiv \frac{\int (\omega-\Delta)^2 h(\omega)d\omega}{\int h(\omega)d\omega} = \sigma_1{}^2 + \sigma_2{}^2.$$

We distinguish the definition of second moment from variance (which is measured from the centroid):

$$M_2 \equiv \frac{\int \omega^2 h(\omega)d\omega}{\int h(\omega)d\omega} = \sigma^2 + \Delta^2$$

$$= \sigma_1{}^2 + \sigma_2{}^2 + (\Delta_1 - \Delta_2)^2. \qquad (6)$$

Generalizing, it is evident from the binomial formula that the kth-moment as measured from the centroid is:

$$\mu_k[h] \equiv \frac{\int (\omega-\Delta)^k h(\omega)d\omega}{\int h(\omega)d\omega} = \sum_{r=0}^{k} \binom{k}{r} \mu_r[G_1]\,\mu_{k-r}[G_2]$$

where the moments of the distribution functions are similarly defined:

$$\mu_s[G_i] \equiv \frac{\int (\omega-\Delta_i)^s G_i(\omega)d\omega}{\int G_i(\omega)d\omega}.$$

The kth moment in terms of the moments of the distributions G_1 and G_2 is given by:

$$M_k = \frac{\int \omega^k h(\omega) d\omega}{\int h(\omega) d\omega} = \sum_{r=0}^{k} \binom{k}{r} \Delta^{k-r} \mu_r[h]$$

$$= \sum_{r=0}^{k} \binom{k}{r} \Delta^{k-r} \sum_{s=0}^{r} \binom{r}{s} \mu_s[G_1] \mu_{r-s}[G_2]. \qquad (7)$$

The above expressions are valid for any functions describing the distribution of states. The functional form enters only in the quantitative values of the moments.

4.2.1 Exact Dynamics

Consider the schematic MQ pulse sequence of Fig. 4.1. The expression for the signal intensity of such a pulse sequence is given by Eq. (1). Expressed in the eigenstates of the Hamiltonian H, this becomes:

$$S(t) = \sum_{j,k} P_{jk}(\tau) Q_{kj}(-\tau') \exp(-i\omega_{jk} t),$$

where $\omega_{jk} = \omega_j - \omega_k$, and $H|j\rangle = \omega_j |j\rangle$. Upon Fourier transforming with respect to t we obtain the frequency spectrum:

$$S(\omega) = \sum_{j,k} P_{jk}(\tau) Q_{kj}(-\tau') \delta(\omega - \omega_{jk}). \qquad (8)$$

By going off-resonance by the amount $\Delta\omega$ or creating an

artificial offset by time proportional phase incrementation,[5] the MQ spectrum is separable into components of order n:

$$S(\omega) = \sum_{n=0}^{N} S_n(\omega)\delta(\omega - n\Delta\omega),$$

assuming ω on the right hand side of the equation contains no offset component. The second moments of the n-quantum order is then:

$$M_2(n) = \frac{\sum_{j,k} \omega_{jk}^2 (P_n)_{jk}(Q_n)_{kj}\delta(\omega-\omega_{jk})}{\sum_{j,k} (P_n)_{jk}(Q_n)_{kj}\delta(\omega-\omega_{jk})}.$$

Evaluation of the Fourier coefficients $(P_n)_{jk}(Q_n)_{kj}$ in the <u>eigenbasis</u> of the Hamiltonian yields a numerical value for $M_2(n)$.

4.2.2 <u>Unique Second Moments Value</u>

A feature not present in conventional single-quantum spectra is the dependence of phase on preparation as a result of the nature of MQ pulse experiments. The Fourier coefficient $P_{jk}Q_{kj}$ [Eq. (8)] is complex and thus contains a phase term. Moreover, the operators P and Q are functions of τ and τ', and thus so are the transition amplitude and phase. Consequently, there is a M_2 value associated with each (τ, τ') value.

We would like to define an <u>unique</u> M_2 value for

discrete transition lines as well as for a continuum of transition lines. A convenient choice is one in which all lines appear in phase and the transition amplitudes show their time-averaged value.[9]

Averaging $P_{jk}Q_{kj}$ over $\tau = \tau'$ in Eq. (8) and assuming magnitude spectra yield an "ultimate τ average"[9] for each transition amplitude. Upon τ averaging, the inherent transition amplitude is realized; thus ultimate τ average spectra should be used to determine the unique M_2 value.

Experimental τ averages are done by superimposing spectra of many randomly chosen preparation times. The phasing of each spectrum can be accomplished by converting it into a magnitude spectrum if lines are resolvable, or incorporating time reversal in the MQ pulse sequence.[10]

The statistical model to be described in the next section implicitly assumes no phase factors.

4.2.3 Statistical Model

For large spin systems, a complete diagonalization of the Hamiltonian for exact dynamics calculations is prohibitively cumbersome. For this reason, we turn to approximation with a statistical model for a qualitative description.

The statistical model assumes a spin system of no apparent symmetry so that all transitions are allowed

and are assigned equal intensity. The assumption of all transitions being allowed is embodied in the construction of <u>one</u> distribution function describing the density of states for each Zeeman manifold, regardless of their classification according to the irreducible representations of the symmetry group. The equality of transition intensity appears in the resulting lineshape of the set of transitions between two manifolds. By taking the cross-correlation between two density of states functions, each transition is assigned unit intensity; that is, the cross-correlation function counts the number of transitions per frequency bandwidth. Any further intensity specification would require exact dynamics treatment.

Our focus will be on the broadening of resonance lines by the dipolar Hamiltonian. Derivation of MQ second moments involves first evaluating the dipolar mean and variance of each Zeeman manifold. Given these two items, a representative distribution of states is constructed for each Zeeman manifold. For a complete description of the distribution of states, higher moments should be included. However, for the second moments of n-quantum orders, only the second moments of the distribution of states are necessary [cf. Eq. (6)]. The second moment of each MQ order is then found by taking the sum of cross-correlations between appropriate Zeeman manifolds.

4.2.3.1 Dipolar Mean and Variance of a Zeeman manifold

The dipolar mean and variance of a p-manifold is given by the following expectation values:

$$\langle H_D \rangle_p = Tr_p\{\rho H_D\} \tag{9}$$

$$\langle H_D{}^2 \rangle_p - \langle H_D \rangle_p^2 = Tr_p\{\rho H_D{}^2\} - Tr_p{}^2\{\rho H_D\} \tag{10}$$

The bracket $\langle\ \rangle_p$ denotes the ensemble average over the p-manifold, $Tr_p\{\ \}$ is the trace over the states in the p-manifold, ρ here is the weighting function of these states, and H_D is the secular part of the dipole-dipole Hamiltonian expressed in units of h:[4]

$$H_D = \sum_{i<j} d_{ij}\{I_{zi}I_{zj} - \tfrac{1}{4}(I_{+i}I_{+j} + I_{-i}I_{-j})\}. \tag{11}$$

The d_{ij}'s (rad/sec) are the dipolar coupling constants between spin i and spin j:

$$d_{ij} = \frac{\gamma^2 h}{r_{ij}{}^3}(1-3\cos\ \theta_{ij}^2).$$

The spin operators I_{zi}, I_{+i}, and I_{-i} are the zth component, the raising operator, and the lowering operator of spin i.

Giving equal weight to each state, as is proper, ρ must be the reciprocal of the number of states. The number of states in the p-manifold is given by $\binom{N}{p}$, the

combinatorial of N with p. With this, Eqs. (9) and (10) become:

$$\langle H_D \rangle_p = \binom{N}{p}^{-1} \mathrm{Tr}\{H_D\}, \tag{12}$$

$$\langle H_D{}^2 \rangle_p - \langle H_D \rangle_p^2 = \binom{N}{p}^{-1} \mathrm{Tr}_p\{H_D{}^2\} - \binom{N}{p}^{-2} \mathrm{Tr}_p^2\{H_D\}. \tag{13}$$

The evaluation of $\mathrm{Tr}_p\{H_D\}$ and $\mathrm{Tr}_p\{H_D{}^2\}$ involves combinatorial arguments. In evaluating these traces, it is convenient to define a quantity f(p) to be the probability that a spin pair will be antiparallel for a given state in the p-manifold. The number of antiparallel spin pairs out of N spins is p(N - p). Thus, f(p) is just this number divided by the number of pairs:

$$f(p) = \frac{p(N - p)}{\binom{N}{2}}. \tag{14}$$

From the form of Eq. (14), f(p) is also the probability that a state in the p-manifold will have a given spin pair (i,j) antiparallel with respect to each other. The explicit evaluations of $\mathrm{Tr}_p\{H_D\}$ and $\mathrm{Tr}_p\{H_D{}^2\}$ are left to appendices 4.A and 4.B. The results are quoted here:

$$\mathrm{Tr}_p\{H_D\} = \binom{N}{p}(1-2f) \sum_{i<j} \frac{1}{4} d_{ij}, \tag{15}$$

$$\mathrm{Tr}_p\{H_D{}^2\} = \binom{N}{p}\{(1+f)a + (1-2f)b + (1-4fg)c\}, \tag{16}$$

where

$$a = \frac{1}{16} \sum_{i<j} d_{ij}^2,$$

$$b = \frac{1}{16} \sum_{i<j} \sum_{k \neq i,j} d_{ij}(d_{ik} + d_{kj}),$$

$$c = \frac{1}{16} \sum_{i<j} \sum_{i'<j'} d_{ij} d_{i'j'}, \qquad (i \neq i', j \neq j')$$

$$g = \frac{(N-p-1)(N-p-2) + (p-1)(p-2)}{(N-2)(N-3)},$$

and f is defined in Eq. (14). We mention here that the number of terms in the summations a, b and c are $\binom{N}{2}$, $2(N-2)\binom{N}{2}$ and $\binom{N-2}{2}\binom{N}{2}$, respectively, and that the total number of terms in a, b and c is $\binom{N}{2}^2$.

Combining Eqs. (12) and (13) with (15) and (16) yields for the p-manifold:

$$h(p) = (1-2f) \sum_{i<j} \frac{1}{4} d_{ij} \tag{17}$$

$$\sigma^2(p) = f(5-4f)a + 2f(1-2f)b + 4f(1-f-g)c. \tag{18}$$

For brevity of notation, we have defined

$$h(p) = \langle H_D \rangle_p$$
$$\sigma^2(p) = \langle H_D{}^2 \rangle_p - \langle H_D \rangle_p{}^2.$$

Written in this form, it is apparent that the dipolar shift h(p) [Eq. (17)] is directly proportional to the

average dipolar coupling.

For the special case of r=1, i.e. all couplings are the same, these quantities reduce to:

$$h(p) = (\tfrac{d}{4})[\binom{N}{2} - 2p(N - p)],$$
$$\sigma^2(p) = (\tfrac{d}{4})^2 p(N - p).$$

where d is the unique coupling constant. That is, in this limit, the width of a Zeeman manifold is proportional to the square root of the number of antiparallel spins.

The features of the dipolar structure of the energy level diagram can be examined. By differentiating $\sigma^2(p)$ with respect to p, the extrema of $\sigma^2(p)$ can be found. Equation (18) can be factored as fF(p), where F(p) is quadratic in p. One extremum is found from df/dp = 0, which yields a root at p = N/2 (or the m=0 manifold for N even). The other two roots can be obtained from solving dF/dp = 0. These roots, which can be either real or complex, occur in pairs since F(p) is symmetric about p = N/2.

The behavior of h(p) and σ(p) versus p for ten randomly-generated sets of couplings between 30 spins of I=1/2 is illustrated in Fig. 4.4(a) for r=1 and in Fig. 4.4(b) for r=0. These plots were generated with the computer programs listed in appendix 4.C. They show that the extreme states are shifted by the largest

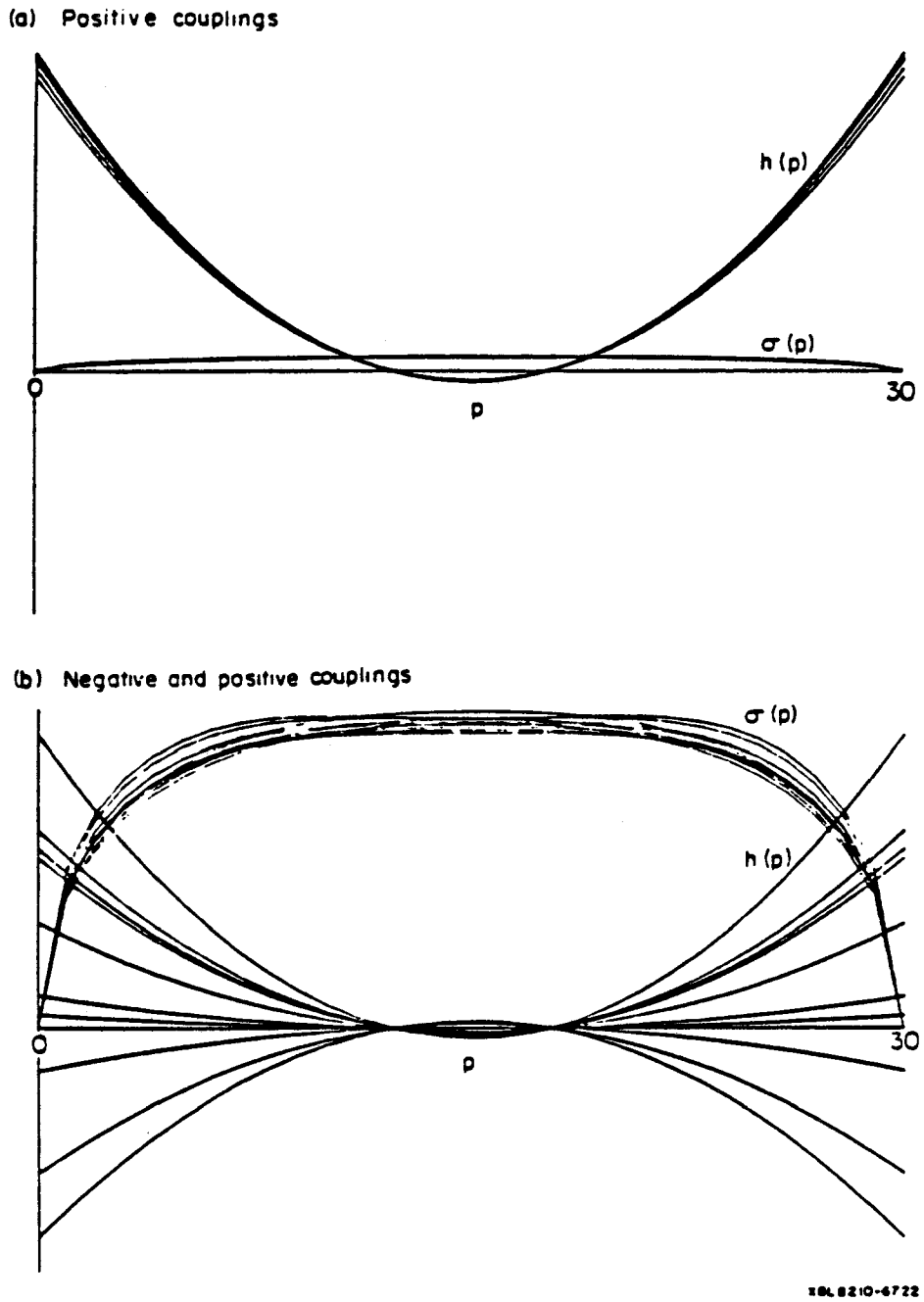

Figure 4.4 The dependence on p of the mean dipolar shift h(p) and the standard deviation σ(p) for ten randomly generated 30-spin systems in the limit of (a) r=1, with couplings in the range 0.0 - 1.0 kHz; (b) r=0, with couplings in the range -1.0 - 1.0 kHz. In (a), the top of the scale is 5.7 kHz, and in (b) is 3.8 kHz.

amount, and the p=N/2 manifold is shifted slightly in the opposite direction. They also show that the width of the distributions is the largest at p=N/2.

One observes that the two cases have distinctly different features. For r=1, the width of the distribution is much smaller than the dipolar shift. For r=0, ideally there is no dipolar shift. Also, given the same upper limit on the magnitude of the couplings, the width is generally larger for r=1 than for r=0. These features dictate the behavior of MQ second moments.

4.2.3.2 Multiple-Quantum Second Moments

For each Zeeman manifold, a distribution function is constructed from h(p) and $\sigma^2(p)$:

$$G_i(\omega) = \binom{N}{p_i} g_i(\omega). \tag{19}$$

The normalized function $g_i(\omega)$ is defined to have the following properties:

$$\int G_i(\omega)d\omega = \binom{N}{p_i}\int g(\omega)d\omega = \binom{N}{p_i}$$
$$\int \omega g_i(\omega)d\omega = \Delta_i,$$
$$\int(\omega-\Delta_i)^2 g_i(\omega)d\omega = \sigma^2(p_i).$$

Evaluating the cross-correlation integral of Eq. (2) using Eq. (19), and summing over the manifolds

yields the final expression of the n-quantum second moments:

$$M_2(n) = Z^{-1} \sum_{p_1=0}^{N-n} \binom{N}{p_1}\binom{N}{p_2}\{\sigma^2(p_1) + \sigma^2(p_2) + [h(p_1)-h(p_2)]^2\} \tag{20}$$

where h(p) and $\sigma^2(p)$ are given in Eqs. (17) and (18). Since each transition is given unit intensity, the normalization constant Z is just the total number of n-quantum transitions:[11]

$$Z = \int I(\omega,n)d\omega = \sum_{p_1=0}^{N-n} \binom{N}{p_1}\binom{N}{p_2}$$

$$= \begin{cases} \binom{2N}{N-n}, & 1 < n < N \\ \frac{1}{2}[\binom{2N}{N} - 2^N], & n=0 \end{cases} \tag{21}$$

Higher moments are readily generalized using Eq.(7) and evaluating $Tr_p\{H_D{}^r\}$, for r=0,1,2,...k.

Shown in Fig. 4.5 are the M_2 values for the same set of ten random spin systems as in Fig. 4.4. Figure 4.6 shows the decomposition into the two contributing terms. As is evident, the M_2 behavior depends almost exclusively on one term or the other. For r=1 [Fig. 4.6(a)], the dominant contribution is from the mean displacements $\Delta^2 = [h(p_1)-h(p_2)]^2$. For r=0 [Fig. 4.6(b)], it is the widths of the lineshape functions $\sigma^2 = \sigma^2(p_1) + \sigma^2(p_2)$ that is dominant. From the dipolar

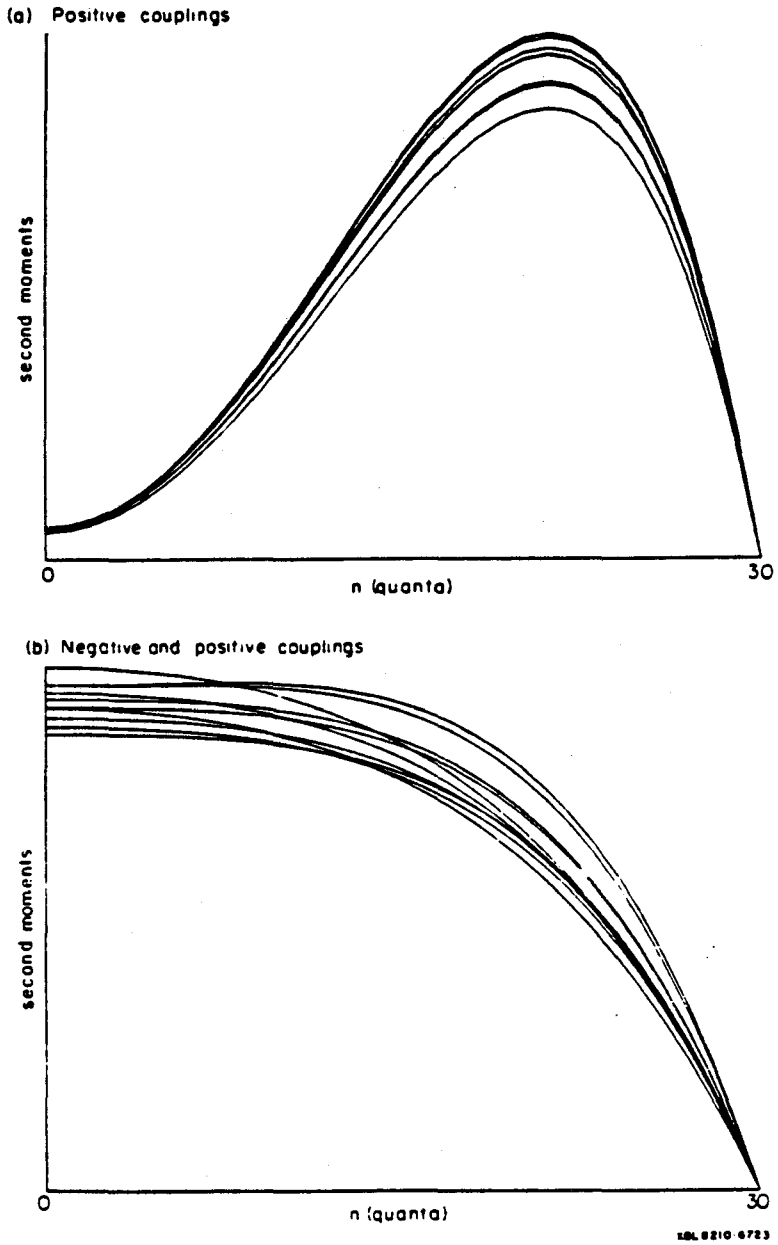

Figure 4.5 Second moments versus the number of quanta n for the same ten systems in the limit (a) $r \approx 1$, and (b) $r \approx 0$. The top of the scale is 240 kHz^2 in (a) and 29 kHz^2 in (b).

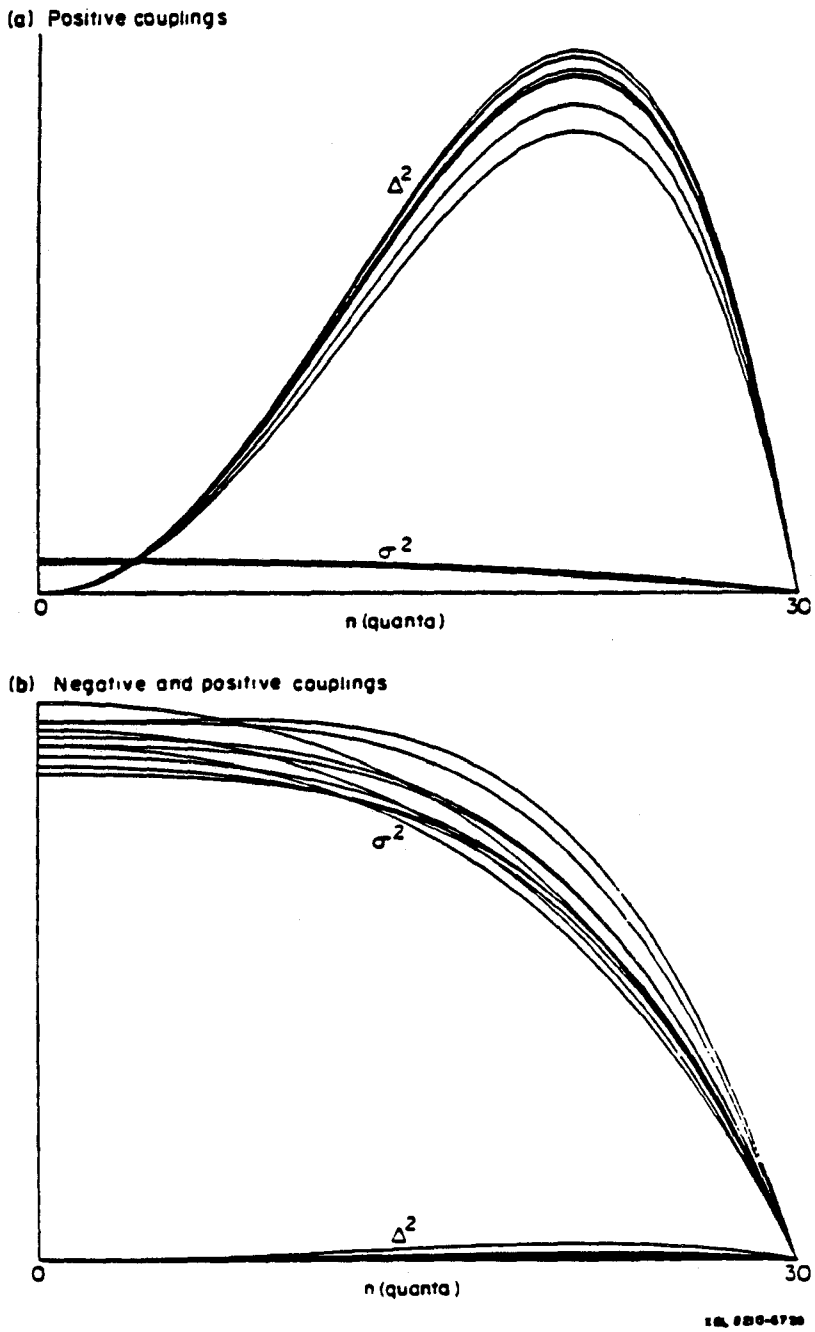

Figure 4.6 Contributions to the second moments. The quantity Δ^2 is the square of the mean shift difference ($[h(p_1) - h(p_2)]^2$) contribution, and σ^2 is the width ($\sigma^2(p_1) + \sigma^2(p_2)$) contribution. Note how different contributions dominate in the two cases.

structure of the energy level diagram, as constructed from Figs. 4.4(a) and 4.4(b), these behaviors are obvious.

For r=1, the mean displacement of an m-manifold is much greater than its width and thus is the dominant contributor. From this and the fact that the higher quantum orders probe only the more extreme states (which differ little in mean dipolar shift), we expect the M_2 of high quantum orders to be small. For the lower quantum orders, the sampling is between adjacent manifolds (which again do not differ much in mean dipolar shift). Thus, we expect the M_2 of low quantum orders to also be small. For the orders that connect $p \approx N/2$ to $p \approx 0$ manifolds, the difference in mean dipolar shift is at its largest, and we expect these orders ($n \approx N/2$) to have the largest M_2.

For r=0, the opposite is true. Since the dipolar shift is ideally zero for all manifolds, only the variances can contribute. The variances are roughly the same except for the more extreme states. This suggests that M_2 should remain roughly constant for the lower quantum orders and then drop to zero at n=N.

Figure 4.5(a) shows that for $r \approx 1$ the maximum M_2 occurs off center toward higher n. This is due to a third competing factor: the normalization constant. Since the number of transitions decreases with n, the maximum M_2 is driven toward higher n.

To summarize, the three competing factors in determining the features of M_2 are:

(1) the difference in mean displacements between transition manifolds.

(2) the distribution widths of transition manifolds.

(3) the normalization constant.

The first term never contributes to the zero-quantum order and drives maximum M_2 toward $n=N/2$. The second term, which is directly proportional to $\bar{d}^2$, drives maximum M_2 towards $n=0$. The smaller the average coupling $\bar{d}$ is, the smaller M_2 is. Finally, the third term favors higher n.

The plots in Figs. 4.5 and 4.6 were generated with the same programs listed in appendix 4.C.

4.3 COMPARISON OF EXPERIMENT WITH COMPUTER SIMULATIONS AND STATISTICAL MODEL

We show examples of systems exhibiting both behaviors predicted by the statistical model. Experimental results can be compared against exact dynamics calculations of ultimate τ averaged spectra[12] and the statistical model using the experimental coupling constants.

The $r=0$ behavior is exhibited by n-hexane-d_6, with the methyl positions deuterated, oriented in a nematic liquid crystal. It is an 8-spin system: only

intramolecular couplings are nonzero since rapid translational diffusion of solutes in a liquid crystal averages to zero intermolecular couplings. The ratio of the average ^1H dipolar coupling to the rms value is measured to be r=0.12. Shown in Fig. 4.7 are the M_2 values of a τ-averaged MQ magnitude spectrum of this system.(13) The τ values range from 9.0 - 11.5 msec, in increments of 0.5 msec. A nonselective three-pulse sec ce was used. The largest second moments occur near n=0, in agreement with the statistical model.

The other extreme is illustrated in the experimental second moments versus n of polycrystalline adamantane, shown in Fig. 4.8. The τ values range from 244.8 - 448.8 μsec, in increments of 40.8 μsec. The transition lines are overlapping, and thus a time-reversal (even-selective) pulse sequence was used to obtain these spectra.(10) Since the sample is a powder, it is hard to assign a single r value to the spin system. Furthermore, there are an Avogadro's number of coupled spins so the system size is essentially infinite. These experiments show that M_2 increases with n up to 16-quantum, indicating that r>0 and the number of spins involved is indeed very large.

4.4 CONCLUSION

Van Vleck's moments formula for single-quantum spectra can be easily extended for MQ spectra. In the

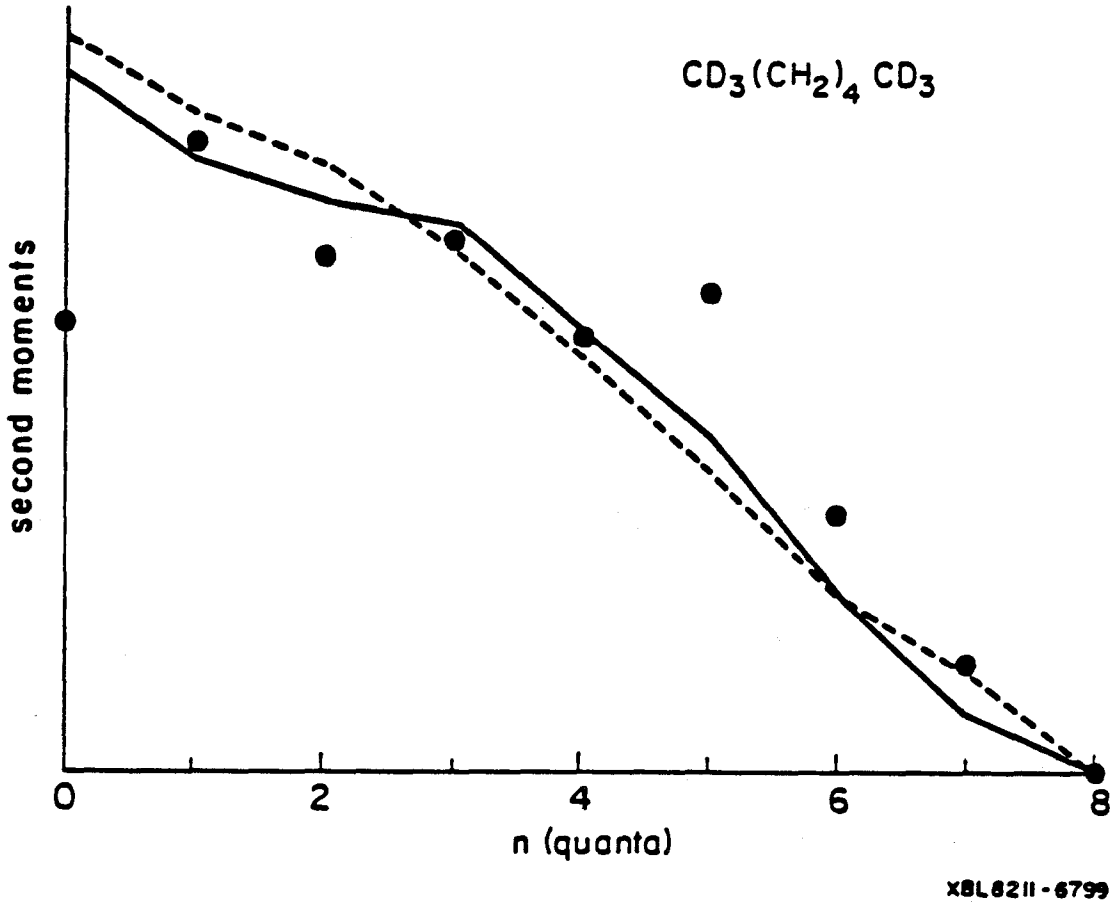

Figure 4.7 Results of n-hexane-d_6 oriented in a nematic liquid crystal: experimental values (solid dots), exact dynamics calculated ultimate τ average M_2 values (solid line), and statistical M_2 values versus n (dashed line). The experimental MQ spectrum used is the average of six magnitude spectra with τ values ranging from 9.0 - 11.5 msec.

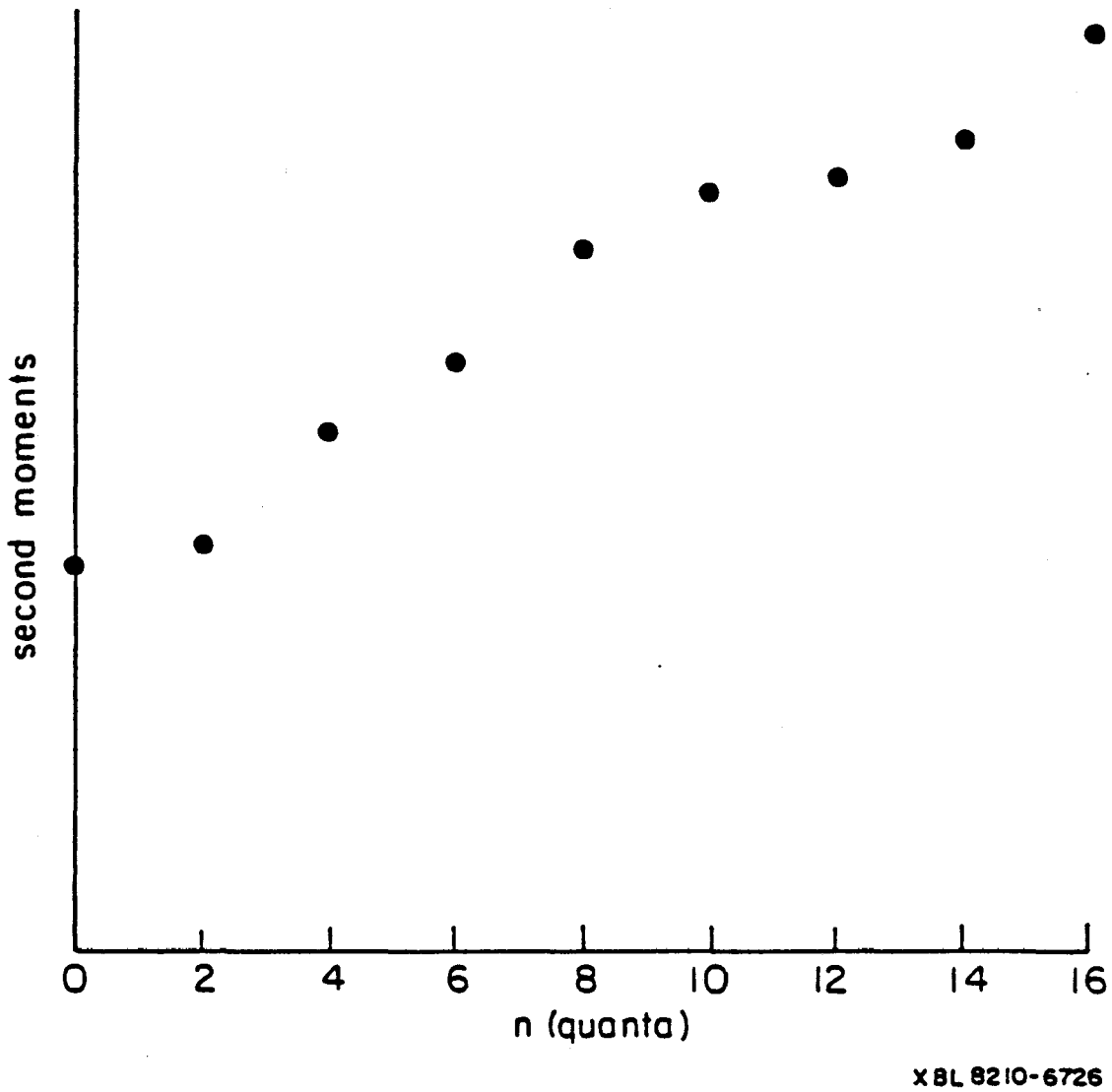

Figure 4.8 The MQ M_2 values of solid adamantane powder. The spectrum used is the average of 5 spectra with preparation times ranging from 244.8 - 448.8 μsec.

process of generalization, we find the dependence of M_2 on the number of quanta. One useful consequence of this is that one can choose to observe the broader orders that are more sensitive to molecular dynamics than the conventional single-quantum order.

Using a statistical assumption, the second moments of MQ orders are rigorously evaluated. The statistical model reveals that two distinct behaviors can occur in M_2 values as a function of n. Both behaviors have been shown to exist experimentally. The experimental results are in accord with statistical model predictions and with exact dynamics calculations. The agreement of the n-hexane-d_6 MQ spectra with the statistical model demonstrates that even for a small 8-spin system with symmetry (C_{2h}), the statistical model predicts the correct general M_2 behavior. This indicates that the manifolds of states grouped according to the irreducible representations must have distributions similar to those of a random spin system. In combination, the two systems demonstrate that a statistical second moments treatment is appropriate for small spin systems as well as for large spin systems.

APPENDIX 4.A

Evaluation of $Tr_p\{H_D\}$ for the p-manifold

Since the trace is independent of the choice of representation, the simple product basis set will be used. Henceforth all states will be referred to in this basis set. Only the operator $I_{zi}I_{zj}$ of H_D is diagonal and contributes to the trace. Thus,

$$Tr_p\{H_D\} = \sum_{k=1}^{\binom{N}{p}} \langle k|H_D|k\rangle$$

$$= \sum_{k=1}^{\binom{N}{p}} \sum_{i<j}^{N} d_{ij}\langle k|I_{zi}I_{zj}|k\rangle. \qquad (A.1)$$

Exchanging the order of the two summations, which are done independently, we sum over the states first. Using the relation:

$$\langle k|I_{zi}I_{zj}|k\rangle = \begin{cases} \frac{1}{4}, & (i,j) \text{ are parallel in } |k\rangle \\ -\frac{1}{4}, & (i,j) \text{ are antiparallel in } |k\rangle \end{cases} \qquad (A.2)$$

the summation over the states k produces:

$$\sum_k \langle k|I_{zi}I_{zj}|k\rangle = \frac{1}{4}[S(N,p) - O(N,p)], \qquad (A.3)$$

where S(N,p) is defined as the number of states in the p-manifold that has spin pair (i,j) parallel, and O(N,p) is the number of states that has (i,j)

antiparallel. These two quantities are determined by combinatorial arguments and are given by:

$$S(N,p) = \binom{N-2}{p} + \binom{N-2}{p-2}, \tag{A.4}$$

$$O(N,p) = \binom{N}{p} \frac{p(N-p)}{\binom{N}{2}}. \tag{A.5}$$

Conservation of states requires:

$$S(N,p) + O(N,p) = \binom{N}{p}.$$

Substituting Eqs. (A.3) - (A.5) in Eq. (A.1) yields

$$Tr_p\{H_D\} = \binom{N}{p}[\binom{N}{2} - 2p(N - p)]\tfrac{1}{4}\bar{d} \tag{A.6}$$

where $\bar{d} = \binom{N}{2}^{-1} \sum_{i<j}^{N} d_{ij}$ is the average dipolar coupling.

APPENDIX 4.B

Evaluation of $Tr_p\{H_D^2\}$ for the p-manifold

As in appendix A, we use the simple product basis set in evaluating $Tr_p\{H_D^2\}$. Written in the form of summation over states, $Tr_p\{H_D^2\}$ can be separated into diagonal and off-diagonal elements of H_D:

$$Tr\{H_D^2\} = \sum_k \langle k|H_D|k\rangle\langle k|H_D|k\rangle + \sum_{k,l}{}' \langle k|H_D|l\rangle\langle l|H_D|k\rangle, \quad (B.1)$$

where the prime on the second summation indicates that the l=k term is excluded. The first term is the sum of squares of the diagonal elements of H_D, and the second term is the corresponding sum for off-diagonal elements. From the form of H_D, we recognize that the operator $I_{zi}I_{zj}$ is purely diagonal and the flip-flop operator $(I_{+i}I_{-j} + I_{-i}I_{+j})$ is purely off-diagonal. This implies that only $I_{zi}I_{zj}$ contributes to the first summation, and only $(I_{+i}I_{-j} + I_{-i}I_{+j})$ contributes to the second summation in Eq. (B.1):

$$Tr_p\{H_D^2\} = \sum_k^{\binom{N}{p}} \sum_{i<j}^{N} \sum_{i'<j'}^{N} d_{ij}d_{i'j'}\langle k|I_{zi}I_{zj}|k\rangle\langle k|I_{zi'}I_{zj'}|k\rangle$$

$$+ \sum_{k,l}{}' \sum_{i<j} \sum_{i'<j'} \frac{1}{16}d_{ij}d_{i'j'}\langle k|I_{+i}I_{-j}+I_{-i}I_{+j}|l\rangle$$

$$\times\langle l|I_{+i'}I_{-j'}+I_{-i'}I_{+j'}|k\rangle. \quad (B.2)$$

1. Consider for now the first summation of Eq. (B.2). This term is more easily evaluated by exchanging the order of summations over states and spins, i.e.

$$\sum_{k}^{\binom{N}{p}} \langle k|H_D|k\rangle\langle k|H_D|k\rangle = \sum_{i<j}^{N} \sum_{i'<j'}^{N} \frac{1}{16} d_{ij} d_{i'j'} Q(N,p)$$

where

$$Q(N,p) = 16 \sum_{k}^{\binom{N}{p}} \langle k|I_{zi}I_{zj}|k\rangle\langle k|I_{zi'}I_{zj'}|k\rangle. \qquad (B.3)$$

The sum Q(N,p) has both positive and negative contributions. The summand in Q(N,p) is positive when $\langle k|I_{zi}I_{zj}|k\rangle$ and $\langle k|I_{zi'}I_{zj'}|k\rangle$ are both either positive (+1/4) or negative (-1/4) [see Eq. (A.2)] and is negative when $\langle k|I_{zi}I_{zj}|k\rangle$ and $\langle k|I_{zi'}I_{zj'}|k\rangle$ are opposite in sign. Performing the summation over states k of Eq. (B.3) yields:

$$Q(N,p) = A - B. \qquad (B.4)$$

Here A is defined to be the number of states within the p-manifold that, given two spin pairs (i,j) and (i´,j´), have both pairs parallel in spin <u>or</u> both pairs antiparallel in spin. B is defined to be the number of states within the p-manifold that have one spin pair parallel in spin <u>and</u> the other antiparallel in spin.

Conservation of states requires:

$$A + B = \binom{N}{p},$$

implying that Eq. (B.4) becomes:

$$Q(N,p) = \binom{N}{p} - 2B. \qquad (B.5)$$

Thus it is only necessary to evaluate B. Three cases can be distinguished:

(a) $(i,j) = (i',j')$,

(b) (i,j) and (i',j') share one common spin,

(c) (i,j) and (i',j') share no common spin.

We will treat each case separately.

<u>Case (a)</u>: $B = 0$, by definition.

<u>Case (b)</u>: Suppose i,j,k are the spins of interest, where $k = i'$ or j'. We divide the N spin system into two parts:

(1) a 3-spin system consisting of spins i,j,k, and

(2) a (N-3)-spin system consisting of the rest of the spins.

Division of the system facilitates the counting argument. We designate the number of spins that are parallel to the magnetic field in the first spin subsystem by p_r, and likewise the same for p_s in the second spin subsystem. Note that conservation of spins requires $p_r + p_s = p$. We also let B_r and B_s have

analogous meanings in the subsystems as B does in the total system [Eq. (B.4)].

For the 3-spin system,

$$B_r = \begin{cases} 0, & p_r=0,3 \\ 2, & p_r=1,2 \end{cases} . \tag{B.6}$$

To treat the (N-3)-spin system, we utilize the facts that $p_s = p - p_r$ and that it is the product of B_r and B_s that is important, i.e.:

$$B = \sum_{p_r} B_r B_s .$$

For $p_r=0,3$, $B_r=0$ and the contribution to B is zero regardless of B_s. We thus will not evaluate B_s for $p_s=p,p-3$. For $p_s=p-1,p-2$, the contribution is nonzero, and

$$B_s = \begin{cases} \binom{N-3}{p-1}, & p_s=p-1 \\ \binom{N-3}{p-2}, & p_s=p-2 \end{cases} .$$

Therefore,

$$B = 2\binom{N-3}{p-1} + 2\binom{N-3}{p-2}$$

$$= f\binom{N}{p}.$$

<u>Case (c)</u>: Evaluation of B here involves the same concept as in case (b). Since (i,j) and (i´,j´) are four distinct spins, we divide the N spin system into a

4-spin system and a (N-4) spin system. The results are:

$$B_r = \begin{cases} 0, & p_r=0,2,4 \\ \binom{4}{1} = \binom{4}{3}, & p_r=1,3 \end{cases},$$

$$B_s = \begin{cases} \binom{N-4}{p-1}, & p_s=p-1 \\ \binom{N-4}{p-3}, & p_s=p-3 \end{cases}.$$

Therefore,

$$B = \binom{4}{1}\binom{N-4}{p-1} + \binom{4}{3}\binom{N-4}{p-3}$$

$$= 2fg\binom{N}{p},$$

where

$$g = \frac{(N-p-1)(N-p-2) + (p-1)(p-2)}{(N-2)(N-3)}. \qquad (B.7)$$

In tabulated form, we have for expressions of B:

	B
case (a)	0
case (b)	$f\binom{N}{p}$
case (c)	$2fg\binom{N}{p}$

The sum Q(N,p) for each of these cases can be found with Eq. (B.5).

The final form of the first summation term is:

$$\sum_{k}^{\binom{N}{p}} \langle k|H_D|k\rangle\langle k|H_D|k\rangle = \binom{N}{p}[a + (1-2f)b + (1-4fg)c], \qquad (B.8)$$

where

$$a = \frac{1}{16} \sum_{i<j}^{N} d_{ij}^2,$$

$$b = \frac{1}{16} \sum_{i<j}^{N} \sum_{k\neq i,j}^{N} d_{ij}(d_{ik} + d_{kj}),$$

$$c = \frac{1}{16} \sum_{i<j}^{N} \sum_{i'<j'}^{N} d_{ij} d_{i'j'}, \qquad (i\neq i',\ j\neq j')$$

are merely constants, and f and g are defined in Eqs. (14) and (B.7).

2. To evaluate the second summation in Eq. (B.2), we realize that for a given pair of states $|k\rangle$ and $|l\rangle$, at most one of the terms $I_{+i}I_{-j}$ and $I_{-i}I_{+j}$ will give a nonzero matrix element. Also, if one spin pair flip-flop term takes $|l\rangle$ into $|k\rangle$, then a different spin pair flip-flop term cannot take the same state $|l\rangle$ into $|k\rangle$. That is,

$$\langle k|I_{+i}I_{-j}+I_{-i}I_{+j}|l\rangle\langle l|I_{+i'}I_{-j'}+I_{-i'}I_{+j'}|k\rangle = \delta_{ij,i'j'}. \tag{B.9}$$

Furthermore, for a given state $|k\rangle$, Eq. (B.9) is satisfied for only one state $|l\rangle$. Thus summation over l of $|\langle k|I_{+i}I_{-j} + I_{-i}I_{+j}|l\rangle|^2$ gives:

$$\sum_{l}{}'|\langle k|I_{+i}I_{-j}+I_{-i}I_{+j}|l\rangle|^2 = \begin{cases} 0, & (i,j) \text{ are parallel in } |k\rangle \\ 1, & (i,j) \text{ are antiparallel in } |k\rangle \end{cases}. \tag{B.10}$$

Performing the summation over k of Eq. (B.10) produces:

$$\sum_{k} \sum_{l}{}'|\langle k|I_{+i}I_{-j}+I_{-i}I_{+j}|l\rangle|^2 = O(N,p), \tag{B.11}$$

where O(N,p) is defined in appendix A, Eq. (A.5).

Making use of Eqs. (B.9) and (B.11) and the freedom of exchanging the order of summations, the second summation term is:

$$\sum_k \sum_l{}' \langle k|H_D|l\rangle\langle l|H_D|k\rangle = \sum_{i<j}^{N} \frac{1}{16} d_{ij}^2 \sum_{k,l}^{\binom{N}{p}}{}' |\langle k|I_{+i}I_{-j}+I_{-i}I_{+j}|l\rangle|^2$$

$$= \sum_{i<j}^{N} \frac{1}{16} d_{ij}^2 \; O(N,p)$$

$$= \binom{N}{p} fa. \qquad \text{(B.12)}$$

Combining the two summations [Eqs. (B.8) and (B.12)], we have as our final expression:

$$\mathrm{Tr}_p\{H_D{}^2\} = \binom{N}{p}\{(1+f)a + (1-2f)b + (1-4fg)c\}, \qquad \text{(B.13)}$$

where a, b, c, f and g are as defined in Eq. (B.8).

APPENDIX 4.C

Computer listings of programs MOMENTS, PLOT1, and PLOT2

These programs were written for use on the VAX/VMS computer system.

MOMENTS calculates the statistical dipolar second moments of each multiple-quantum order. It requires as inputs the number of spins and the dipolar coupling constants. An option is provided for generating random couplings, given a range of couplings and the number of spins. The program also has the capability of running consecutively up to seven different systems having the same number of spins.

The second moments for the multiple-quantum orders are gathered in the datafile PLOT1.DA. If the mean dipolar shifts and standard deviations for the Zeeman manifolds are also desired as outputs, the datafile PLOT2.DA is created.

Running PLOT1 and PLOT2 will allow the plotting of the data arrays PLOT1.DA and PLOT2.DA, respectively, on the Tektronix 4014 and 4662 plotters.

The plotting routines were supplied by Jim Murdoch.

```
      program moments
c
c     This program calculates the multiple-quantum
c     second moments for a spin system containing up
c     to 20 spin-1/2's.  The calculation is based on
c     a statistical model, which disregards symmetry.
c
      dimension d(4950),var(101),sqvar(101),h(101)
      integer p,p2
      real mom(101),mom1(101),mom2(101),norm
c
      f(p)=p*(n-p)*2.0/float(n*(n-1))
      rand(j)=2.2*ran(j) - 1.0
c
      open(unit=21,name='plot1.da',type='new')
      open(unit=22,name='plot2.da',type='new')
c
12    type 501
501   format(//,' enter the number of spins: ',$)
      accept *,n
      n2=n+n
      n1=n+1
c
      type 513,n
513   format(/,' how many ',i3,' spin systems should be tried? ',$)
      accept *,nsets
c
      type 503
503   format(/,' should the width and the mean contribution be plotted'/
     1  ' in addition to the second moment ? (0=no,1=yes) ',$)
      accept *,isep
      mm=n1
      nn=2*n1
      if(isep .eq. 1) mm=3*n1
      write(1,701) nsets,mm
      write(2,701) nsets,nn
c
      do 496 iset=1,nsets
      if(nsets .gt. 1) type 514,n,iset
514   format(//,i4,' SPIN SYSTEM #',i3,' .....',/)
c
      type 502
502   format(/,' do you want random couplings? (0=no,1=yes) ',$)
      accept *,icnoice
      if(icnoice .eq. 1) go to 30
c
      type 503
503   format(//,' enter the dipolar coupling constants in hz.....',/)
      do 20 i=1,n-1
      do 20 j=i+1,n
      k=n*(i-1) - i*(i+1)/2 + j
      type 504, i,j
504   format(5x,'d(',i3,',',i3,') :  ',$)
      accept *,d(k)
20    continue
      go to 50
c
30    type 505
505   format(//,' enter a maximum magnitude for couplings in hz: ',$)
      accept *,dmax
      type 506
506   format(' should all couplings be positive ? (0=no,1=yes) ',$)
      accept *,ipos
      type 507
```

```
507     format(' enter a randomizing integer: ',$)
        accept *,jr
        jr0=jr
c
        do 40 i=1,n-1
        do 42 j=i+1,n
        k=n*(i-1) - i*(i+1)/2 + j
        d(k)=dmax*rand(jr)
        if(ipos .eq. 1) d(k)=abs(d(k))
42      continue
c
50      ncoup=comb(n,2)
        type 528, ncoup
528     format(/,' do you want the ',i3,' couplings printed out? ',$)
        accept *,iprint
c
c       compute the dipolar variables t,a,b
c
        a=0.2
        b=0.0
        t=0.2
        do 220 i=1,n-1
        do 200 j=i+1,n
        do 222 k=1,n-1
        do 200 l=k+1,n
        k1=n*(i-1) - i*(i+1)/2 + j
        k2=n*(k-1) - k*(k+1)/2 + l
        if((i.eq.k).or.(i.eq.l).or.(j.eq.k).or.(j.eq.l))
     1   b=b + d(k1)*d(k2)
        go to 220
110     t=t + d(k1)
        a=a + d(k1)*d(k2)
200     continue
        t=t/4
        a=a/16
        b=b/16
c
c
        do 450 m=0,n
        m1=m+1
c
c       compute the normalization factor .....
c
        nm=n-m
        if(m .eq. 0) norm=comb(n2,n) - 2.0**n
        if(m .ne. 0) norm=comb(n2,nm)
c
c       compute the variance and the mean of the zeeman manifolds .....
c
        do 320 p=0,n
        p1=p+1
        var(p1)=t(p)* ((5-4*f(p))*a + (2-4*f(p))*b + 4*(f(p)*
     1   (4*n-5)-2*(n-1))/((n-2)*(n-3))*(t*t-a-b))
        m(p1)=(1-2*f(p))*t
320     continue
c
c       compute the second moment .....
c
        mom(m1)=0.0
        mom1(m1)=0.0
        mom2(m1)=0.0
        do 400 p=0,nm
        p1=p+1
```

```
      p2=p1+m
      mom1(m1)=mom1(m1) + comb(n,p)*comb(n,m+p)*(var(p1)+var(p2))/norm
      mom2(m1)=mom2(m1) + comb(n,p)*comb(n,m+p)*(h(p2)-h(p1))**2/norm
460   continue
      mom(m1) = mom1(m1) + mom2(m1)
c
450   continue
c
c
      print 621,n
621   format(1x1//' second moments for a ',i3,' spin system .....'//)
      if(icroice .eq. 1) go to 450
      print 622
622   format(5x,' couplings entered by hand')
      go to 470
450   dlow=-dmax
      if(ipos .eq. 1) dlow=0.0
      print 623, dlow,dmax
623   format(5x,' range of randomly-chosen couplings   ',f9.2,
     1  ' hz to ',f9.2,' hz')
      print 624,jr0
624   format(//,5x,'initial randomizing integer =  ',i14)
c
470   if(iprint .eq. 0) go to 460
      print 625
625   format(////,' the coupling constants in hz .....',/)
      do 475 i=1,n-1
      do 475 j=i+1,n
      k=n*(i-1) - i*(i+1)/2 + j
      print 626, i,j,d(k)
626   format(5x,'d(',i3,',',i3,') = ',f9.2)
475   continue
c
c
450   print 627
627   format(/////,73x,' width',16x,'mean'/'  m',8x,'second moments',
     1  12x,'ratio',32x,'contribution',9x,'contribution',/,
     1  ' ---',7x,13('-'),12x,'-----',30x,12('-'),9x,12('-'),/)
      do 450 m=0,n
      m1=m+1
      ratmom=mom(m1)/mom(2)
      print 628, m,mom(m1),ratmom,mom1(m1),mom2(m1)
628   format(i4,7x,e13.6,8x,e13.6,25x,e13.6,8x,e13.6)
450   continue
c
      print 611
611   format(1x1/////' p',12x,'width',16x,'ratio',34x,'mean'/
     1  ' ---',11x,13('-'),16x,'-----',34x,'----'/)
      do 477 p=0,n
      p1=p+1
      sqvar(p1)=sqrt(var(p1))
      ratvar=sqvar(p1)/sqrt(var(2))
      print 612, p,sqvar(p1),ratvar,h(p1)
612   format(i4,7x,e13.6,8x,e13.6,25x,e13.6)
477   continue
c
c
c     create data arrays for plotting .....
c
      write(1,702) (mom(i),i=1,n1)
      if(isep.eq.1) write(1,702) (mom1(i),i=1,n1),(mom2(i),i=1,n1)
      write(2,702) (sqvar(i),i=1,n1)
      write(2,702) (h(i),i=1,n1)
```

```
c
498     continue
c
        type 503
623     format(//,' do you want another spin system ? (0=no,1=yes) ',$)
        accept *,ispin
        if(ispin .eq. 1) go to 12
c
        print 610
610     format(1a1)
c
701     format(i6)
702     format(e16.8)
c
499     close(unit=1)
        close(unit=2)
        end
c
c
c
c
c
        function comb(n,m)
c
c       computes the binomial coefficient for n "things" taken
c       m at a time
c
        comb=1
        if(m .le. 2) return
        if(m .ge. n) return
        mm=m
        if(m .gt. n/2) mm=n-m
        comb=n
        if(mm .eq. 1) return
        mm1=mm-1
        qd=mm
        do 20 i=1,mm1
        comt=comt*(n-i)
        qd=qd*(mm-i)
        if(mod(i,10) .ne. 0) go to 20
        comb=comb/qd
        qd=1.0
20      continue
        comb=comt/qd
        return
        end
```

```
      program plot1
c
c     a program for plotting equally-spaced data points on the
c     Tektronix 4014 and 4662
c
      dimension dat(10,1021),dmax(10),ipos(10),imer(10),xy(4),
     1 corr(4)
      character*8 word(3)
c
      word(1)='ensemble'
      word(2)='ensemble'
      word(3)='data set'
c
      type 521
521   format(/,' enter plotter used: 0= 4014, 1= 4662  ',$)
      accept *,ipl
      jp=0
      if(ipl .ne. 0) jp=2
c
      type 502
502   format(/,' in which "plot" file is the data ? ',$)
      accept *,ifl
c
      call defile('plot',ifl,1)
c
      type 503
503   format(/,' how many data ENSEMBLES ? ',$)
      accept *,nens
c
      type 505
505   format(/,' which units do you prefer - inches (0) or cm ',
     1 '(1) ? ',$)
      accept *,iun
c
      corr(1)=0.38465
      corr(2)=0.59842
      corr(3)=0.52226
      corr(4)=0.53685
c
      xy(1)=6.33
      xy(2)=6.25
      xy(3)=13.8
      xy(4)=6.5
c
      if(iun .eq. 0) go to 20
      do 10 i=1,4
10    xy(i)=xy(i) * 2.54
c
22    call grstrt(4014,2)
      call dasnpt(0)
      call clip
      call inches
c
c
c
      do 400 ien=1,nens
c
      type 506, ien
506   format(//,' data ensemble ',i2,' .....')
c
      read(1,622) nsets,np
      read(1,603) ((dat(i,j), j=1,np), i=1,nsets)
c
      type 508, nsets
```

```
508     format(/,i7,' data SETS in this ensemble')
c
c
21      ips=1
        if(nsets .eq. 1) go to 22
        type 510
510     format(/,3x,'enter the desired plotting style .....',/,
     1   6x,'1 = all data sets on the same page',/,
     2   6x,'2 = separate pages but consistent scaling',/,
     3   6x,'3 = separate pages and independent scaling      ',$)
        accept *,ips
c
22      if(ips .lt. 3) nreps=1
        if(ips .eq. 3) nreps=nsets
c
        do 300 irep=1,nreps
c
        if(nreps .gt. 1) type 511, irep
511     format(/,3x,'data set ',i1,' .....')
c
        type 512, np
512     format(/,4x,'horizontal scaling for your',i5,' data points',
     1   ' .....')
23      type 513
513     format(/,5x,'enter low and high point limits to be',/,
     1   6x,'displayed :  (for all points, enter 0,0)   ',$)
        accept *,nlo,nhi
        if(nlo .eq. 0) nlo=1
        if(nhi .eq. 0) nhi=np
        if(nhi .le. nlo) go to 23
        npp=nhi - nlo
        type 514, xy(jp+1)
514     format(/,5x,'enter the desired plot width in your preferred',
     1   /,6x,'units :  (',f5.1,' maximum)  ',$)
        accept *,xxx
        if(iun .eq. 1) xxx=xxx / 2.54
        xxx=xxx / corr(jp+1)
c
        nback=nsets
        if(ips .eq. 3) nback=irep
c
        do 25 is=irep,nback
        ipos(is)=0
        ineg(is)=0
25      dmax(is)=0.0
        jpos=0
        jneg=0
        smax=0.0
c
        do 30 is=irep,nback
        do 28 ip=nlo,nhi
        if(dat(is,ip) .le. .001) go to 26
        ipos(is)=1
        jpos=1
26      if(dat(is,ip) .ge. -.001) go to 27
        ineg(is)=1
        jneg=1
27      dmax(is)=amax1(dmax(is),abs(dat(is,ip)))
28      continue
        smax=amax1(dmax(is),smax)
30      continue
c
        type 515
```

```
515     format(//,4x,'vertical scaling .....')
c
        if(ips .eq. 3) go to 45
        pmax=smax
        kpos=jpos
        kneg=jneg
        go to 50
45      pmax=imax(irep)
        kpos=ipos(irep)
        kneg=ineg(irep)
c
50      itop=0
        ibot=0
        if(kneg .ne. 0) go to 55
        type 516
516     format(/,5x,'your data points are all positive.  do you',/,
     1   6x,'want the negative half-plane suppressed ? (0=no,1=yes) ',
     2   $)
        accept *,itop
55      if(kpos .ne. 0) go to 60
        type 517
517     format(/,5x,'your data points are all negative.  do you',/,
     1   6x,'want the positive half-plane suppressed ? (0=no,1=yes) ',
     2   $)
        accept *,ibot
c
60      type 518, pmax
518     format(/,5x,'the beefiest data point has abs. value = ',G14.6)
        type 519
519     format(/,5x,'for "automatic" full-value scaling, enter 2.0;',
     1   /,6x,'otherwise enter the number which corresponds to',/,
     2   6x,'maximum magnitude on the plot:  ',$)
        accept *,fv
        if(fv .eq. 0.0) ymax=pmax
        if(fv .gt. 2.0) ymax=fv
c
        type 520, xy(jp+2)
520     format(/,5x,'enter the desired plot height in your preferred',
     1   /,6x,'units :  (',f5.1,' maximum)  ',$)
        accept *,yyy
        if(iun .eq. 1) yyy=yyy / 2.54
        yyy=yyy / corr(jp+2)
        ytop=yyy - 100
c
        if(ips .ne. 2) type 521
521     format(/,5x,'should a y-axis be drawn ? (0=no,1=yes) ',$)
        if(ips .eq. 2) type 522
522     format(/,5x,'should a y-axis be drawn ? (0=no,1=yes,',/,
     1   6x,'2=yes, but only on the first page) ',$)
        accept *,iax
c
        if(jp .eq.    go to 70
        type 525,      ips)
525     format(//,     enter 1 if you are ready to plot, 0 if you',/,
     1   4x,'want  skip THIS ',a,', or -1 if you want to quit : ',$)
        accept *,ichoice
        if(ichoice .eq. 0) go to 300
        if(ichoice .lt. 0) go to 490
c
c
70      npages=1
        if(ips .eq. 2) npages=nsets
c
```

```
      do 150 ipage=1,npages
c
      if(ips .ne. 2) go to 72
      type 526, ipage
526   format(/,5x,'data set ',i2,' -- plot it ?? (0=no,1=yes) ',$)
      accept *,igo
      if(igo .eq. 0) go to 150
c
72    call newpag
      xlo=nlo
      xhi=nhi
      if(itop .eq. itot) call window(xlo,xhi,-ymax,ymax)
      if(itop .eq. 1) call window(xlo,xhi,0.0,ymax)
      if(ibot .eq. 1) call window(xlo,xhi,-ymax,0.0)
      call viewport(2.0,xxx,0.100,ytop)
73    if(iax .eq. 0) go to 75
      if((iax .eq. 2) .and. (ipage .gt. 1)) go to 75
      yaxt= ymax * (1 - ibot)
      yaxb=-ymax * (1 - itop)
      call move(xlo,yaxt)
      call draw(xlo,yaxb)
75    call move(xlo,0.0)
      call draw(xhi,0.0)
c
      nlines=1
      if(ips .eq. 1) nlines=nsets
c
82    do 100 iline=1,nlines
      im=max0(irep,ipage,iline)
      call move(xlo,dat(im,nlo))
      do 90 k=1,npp
92    call draw(xlo+k,dat(im,nlo+k))
      call grsend
100   continue
c
c
      type 530
530   format(/,10x,'ONeAEB ?? (0=no,1=yes,2=new style,',
     1 '3=new ensemble,4=quit) ',$)
      accept *,ion
      if(ion .eq. 2) go to 73
      if(ion .eq. 2) go to 21
      if(ion .eq. 3) go to 400
      if(ion .eq. 4) go to 450
c
150   continue
320   continue
420   continue
c
c
450   call grstop
      close(unit=01)
c
602   format(i6)
603   format(e16.8)
c
      end
```

```
      program plot2
c
c     a program for plotting equally-spaced data points on the
c     Tektronix 4014 and 4662 -- similar to PLOT1, but combines
c     up to seven different data ensembles on the same graph.
c
      dimension dat(10,601,7),dmax(10),ipos(10),ineg(10),xy(4),
     1  corr(4)
      character*8 word(3)
c
      word(1)='NAT ACLE'
      word(2)='POPSIAND'
      word(3)='data set'
c
      type 501
501   format(/,' enter plotter used: 0= 4014, 1= 4662  ',$)
      accept *,ipl
      jp=0
      if(ipl .ne. 0) jp=2
c
      type 502
502   form[illegible]' in which "plot" file is the data ? ',$)
      acc[illegible]1
c
      call defile('plot',ifl,1)
c
      type 503
503   format(/,' how many data ENSEMBLES ? ',$)
      accept *,nens
c
      type 505
505   format(/,' which units do you prefer - inches (0) or cm ',
     1  '(1) ? ',$)
      accept *,iun
c
      corr(1)=0.3e465
      corr(2)=0.59642
      corr(3)=0.92226
      corr(4)=0.92265
c
      x[illegible]
      xy[illegible]5
      xy([illegible].8
      xy(4)=8.9
c
      if(iun .eq. 0) go to 15
      do 10 i=1,4
10    xy(i[illegible] xy(i) * 2.54
c
15    call [illegible]strt(4014,2)
      call [illegible]asnpt(0)
      call clip
      call inches
c
c
c
      do 20 k=1,nens
      read(1,602) nsets,np
      read(1,603) ((dat(i,j,k), j=1,np), i=1,nsets)
20    continue
c
      type 506, nsets
506   format(/,'    (',i2,' data SETS per ensemble)')
c
```

```
21      ips=1
        if(nsets .eq. 1) go to 22
        type 512
512     format(/,5x,'enter the desired plotting style .....',/,
     1   5x,'1 = all data sets on the same page',/,
     2   5x,'2 = separate pages but consistent scaling',/,
     3   5x,'3 = separate pages and independent scaling     ',$)
        accept *,ips
c
22      if(ips .lt. 3) nreps=1
        if(ips .eq. 3) nreps=nsets
c
        do 300 irep=1,nreps
c
        if(nreps .gt. 1) type 511, irep
511     format(/,3x,'data set ',i1,' .....')
c
        type 512, np
512     format(/,4x,'horizontal scaling for your',i5,' data points',
     1    ' .....')
23      type 513
513     format(/,5x,'enter low and high point limits to be',/,
     1   5x,'displayed :  (for all points, enter 0,0)   ',$)
        accept *,nlo,nhi
        if(nlo .eq. 0) nlo=1
        if(nhi .eq. 0) nhi=np
        if(nhi .le. nlo) go to 23
        npp=nhi - nlo
        type 514, xy(jp+1)
514     format(/,5x,'enter the desired plot width in your preferred',
     1   /,5x,'units :  (',f5.1,' maximum)  ',$)
        accept *,xxx
        if(iun .eq. 1) xxx=xxx / 2.54
        xxx=xxx / corr(jp+1)
c
        nhack=nsets
        if(ips .eq. 3) nhack=irep
c
        do 25 is=irep,nhack
        ipos(is)=0
        ineg(is)=0
25      dmax(is)=0.0
        jpos=0
        jneg=0
        smax=0.0
c
        do 30 is=irep,nhack
        do 29 k=1,nens
        do 28 ip=nlo,nhi
        if(dat(is,ip,k) .le. .001) go to 28
        ipos(is)=1
        jpos=1
26      if(dat(is,ip,k) .ge. -.001) go to 27
        ineg(is)=1
        jneg=1
27      dmax(is)=amax1(dmax(is),abs(dat(is,ip,k)))
28      continue
29      continue
        smax=amax1(dmax(is),smax)
30      continue
c
        type 515
515     format(//,4x,'vertical scaling .....')
```

```
c
        if(ips .eq. 3) go to 45
        pmax=smax
        kpos=jpos
        kneg=jneg
        go to 30
45      pmax=dmax(irep)
        kpos=ipos(irep)
        kneg=ineg(irep)
c
30      itop=0
        icot=0
        if(kneg .ne. 0) go to 55
        type 516
516     format(/,5x,'your data points are all positive.  do you',/,
     1   6x,'want the negative half-plane suppressed ? (0=no,1=yes) ',
     2   $)
        accept *,itop
55      if(kpos .ne. 0) go to 60
        type 517
517     format(/,5x,'your data points are all negative.  do you',/,
     1   6x,'want the positive half-plane suppressed ? (0=no,1=yes) ',
     2   $)
        accept *,icot
c
60      type 518, pmax
518     format(/,5x,'the beefiest data point has abs. value = ',g14.6)
        type 519
519     format(/,5x,'for "automatic" full-value scaling, enter 0.0;',
     1   /,6x,'otherwise enter the number which corresponds to',/,
     2   6x,'maximum magnitude on the plot:  ',$)
        accept *,fv
        if(fv .eq. 0.0) ymax=pmax
        if(fv .gt. 0.0) ymax=fv
c
        type 520, xy(jp+2)
520     forma[illegible] .5x,'enter the desired plot height in your preferred',
     1   /,6x [illegible] ts :  (',f5.1,' maximum)  ',$)
        accept [illegible],yyy
        if(iun .eq. 1) yyy=yyy / 2.54
        yyy=yyy / corr(jp+2)
        ytop=yyy + .100
c
        if(ips .ne. 2) type 521
521     format(/,5x,'should a y-axis b[illegible] drawn ? (0=no,1=yes) ',$)
        if(ips .eq. 2) type 522
522     format(/,5x,'should a y-axis be drawn ? (0=no,1=[illegible]es,',/,
     1   6x,'2=yes, but only on the first page) ',$)
        accept *,iax
c
        if(jp [illegible] 6) go to 70
        type [illegible] word(ips)
525     form[illegible] /,3x,'enter 1 if you are ready to plot, 0 if you',/,
     1   4x,'want to skip THIS ',a,', or -1 if you want to quit : ',$)
        accept *,icnoice
        if(icnoice .eq. 0) go to 300
        if(icnoice .lt. 0) go to 400
c
c
70      npages=1
        if(ips .eq. 2) npages=nsets
c
        do 150 ipage=1,npages
```

```
c
        if(ips .ne. 2) go to 72
        type 526, ipage
526     format(/,3x,'data set ',i2,' -- plot it ?? (0=no,1=yes) ',$)
        accept *,igo
        if(igo .eq. 0) go to 100
c
72      call newpag
        xlo=nlo
        xhi=nhi
        if(itop .eq. itot) call window(xlo,xhi,-ymax,ymax)
        if(itop .eq. 1) call window(xlo,xhi,0.0,ymax)
        if(ibot .eq. 1) call window(xlo,xhi,-ymax,0.0)
        call vwport(2.0,xxx,0.100,ytop)
73      if(iax .eq. 0) go to 75
        if((iax .eq. 2) .and. (ipage .gt. 1)) go to 75
        yaxt= ymax * (1 - ibot)
        yaxb=-ymax * (1 - itop)
        call move(xlo,yaxt)
        call draw(xlo,yaxt)
75      call move(xlo,0.0)
        call draw(xhi,0.0)
c
        nlines=1
        if(ips .eq. 1) nlines=nsets
c
        do 100 iline=1,nlines
        im=max0(irep,ipage,iline)
c
        do 50 k=1,nens
        call move(xlo,dat(im,nlo,k))
        do 50 j=1,npp
54      call draw(xlo+j,dat(im,nlo+j,k))
55      continue
c
        call grsend
100     continue
c
c
        type 530
530     format(/,10x,'OK.ARD ?? (0=no,1=yes,2=new style,',
     1   'b=quit) ',$)
        accept *,ion
        if(ion .eq. 0) go to 73
        if(ion .eq. 2) go to 21
        if(ion .eq. 3) go to 400
c
100     continue
300     continue
c
c
400     call grstop
        close(unit=21)
c
602     format(i6)
603     format(e16.6)
c
        end
```

CHAPTER 4 REFERENCES

1. W.S. Warren, Ph.D. thesis, University of California, Berkeley, 1980.
2. G. Bodenhausen, Prog. NMR Spectrosc. 14, 137 (1981).
3. D.P. Weitekamp, submitted to Adv. Magn. Resonance.
4. A. Abragam, Principles of Nuclear Magnetism, (Oxford, London, 1961).
5. G. Drobny, A. Pines, S. Sinton, D.P. Weitekamp, and D. Wemmer, Faraday Symp. Chem. Soc. 13, 49 (1979); G. Bodenhausen, R.L. Vold, and R.R. Vold, J. Magn. Reson. 37, 93 (1980).
6. J.H. Van Vleck, Phys. Rev. 74, 1168 (1948).
7. J. Tang, Ph.D. thesis, University of California, Berkeley, 1981.
8. R. Bracewell, The Fourier Transform and Its Applications, (McGraw-Hill, New York, 1965).
9. J.B. Murdoch, W.S. Warren, D.P. Weitekamp, and A. Pines, submitted to J. Magn. Reson.
10. Y.S. Yen and A. Pines, J. Chem. Phys., accepted for publication.
11. A. Wokaun and R.R. Ernst, Molec. Phys. 36, 317 (1978).
12. Computer simulation performed by J.B. Murdoch, University of California, Berkeley.
13. MQ spectrum supplied by Gary Drobny, University of Washington.

CHAPTER 5

SENSITIVITY ENHANCEMENT BY SPINLOCKING IN THE DETECTION PERIOD

5.1. INTRODUCTION AND THEORY

A MQ experiment is a two-dimensional experiment.[1] That is, one of the dimensions is scanned in real time, and the other is scanned by successive incrementation from shot to shot. Every two-dimensional experiment suffers from two sources of noise: the real time noise, and the successive shot to shot noise. The first type of noise, the t_2 noise, is predominantly thermal noise in the electronics, and is also common to single-dimension experiments. The second type of noise, which has been termed the t_1 noise,[2] is due to the irreproducibility of the experiment and is inherent in any two-dimensional experiment.

A simple scheme is proposed to improve S/N by minimizing the t_2 noise. The idea is to acquire more signal energy[3] in the detection period.

The pulse sequence used is shown in Fig. 5.1. It is a typical MQ sequence but with a train of pulses in the detection period. The first three pulses allow even-quantum selection and are phase-shifted by $\Delta\phi = \frac{2\pi}{2M}$, where M is the maximum order desired, for each incrementation in t_1 to effect separation of

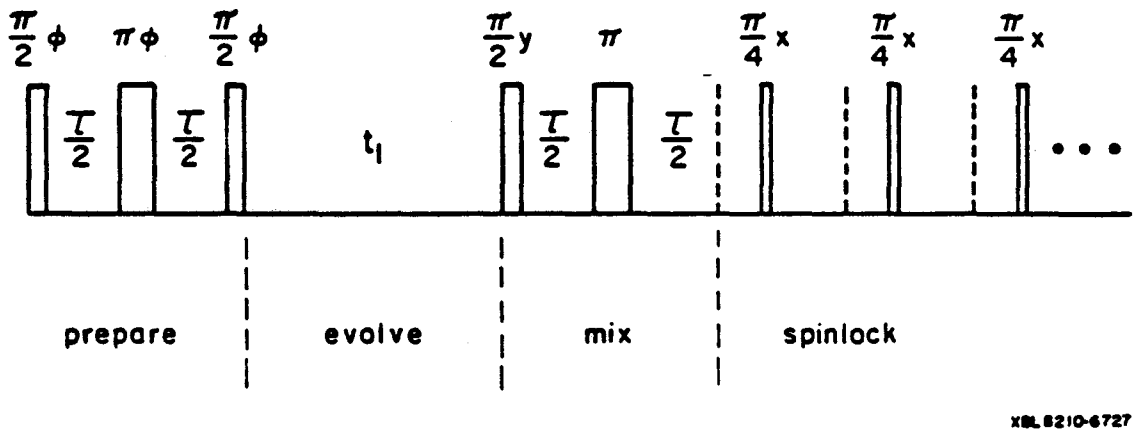

Figure 5.1 Even-selective multiple-quantum pulse sequence with spinlocking pulses in the detection period. The preparation pulses are incremented by an amount $\Delta\phi$ for each incrementation in t_1 (TPPI).

orders (TPPI[4]). The π pulse in t_1 removes offset terms in the ω_1 spectrum. The next two rf pulses mix the MQ coherences into single-quantum (SQ) coherences. Detecting the amplitude modulation of the SQ coherences as a function of t_1 maps out the MQ evolution.

Because the evolution in t_2 is uninteresting for our purposes, it is unnecessary to acquire the entire F.I.D. in t_2. In fact, typically only one point in t_2 is sampled for each incrementation in t_1. Only the amplitude modulation of the SQ coherences in t_2 is desired. Therefore, instead of subjecting the SQ coherences to decay under the full Hamiltonian, which may contain rapidly dephasing terms, one can increase the signal energy available for detection by removing the rapidly decaying terms. The main source in solids is the dipolar Hamiltonian. One solution is to apply WAHUHA[5] in t_2 to remove this term. Best yet is to remove all such terms by pulsed spinlocking.[6,7] Under perfect spinlocking conditions, the only decay that will occur will be due to the spin-lattice relaxation in the rotating frame.

The multiple pulses in t_2 (Fig. 5.1) are applied for just that effect. Rhim et al[7] have shown that optimal spinlocking is achieved with a series of $\pi/4$ pulses at a repetition rate Ω satisfying

$$\Omega > \bar{\omega}_1, \ \gamma H_{loc}$$

where $\overline{\omega}_1 = \gamma\overline{H}_1$ is proportional to the average rf irradiation strength and H_{loc} is the local field strength.

By spinlocking the SQ coherences in t_2, we are in essence preserving the signal amplitude as modulated by the evolution in t_1. By sampling in the pulse windows and averaging over all the signal that is available in the detection period, we have performed an integration of the signal in t_2. The integral is proportional to the signal amplitude at $t_2 = 0$ averaged over the t_2 noise.

5.2 EXPERIMENTAL RESULTS AND DISCUSSION

The sample is polycrystalline adamantane, $C_{10}H_{16}$. Experiments were performed at a regulated temperature of 25°C.

The following observations on the effective relaxation rates were made. The SQ transverse decay time under free evolution was measured to be ≈ 100 μsec. A series of π/4 pulses was applied at various repetition rates to the SQ coherences. The observed decay times in the rotating frame were

$\Omega^{-1} = 15.9$ μsec, $T_{1e} > 1.2$ sec

$\Omega^{-1} = 25.9$ μsec, $T_{1e} \approx 1.0$ sec

$\Omega^{-1} = 35.9$ μsec, $T_{1e} \approx 0.2$ sec

$\Omega^{-1} > 90$ μsec, saw no spinlocking effect .

With $\pi/2$ spinlocking rf pulses at a repetition time of Ω^{-1} = 54.8 μsec, T_{1e} = 2.2 msec.

For our MQ experiments, the repetition rate was Ω = (39 μsec)$^{-1}$ = 25.6 kHz and the pulse duration for a π pulse was 8.0 μsec. Thus the average irradiation strength was $\overline{\omega}_1/2\pi$ = 3.2 kHz. From second moments measurements, $\gamma H_{loc}/2\pi$ is roughly 15 kHz for adamantane. Thus the condition for spinlocking was modestly satisfied, and for our purposes sufficient.

The preparation time was τ=60 μsec in all our MQ experiments.

The first sampled point occurs at t_2 = 0, the normal sampling point. This is to be compared with the integrated spinlocked signal. Integration was simulated by taking the average of 1000 points sampled in the spinlocking windows. These points were taken after the first 25 $\pi/4$ pulses, or at a delay of $25\Omega^{-1}$ = 1.00 msec after the mixing period. This delay moves the sampling far away from any transients that were not spinlocked.

Shown in Fig. 5.2 is a comparison of MQ spectra obtained with one point sampled at t_2 = 0 and the average of 1000 points sampled between spinlocking pulses. There is an improvement in S/N of roughly ×2 by sampling more points, indicating that the signal was large enough so that t_1 noise dominates.

To effect t_2 limitation in noise, the signal was

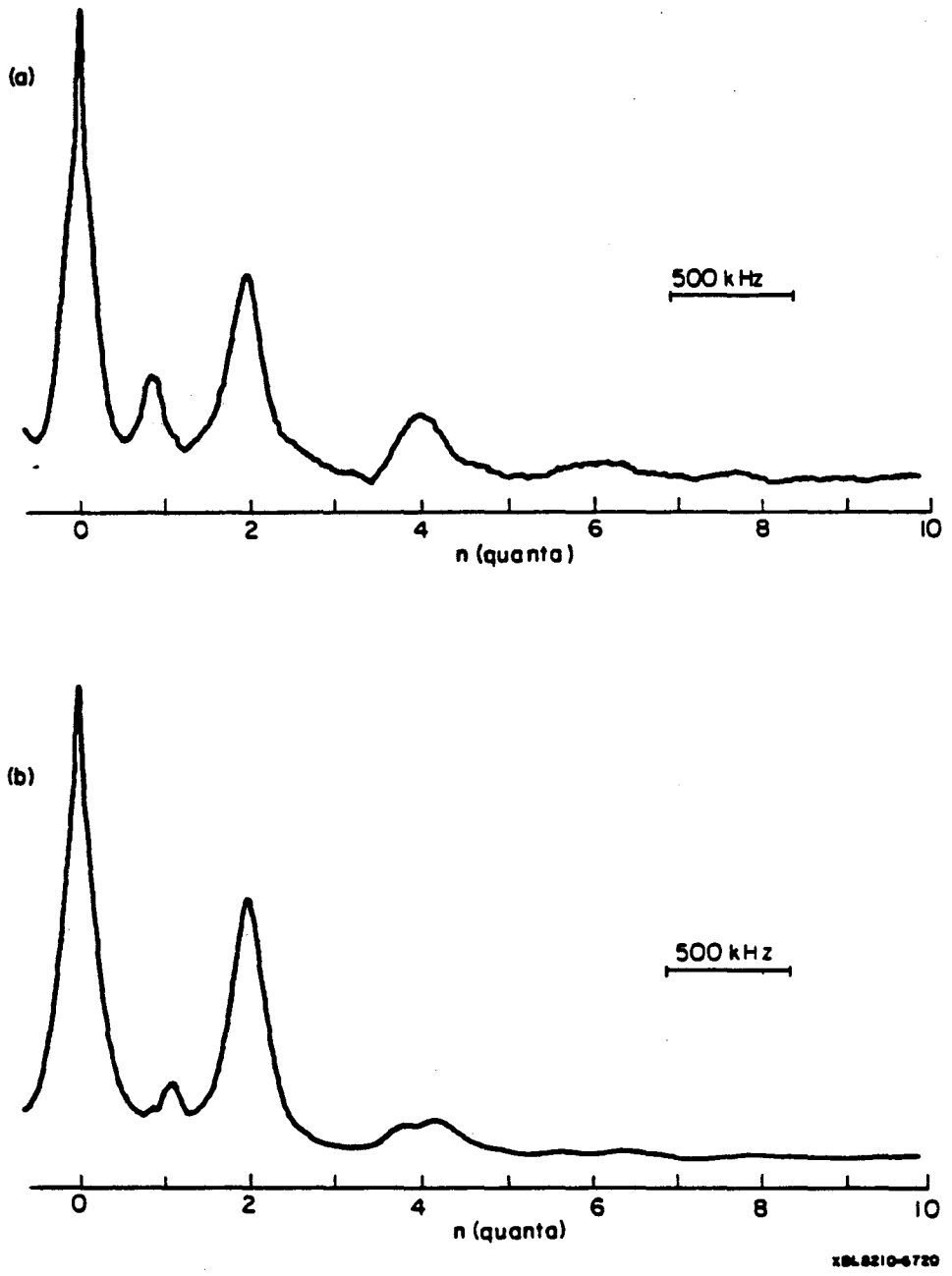

Figure 5.2 MQ spectrum obtained with pulse sequence of Fig. 5.1 using (a) the first sampled point, yielding the normal spectrum, (b) an average of 1000 points sampled between the spinlocking pulses, yielding the spinlocked spectrum. The comparison shows lit: improvement by t_2 spinlocking, indicating that t_1 n e dominates.

attenuated by 30dB and the receiver amplifier gain was increased appropriately to achieve its full dynamic range. Figure 5.3 shows the large improvement in S/N by spinlocking. The S/N is increased by 20 - 30 times, which is near the maximum improvement possible. That is, for t_2 limited sensitivity, the spinlocking spectrum is equivalent to an accumulation of runs roughly equal to the number of points sampled in t_2.

In both instances, Figs. 5.2 and 5.3, we observe the intensity in the odd-quantum order relative to the even-quantum order is less in the spinlocking spectrum. The odd-quantum coherences appear as a result of imperfect even-selection, and must be a result of imperfect offset cancellation in the preparation and mixing periods. If even-selection is perfect, the signal should appear as $\langle I_x \rangle$ for the pulse sequence shown in Fig. 5.1. A small offset term causes signal to appear in the orthogonal channel. It also creates a small amount of odd-quantum in both channels in addition to even-quantum coherences, but in different amounts. The difference in the spinlocked spectrum and the normal spectrum reflects this difference in the preparation of even and odd quantum coherences in the two channels: the spinlocked signal pertains to only one of the channels. Based on this argument, we should expect to see a difference in spectra obtained with t_2 spinlocking if selectivity is

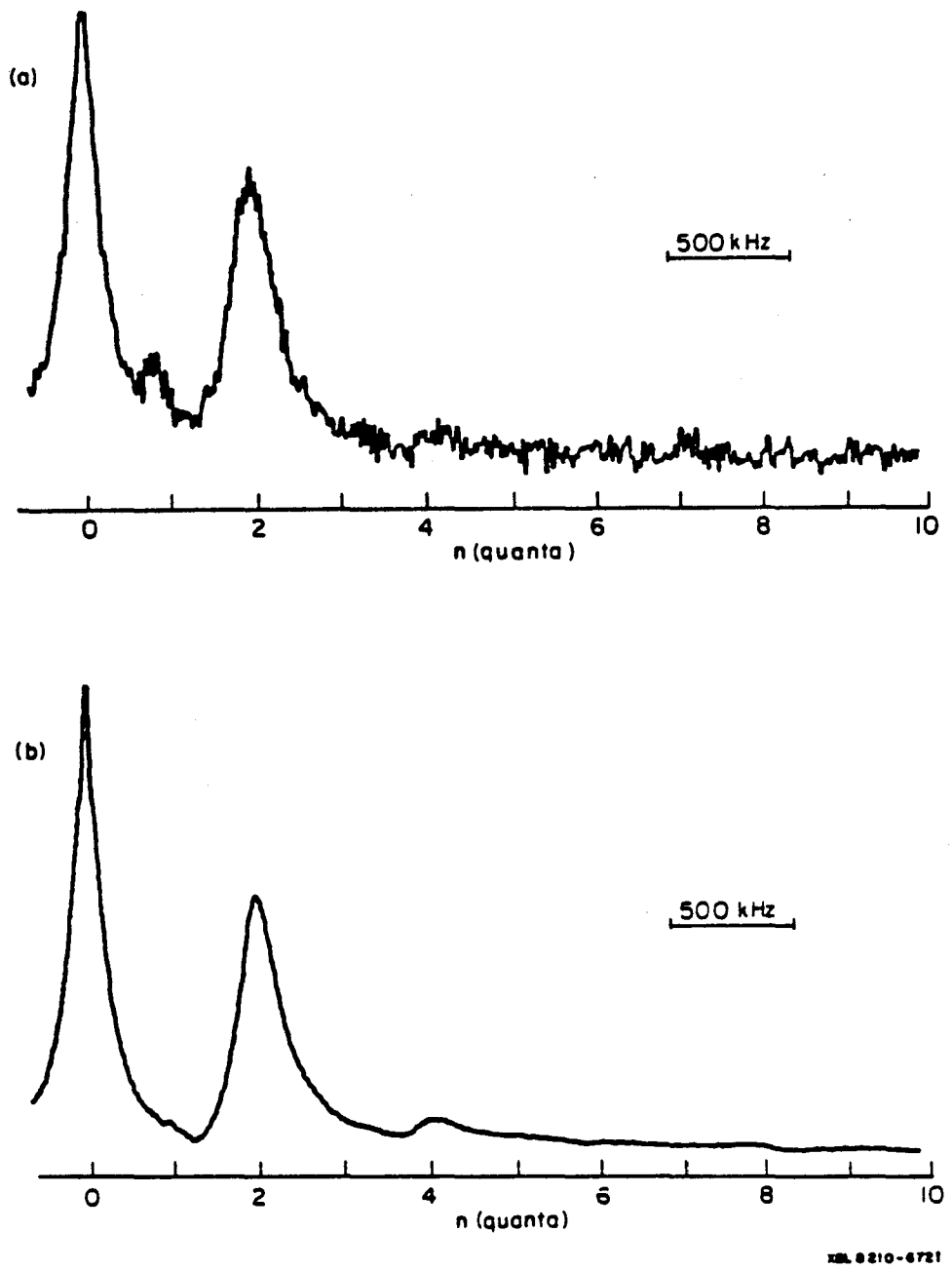

Figure 5.3 MQ spectra obtained in the same way as Fig. 5.2 but with attenuated signal input to receiver. The comparison shows large improvement by t_2 spinlocking when the S/N in the spectrum is limited by t_2 noise.

imperfect.

For nonselective sequences, signal in the other channel can be obtained by repeating the experiment a second time with the spinlocking pulses changed in phase by 90°. Another strategy is to phase the spinlocking pulses at 45° with respect to the mixing pulses, thereby spinlocking both channels simultaneously and with equal weighting.

In conclusion, the experiments show that the proposed scheme can improve sensitivity of detection. The t_1 noise is proportional to the magnetization and cannot be minimized by increasing sample size. In contrast, the t_2 noise can be made insignificant by doing so. However, given the situation that the t_2 noise is an important limitation, these preliminary experiments show that pulsed spinlocking in the detection period and with integration of signal in the windows is successful in enlarging S/N.

CHAPTER 5 REFERENCES

1. A. Wokaun and R.R. Ernst, J. Chem. Phys. 67, 1752 (1977).
2. K. Nagayama, P. Bachmann, K. Wuthrich, and R.R. Ernst, J. Magn. Reson. 31, 133 (1978); D.P. Weitekamp, Advan. Magn. Reson., submitted for publication.
3. W.P. Aue, P. Bachmann, A. Wokaun, and R.R. Ernst, J. Magn. Reson. 29, 523 (1978).
4. G. Drobny, A. Pines, S. Sinton, D.P. Weitekamp, and D. Wemmer, Fraadav Symp. Chem. Soc. 13, 49 (1979); G. Bodenhausen, R.L. Vold, and R.R. Vold, J. Magn. Reson. 37, 93 (1980).
5. M. Mehring, High Resolution NMR Spectroscopy in Solids, (Springer-Verlag, New York, 1976).
6. E.D. Ostroff and J.S. Waugh, Phys. Rev. Lett. 16, 1097 (1966).
7. W.-K. Rhim, D.P. Burum, and D.D. Elleman, Phys. Rev. Lett. 37, 1764 (1976).

CHAPTER 6

CORRELATION OF MOTION OF TWO METHYL GROUPS

6.1 INTRODUCTION

Two interacting methyl groups serve as a model system for studying hindered internal rotation. Because it involves only six nuclear spins, the calculations involved are tractable. Definitions of correlated and uncorrelated motion are well defined and thus exact treatment is possible.

We wish to utilize the fact that molecular motion modifies the observed couplings between nuclear spins. In oriented systems, such as solids or solutes dissolved in a liquid crystal, the dipolar interaction is typically two or three orders of magnitude larger than the J couplings. Our studies will be in such systems; thus we will concentrate on motional averaging of the dipolar couplings and neglect the J couplings.[1]

The definitions of correlated and uncorrelated motion of two methyl groups are first stated. The form of the Hamiltonians is thus defined and is different for the two motions, ensuring that NMR is sensitive to correlation of motion. The NMR spectrum for each of these cases can be calculated as a function of the dipolar coupling constants. Group theory for nonrigid molecules is used to simplify the calculations in these

two extremes and in the intermediate region. The transition from correlated to uncorrelated motion can be likened to an exchange process and hence is amenable to treatment with exchange theory. Multiple-quantum NMR enters as a simplification tool in the extraction of coupling constants. A computer simulation of the 4-quantum spectra for the molecule 1,8-dimethylnaphthalene-d_6 undergoing exchange processes at a particular crystal orientation is presented. Experiments on the same molecule dissolved in a nematic liquid crystal reveals that at room temperature this system has uncorrelated equivalent methyl groups. Finally, we present the analysis of a simple two-spin system, diprotonated 1,8-dimethylnaphthalene-d_{10}, in the limit of correlated and uncorrelated motion.

6.2 DEFINITION OF CORRELATED AND UNCORRELATED MOTION

In both limits, the methyl groups are undergoing rapid torsional motions about their C_3 axes. The distinction we would like to make here is in the relative motion of the methyl groups. We define the motions as follows. If the methyl groups are correlated, the motion of one methyl group completely determines the motion of the other group. If the methyl groups are uncorrelated, the relative orientation of the methyl groups is completely random in time.

The above definition of correlated motion is independent of how the motion is executed. The methyl groups can either be correlated in an "eclipsed" or "staggered" configuration, as shown in Fig. 6.1, or in an intermediate configuration. The motionally averaged values of the dipolar couplings are modified by the type of correlated motion the spin system undergoes, but the number of coupling constants remains the same. Experimental determination of the dipolar coupling constants, assuming a certain fixed distance between the two C_3 axes, can lead to information on how the methyl groups move in a correlated manner. The C_3 axes distance can be determined by other means, such as X-ray diffraction or neutron scattering methods.[2]

The symmetry group of the spin Hamiltonian is also independent of how the correlated motion is executed, and can be found based on the above definition.

Correlation of two methyl groups can be viewed as two wheels in gear, however the methyl groups are positioned. In the transition to becoming uncorrelated, there is an occasional slipping of gears. The rate of slippage depends on the potential barrier determined by the environment and on the temperature of observation.

6.3 DETERMINATION OF THE SPIN HAMILTONIAN

We will assume a system of isolated molecules

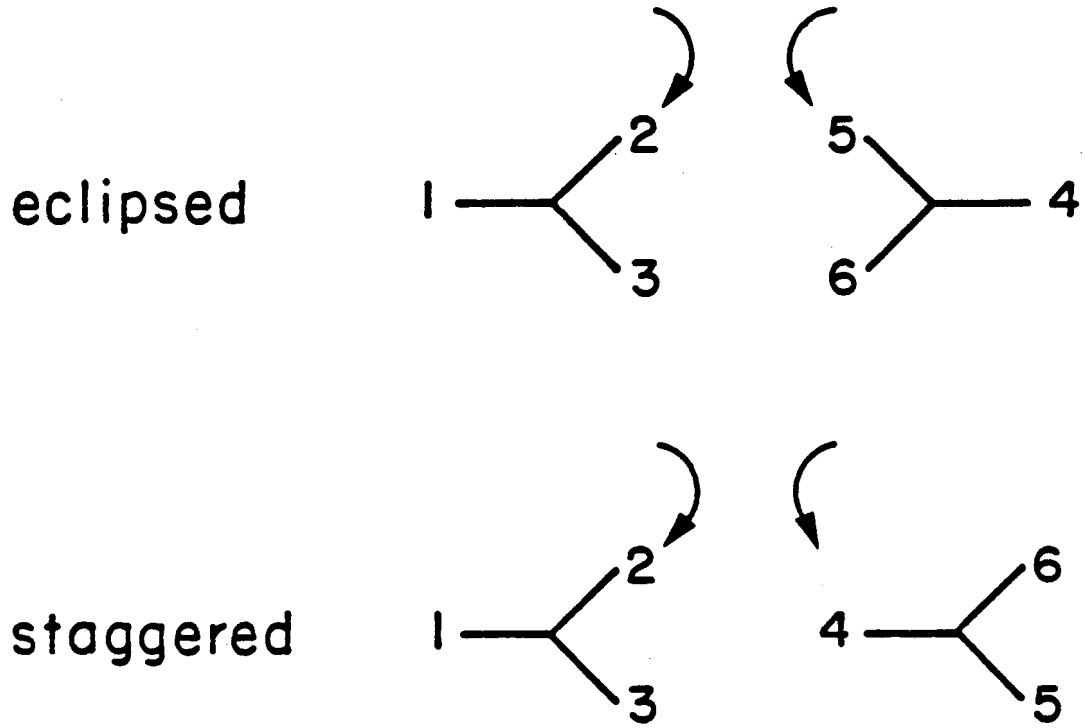

XBL 8210-2925

Figure 6.1 When the correlated motion of two methyl groups occur in an "eclipsed" manner, the methyl groups are mirror images. In a "staggered" configuration, they act as gears in a cogwheel mesh.

oriented in a matrix. The relevant Hamiltonian is the one that is averaged over the nuclear motion. The Hamiltonian also has to be consistent with the spacial symmetry of the molecule.

At room temperature, the correlation time of rotation τ_c is typically 10^{-9} - 10^{-11} sec for methyl groups.[2] To observe the effect on dipolar spectrum the inherent time scale is roughly 10^{-3} - 10^{-4} sec for typical dipolar couplings. Thus, on the NMR time scale, at room temperature the methyl groups are motionally averaged.

To determine the Hamiltonian of the spin system, one must know the number of spins involved, the number of unique dipolar couplings according to the molecular motion, and the molecular orientation with respect to the external magnetic field. Specification of the molecular orientation is essential since the magnitude of the coupling depends on the polar angle θ that the internuclear vector r makes with the external magnetic field $\vec{H}_o$:

$$d_{ij} \propto \frac{1}{r_{ij}^3} (3\cos^2\theta_{ij} - 1).$$

We will first treat a hypothetical case of rigid lattice structure with one molecule per unit cell. The influence on the spin Hamiltonian by molecular reorientation, such as happens in a liquid crystal,

will be treated in section 6.6. The determination of the number of motionally averaged dipolar coupling constants is discussed separately for the intramethyl and intermethyl parts of the dipolar Hamiltonian.

6.3.1 Intramethyl Couplings

Due to the fast C_3 reorientation of the methyl groups, the dipolar couplings within each methyl group is averaged to the same value. If the orientation of the crystal is such that the two C_3 axes make the same angle with respect to $\vec{H}_o$, then the methyl groups are equivalent and there is only one unique intramethyl coupling constant. Otherwise, the methyl groups are inequivalent and there are two distinct intramethyl coupling constants. The above statements are true regardless of whether the methyl groups are correlated or not. Thus, intramethyl couplings do not lead to information on correlation.

6.3.2 Intermethyl couplings

The determination of the number of intermethyl couplings is more complicated as a result of two factors: the relative motion of the methyl groups and the direction of the C_3 axes with respect to $\vec{H}_o$. We will assume for simplicity that each methyl group can hop between three equivalent equilibrium positions.

6.3.2.1 Uncorrelated Motion

If the methyl groups are uncorrelated [Fig. 6.2(a)], a proton on one group senses the same coupling to all three protons on the other group. But all the protons on a methyl group are equivalent as a result of the rapid methyl reorientation. Averaging the couplings over this motion yields one unique intermethyl coupling constant. Any type of molecular reorientation will not alter this uniqueness.

6.3.2.2 Correlated Motion

This case is the most difficult one to contend with. Determination of the couplings depends on the factors mentioned at the beginning of section 6.3.2. In Fig. 6.2(b), for the sake of discussion, we have assumed a particular relative positioning of the methyl groups. However, the results remain unaltered by the relative positioning or by whether the methyl reorientation is discrete or continuous. According to Fig. 6.2(b), there are three configurations that are possible.

When the motion is correlated, the number of unique intermethyl couplings depends on the orientation of the molecule, and thus the symmetry group of the Hamiltonian will vary with the orientation. (Take note that this fact does not hold when the motion is uncorrelated.) Three situations can occur.

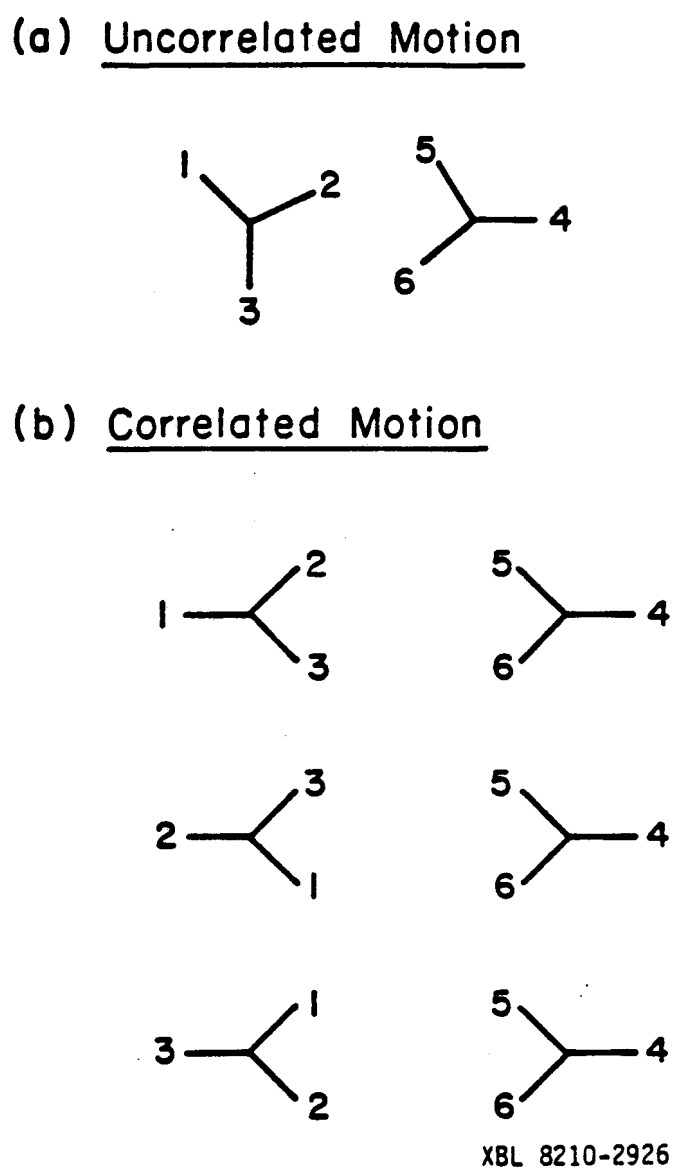

Figure 6.2 (a) In uncorrelated motion, the methyl groups have a random relationship with respect to each other. (b) Assuming the methyl rotor can hop only between equilibrium positions, there are only three possible configurations for correlated motion.

(i) Equivalent Methyl Groups

When the two methyl C_3 axes make the same polar angle with respect to H_o, they are NMR equivalent. Averaging the dipolar couplings over the three possible configurations results in:

$$d_{14}=d_{25}=d_{36}$$

$$d_{15}=d_{16}=d_{24}=d_{26}=d_{34}=d_{35},$$

where the subscripts are consistent with the labeling scheme of Fig. 6.2(b). Thus there are two unique intermethyl coupling constants when the methyl groups are equivalent. The net result is that the dipolar Hamiltonian is of the form:

$$H_D = u \sum_{i,j} U_{ij} + v \sum_{k,l} V_{kl} + w \sum_{m,n} W_{mn},$$

where u is the unique intramethyl coupling constant, v and w are the two unique intermethyl coupling constants. The spin operators U, V, and W are of the same form:

$$U_{ij} = I_{zi}I_{zj} - \frac{1}{4}(I_{+i}I_{-j} + I_{-i}I_{+j}),$$

and the indices run through the following labels:

$(i,j) = \{(1,2), (2,3), (1,3), (4,5), (5,6), (4,6)\}$

$(k,l) = \{(1,4), (2,5), (3,6)\}$

$(m,n) = \{(1,5), (1,6), (2,4), (2,6), (3,4), (3,5)\}.$

(ii) $\vec{H}_o$ and the Methyl C_3 Axes are Contained in a Plane

The two methyl C_3 axes define a plane in the Cartesian space. The orientation of interest here is the one where this plane contains also the direction of $\vec{H}_o$. We distinguish here the case where the methyl groups are inequivalent. In this orientation, assuming the same proton labeling scheme as before, one finds that the equivalency of the intermethyl couplings are the same as in case (i). Thus, the dipolar Hamiltonian is of the form:

$$H_D = u_1 \sum_{i,j} U_{ij}^{(1)} + u_2 \sum_{i',j'} U_{i'j'}^{(2)} + v \sum_{k,l} V_{kl} + w \sum_{m,n} W_{mn}.$$

and the indices run through the following sets:

$$(i,j) = \{(1,2), (2,3), (1,3)\}$$

$$(i',j') = \{(4,5), (5,6), (4,6)\},$$

and (k,l) and (m,n) run through the same sets as before.

(iii) Arbitrary Orientation

Excluding the particular orientations listed in the above two cases (i) and (ii), all other orientations fall in this class. The averaging of the intermethyl couplings is different and yields:

$$d_{14}=d_{25}=d_{36}$$

$$d_{15}=d_{26}=d_{34}$$

$$d_{16}=d_{24}=d_{35}.$$

Thus for an arbitrary orientation, the number of unique intermethyl couplings is three. The dipolar Hamiltonian is then of the form:

$$H_D = u_1 \sum_{i,j} U_{ij}^{(1)} + u_2 \sum_{i',j'} U_{i'j'}^{(2)} + v \sum_{k,l} V_{kl} + w_1 \sum_{m,n} W_{mn}^{(1)}$$

$$+ w_2 \sum_{m',n'} W_{m'n'}^{(2)}.$$

The indices run through the following sets:

$$(i,j) = \{(1,2), (2,3), (1,3)\}$$

$$(i',j') = \{(4,5), (5,6), (4,6)\}$$

$$(k,l) = \{(1,4), (2,5), (3,6)\}$$

$$(m,n) = \{(1,5), (2,6), (3,4)\}$$

$$(m',n') = \{(1,6), (2,4), (3,5)\}$$

The number of unique intramethyl and intermethyl couplings are displayed in Table 6.1.

6.4 NMR PERMUTATION GROUP OF NON-RIGID MOLECULES

The commutability of I_z and H implies that the Hamiltonian in the eigenbasis of I_z is already in block diagonal form according to the Zeeman quantum number m. By finding the symmetry group of the spin system, each Zeeman block can be further block diagonalized according to the irreducible representations of the symmetry group. This reduces substantially the amount

Table 6.1

Number of unique dipolar couplings

		intramethyl	intermethyl
uncorrelated:	$(S_3 \times S_3) \wedge S_2$	1	1
	$S_3 \times S_3$	2	1
correlated:	D_{3h}	1	2
	S_3	2	2
	C_3	2	3

of time and effort in diagonalizing the Hamiltonian to solve for eigenenergies, and even more so when solving for the equation of motion of the density matrix.

The objective is to find all operations that leave the spin Hamiltonian invariant. This defines the symmetry group of the Hamiltonian. The following procedure for group determination applies also to rigid systems:

1. Find equalities among dipolar couplings. This contains the symmetry of the dipolar Hamiltonian, including the motionally averaged symmetry as well as the spacial symmetry of the molecule. Form sets of equal dipolar couplings $\Omega_k = \{(i,j): d_{ij}=d_k\}$, where d_k represents the unique coupling constant for the set Ω_k.

2. Find all permutations of labels such that the dipolar couplings remain in the same set. These permutations are the elements of the symmetry group of the dipolar Hamiltonian:

$$G = \{P_r : P_r\Omega_k = \Omega_k\},$$

where

$$P_r\Omega_k \equiv \{P_r d_{ij} = d_{mn} : d_{ij} \text{ and } d_{mn} \text{ are both in } \Omega_k\}.$$

One must be careful to locate <u>all</u> symmetry operations. It is more likely the case that a symmetry operation is missed, and <u>more</u> transition lines are predicted than is really the case.

3. Given the identity of the group, the goal is to ultimately determine the energy level diagram according to the irreducible representations of the group. This can be accomplished by calculating the coefficients of generating functions of wreath products,[3,4] or by obtaining the character table of the group and decomposing constructed reducible representations of the Zeeman manifolds into the group's irreducible representations.

Often it is difficult to identify the group even when the elements of the group are known. One may use elementary group theory, i.e. construct a multiplication table of the elements, extract the classes and subgroups from this table, etc., and eventually construct the character table. This is usually a difficult problem. Sometimes through recognition one may find an isomorphism[5] with a known group and the obtainment of the group's character table is automatic, since isomorphic groups have identical character tables. Fortunately, there is a systematic approach to group determination of nonrigid molecules that involves decomposing a larger group into products of smaller groups, which are easier to handle.

Two types of products are relevant, the direct product and the semidirect product. The conditions in which they are applicable are discussed below.

A direct product can be formed between two groups

only if they commute. An obvious case to recognize is the following. Physically, if two subgroups involve permutations of labels only between disjoint parts of the molecule, and no other operations in the group will connect the two subgroups, then these parts of the molecules can be considered as separate entities. The operations on separate entities commute, and a direct product can be formed.

Semidirect products is used when one of the subgroups is the set of all operations that permute entire identical molecular parts, but that do not involve any permutations within the molecular parts.[7,8] Note that the frame subgroup does not commute with the internal subgroups.

It is useful to realize that all NMR semidirect product groups of spin systems undergoing uncorrelated internal motion can be categorized as generalized wreath products. Wreath products are a subset of semidirect products. In general for nonrigid systems, the molecular symmetry group can be decomposed into a semidirect product of internal torsional subgroups and a skeletal frame subgroup. When a frame subgroup which permutes a set of identical rotors can be defined, it can be decomposed into a wreath product.[5] When more than one set of rotors are to be permuted, the generalized wreath product should be used.[6]

When the molecule is undergoing correlated

internal motion, the group is isomorphic to a point group. More specifically, the subgroup for the parts of the molecule that move in a relative manner are isomorphic to point groups.

As an example, consider the para-disubstituted biphenyl molecule $X-C_6H_4-C_6H_4-Y$.[9] At room temperature rapid torsional motion occurs about the phenyl-phenyl bond. We will analyze the composition of its symmetry group based on the above concepts. Each phenyl ring has C_{2v} symmetry. Juxtaposed to another phenyl ring, its symmetry is reduced to C_2. If the para-substituents X and Y distort the phenyl structures inequivalently, then the group of the whole molecule is just the direct product $C_2 \times C_2$, which is isomorphic to D_2. If the para-substituents distort the phenyl structure equivalently, then an additional subgroup, that contains the permutation of the two phenyl rings, must be included. This group C_2 does not commute with either of the phenyl C_2's nor with their direct product. The group for the symmetrically disubstituted biphenyl molecule is $(C_2 \times C_2) \hat{} C_2$, which can be shown to be isomorphic to D_4. Here the symbol $\times$ represents a direct product, and $\hat{}$ represents a semidirect product.

Finally, we consider the importance of separation of motional time scales. To cite an example, consider the n-hexane molecule, $CH_3(CH_2)_4CH_3$. Suppose the hexane molecule is undergoing slow conformational

changes but rapid torsional motions about the C-C bonds. A different symmetry group may exist for each conformation. Each conformation must be considered as a separate motionally averaged nonrigid specie, each contributing individually to the NMR spectrum. If the hexane molecule is also undergoing rapid conformational changes, then the molecule is considered as one specie which is averaged over the conformations as well as the torsional motions.

6.5 DETERMINATION OF THE HAMILTONIAN SYMMETRY GROUP

Molecules undergoing rapid internal motion must be treated with group theory appropriate for nonrigid systems, as discussed in the previous section. As the environment of the spin system changes, so may the symmetry group of the Hamiltonian. Specifically, if one is dealing with a single crystal, as the orientation changes, the Hamiltonian changes and the symmetry of the Hamiltonian may change. In the case of two coupled methyl groups, there are five symmetry groups to consider. We demonstrate the determination of the Hamiltonian group on the different motional cases.

6.5.1 Uncorrelated Equivalent Methyl Groups

The group for the case of an equivalent pair of methyl groups undergoing uncorrelated motion is G =

$(S_3 \times S_3') \wedge S_2$. The prime on the second subgroup allows differentiation between the two methyl groups. The notation S_n represents the group of permutation of n identical objects (nuclei). In wreath notation, $G = S_2[S_3]$. The elements of S_3, S_3', and S_2 are listed below:

S_3

(1)(2)(3)

{(12), (23), (13)}

{(123), (132)}

S_3'

(4)(5)(6)

{(45), (56), (46)}

{(456), (465)}

S_2

(1)(2)(3)(4)(5)(6)

(14)(25)(36)

The notation $(a_1\ a_2\ \ldots\ a_p)$ represents a cyclic permutation of p objects, i.e. a_1 becomes a_2, a_2 becomes a_3, ..., and a_p becomes a_1. The above permutations can be related to point group operations. As examples, the permutation (123) has C_3 character and (12) has C_2 character on an individual

methyl group.

There are a total of $(6\times6)\times2=72$ elements in the group $(S_3\times S_3')\wedge S_2$. The construction of the group G in terms of products of smaller groups can be formulated in the following manner. S_3 and S_3' are obvious subgroups; they represent the rapid reorientations of individual methyl groups. All the elements of the S_3 commute with all the elements of S_3' since they permute disjoint sets of nuclear labels. One can then form a direct product $S_3\times S_3'$, which is also a subgroup of G. The product of $S_3\times S_3'$ with S_2 is a semidirect product since S_2 does not commute with either S_3 and S_3'.

The character table of $(S_3\times S_3)\wedge S_2$ can be obtained from the subgroups S_3 and S_2, as prescribed in many references.[7,8] However, we will utilize the identity of a pair of coupled methyl groups to gaseous ethane, of which the character table has already been derived.[10] Given the character table, projection operators are used to obtain the energy level diagram according to the irreducible representations of G, up to the number of states for each Zeeman manifold.

6.5.2 Uncorrelated Inequivalent Methyl Groups

When the methyl groups are inequivalent and uncorrelated in motion, the S_2 subgroup present in the previous group that characterizes the symmetry of two identical rotors is removed. The appropriate group is

then $S_3 \times S_3$. The elements of the group can obtained from a direct product of S_3 with S_3'.

6.5.3 Correlated Equivalent Methyl Groups

If the methyl groups are correlated and equivalent, the operations on this spin system are isomorphic to those that are performed on cyclopropane. That is, the protons in both cases are restricted to move in a relative manner. The group for this case is D_{3h}. The elements of this group are:

(1)(2)(3)(4)(5)(6)

{(123)(456), (132)(465)}

{(12)(45), (23)(56), (13)(46)}

(14)(25)(36)

{(153426), (162435)}

{(15)(24)(36), (14)(26)(35), (16)(25)(34)}

6.5.4 Correlated Inequivalent Methyl Groups in a "Planar" Orientation

If the methyl groups are inequivalent and in an orientation such that the methyl C_3 axes and $\vec{H}_o$ lie in a plane, then the appropriate group is S_3. That is, since the methyl groups are constrained to move together but are not interchangeable, this system acts isomorphically as a single methyl group, and thus its symmetry group must be the same as that of a methyl group. The elements of the S_3 group are:

(1)(2)(3)(4)(5)(6)

{(123)(456), (132)(465)}

{(23)(56), (13)(46), (12)(45)}

6.5.5 Correlated Inequivalent Methyl Groups at an Arbitrary Orientation

For an arbitrary orientation of the methyl C_3 axes but with correlated motion, the group is C_3. This group has the lowest symmetry of all the cases. It is easy to show that the elements of the C_3 group are:

(1)(2)(3)(4)(5)(6)

(123)(456)

(132)(465)

The list of groups for all five cases are tabulated in Table 6.2.

6.6 EFFECT OF SPINNING OR MOLECULAR REORIENTATION ABOUT A FIXED AXIS

Molecular reorientation is of particular concern in a liquid crystalline environment where solutes have rotational freedom, although usually it is axially restricted. Molecular reorientation can also occur in a solid matrix if spacial symmetry allows it.

To treat this matter, we first determine the effect of spinning on an internuclear vector $\vec{r}$. Figure 6.3 shows the vector $\vec{r}$ being spun about an axis $\vec{\omega}_s$ with

Table 6.2

Symmetry groups of two interacting methyl groups

	equivalent	inequivalent
uncorrelated:	$(S_3 \times S_3) \wedge S_2$	$S_3 \times S_3$
correlated:	D_{3h}	S_3
		C_3

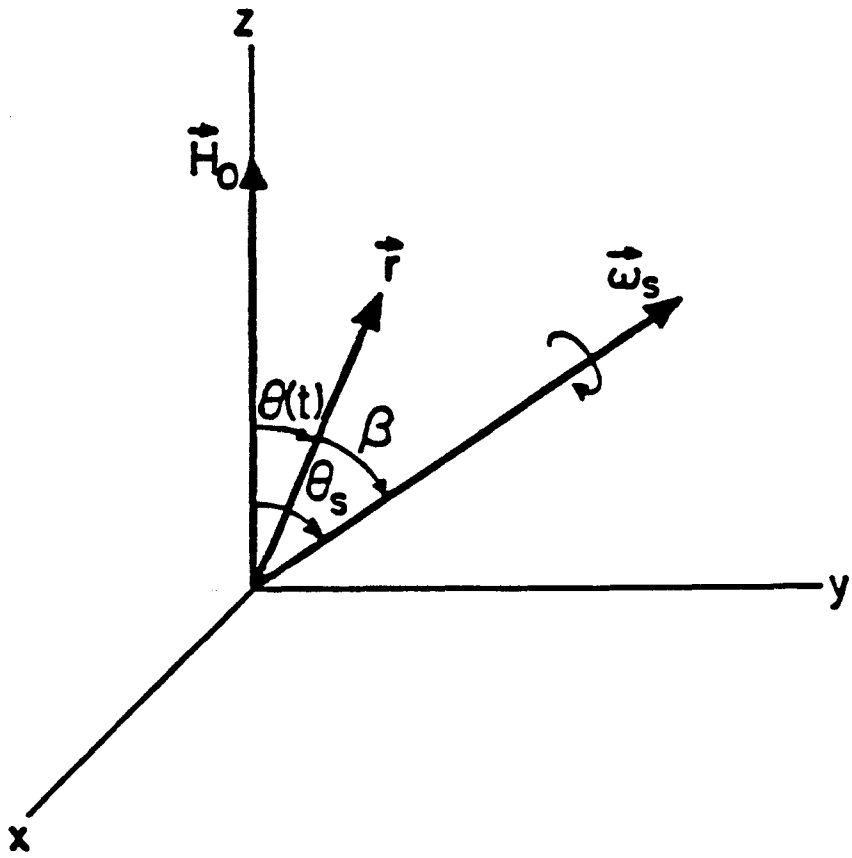

XBL 8210-6728

Figure 6.3 A vector diagram showing the relevant angles when an internuclear vector $\vec{r}$ is being spun about an axis at a rate ω_s. The spinning axis has a fixed angle θ_s relative to the external magnetic field $\vec{H}_o$, and the vector $\vec{r}$ has a fixed angle β relative to the spinning axis. As a result of spinning, the angle θ that $\vec{r}$ makes with $\vec{H}_o$ is time-dependent.

an angle θ with respect to $\vec{H}_o$ and an angle β with respect to $\vec{\omega}_s$. Assuming the rate of spinning ω_s is much faster than the inverse of the coupling, the time-average value of $\cos^2\theta(t)$ is given by:[11]

$$\overline{\cos^2\theta(t)} = \cos^2\beta(\cos^2\theta_s - \tfrac{1}{2}\sin^2\theta_s) + \tfrac{1}{2}\sin^2\theta_s .$$

If two internuclear vectors $\vec{r}_{ij}$ and $\vec{r}_{kl}$ of equal magnitude in this spinning system have angles β_{ij} and β_{kl} such that

$$\cos^2\beta_{ij} = \cos^2\beta_{kl},$$

$$\text{or} \quad \beta_{ij} = \pm\beta_{kl} + p\pi \quad (p=0, \pm1, \pm2, \ldots) \qquad (1)$$

then the two coupling constants $\bar{d}_{ij}$ and $\bar{d}_{kl}$ are made equal.

The case of two methyl groups has three axes of rotation: the two C_3 axes and the spinning axes. To treat the combined motions, it is convenient to relate the spinning axis with respect to a "molecular" coordinate system defined by the two C_3 axes.

Figure 6.4 depicts the methyl groups as planar rotors with their C_3 axes at some orientation with respect to $\vec{H}_o$. The a-axis is defined to have the highest symmetry; it bisects the two C_3 axes and is contained in the same plane. The b-axis lies perpendicular to the a-axis in this plane, and the c-

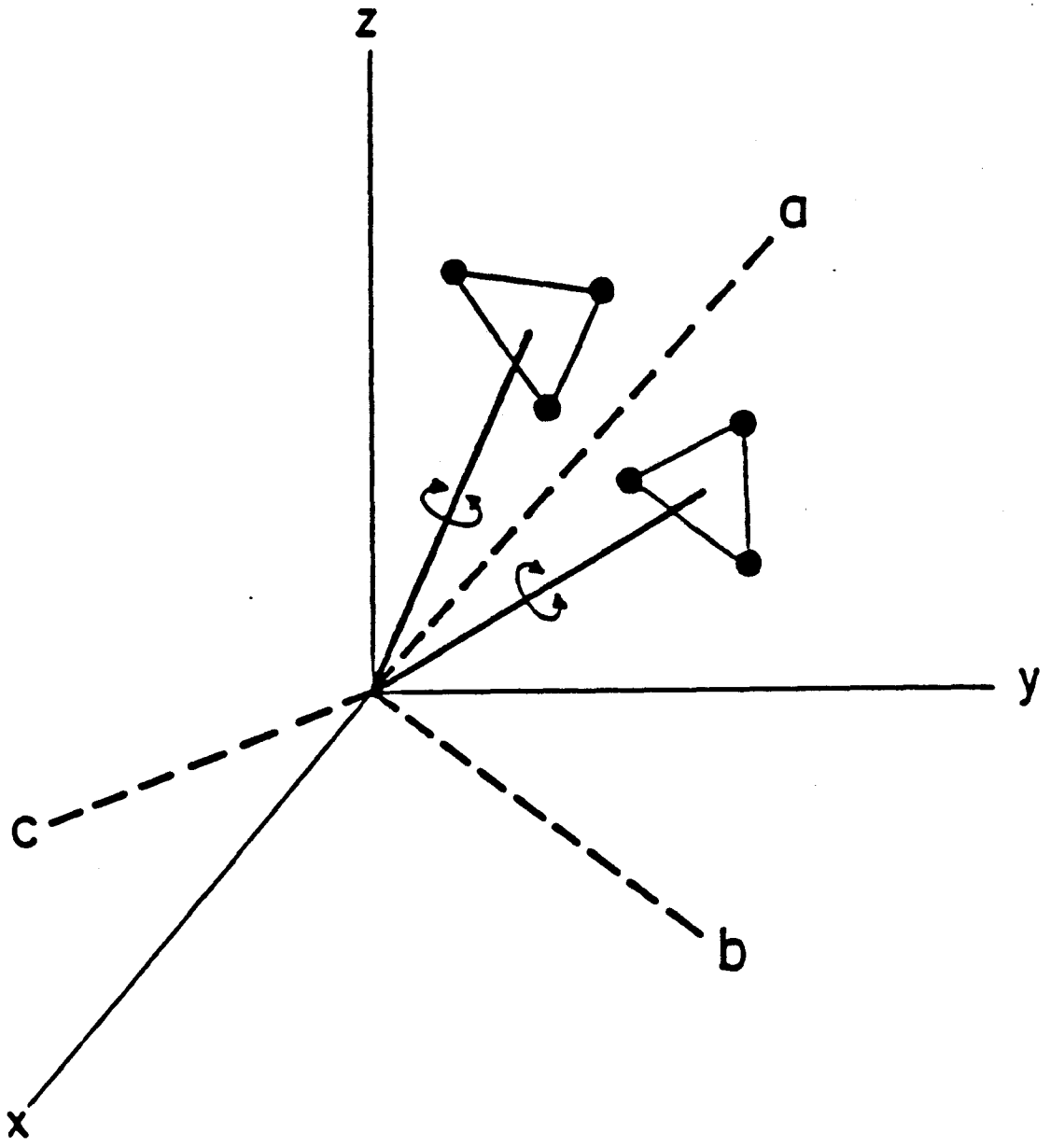

XBL 8210-6729

Figure 6.4 Definition of the molecular frame (abc), shown here with the laboratory frame (xyz). The plane defined by the two C_3 axes will be labeled the ab-plane, with the a-axis (the axis of highest symmetry) bisecting the two C_3 axes. The c-axis is perpendicular to this plane.

axis is perpendicular to this plane.

Using Eq. (1) and some elementary geometry arguments, the following conclusions are drawn and are applicable regardless of the direction of the C_3 axes with respect to $\vec{H}_o$:

(1) If the spinning axis is contained in the ac-plane or bc-plane, then the two methyl groups are made equivalent. Any other spinning axis will make the methyl groups inequivalent. The groups that can arise from spinning at this axis are $(S_3 \times S_3)\hat{}S_2$ if uncorrelated and D_{3h} if correlated.

(2) If the methyl groups are uncorrelated, spinning about an axis anywhere but in the ac- or bc-plane will leave the methyl groups inequivalent. The group that results is $S_3 \times S_3$.

(3) Consider correlated methyl groups. Suppose the C_3 axes are parallel and the two methyl groups are mirror images. Spinning about an axis in the ab-plane, but excluding the a- and b-axis, will result in the group S_3. If there is any deviation from this ideal geometry, the S_3 group will never occur and the C_3 group is the appropriate one. The C_3 group also encompasses any spinning axis not contained in the ab-, ac-, or bc-planes.

6.7 ENERGY LEVEL DIAGRAMS

The corresponding energy level diagrams are in

Figs. 6.5 - 6.9. Group theory allows the determination of the energy level diagram up to the number of levels in each irreducible representation of a given Zeeman quantum number. It requires no quantitative values of the couplings, only the equivalence in the couplings, and thus cannot lead to information on the eigenenergies. Further determination of the energy level diagram requires diagonalization of the Hamiltonian within each subblock, or interpretation of the experimental dipolar spectrum, depending on one's objective.

Correlated systems have a lower symmetry than uncorrelated systems. The uncorrelated representations must be reducible in correlated representations. By decomposing the uncorrelated representations into correlated irreducible representations, one can find how uncorrelated states transform under the correlated group. This decomposition shows how the levels split under a small perturbation. The method of decomposition is called subduction of a higher symmetry group into a lower symmetry group. The reverse is called an induction. To perform a subduction, one first finds the correspondence between classes of the two symmetry groups and thereby obtain the character of the higher symmetry group's representations for each of the classes of the lower symmetry group. With the great orthogonality theorem, one can decompose the

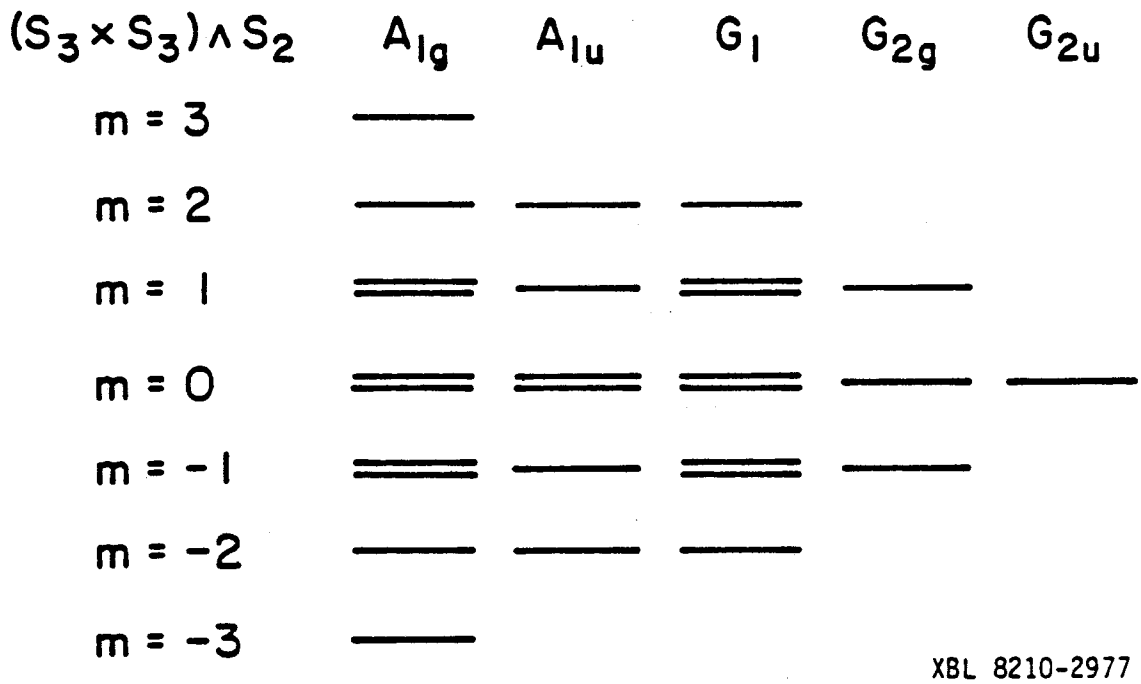

Figure 6.5 Energy level diagram for $(S_3 \times S_3) \wedge S_2$: uncorrelated equivalent methyl groups.

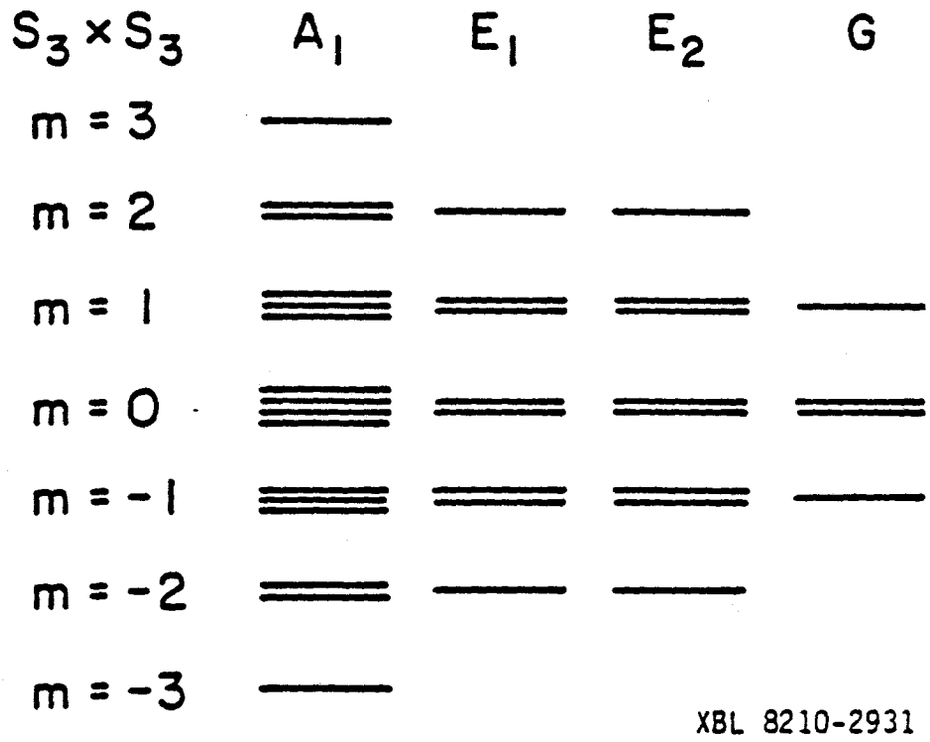

Figure 6.6 Energy level diagram for $S_3 \times S_3$: uncorrelated inequivalent methyl groups.

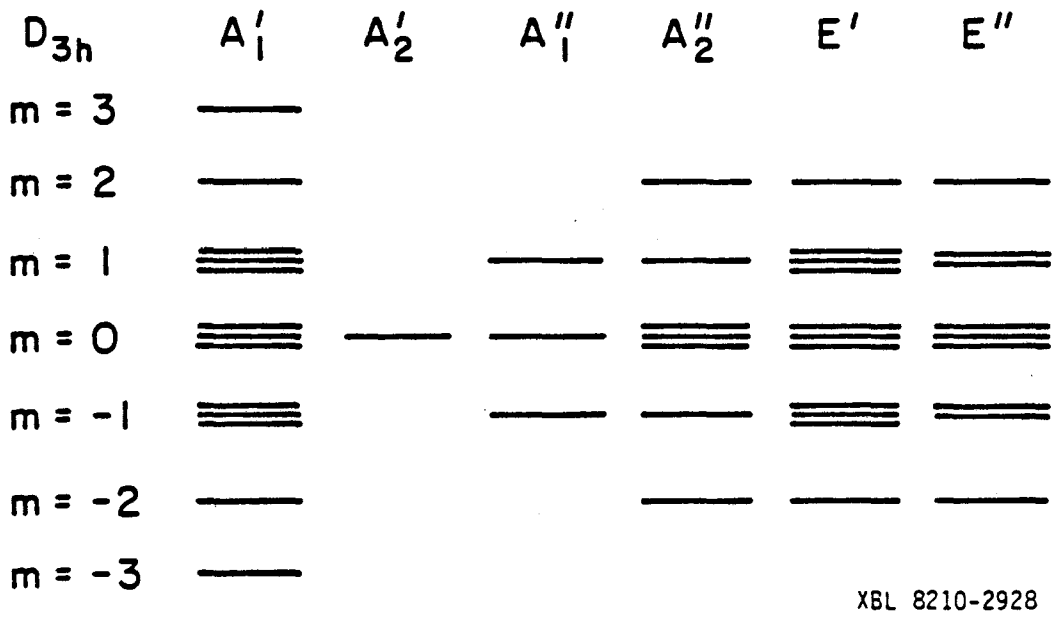

Figure 6.7 Energy level diagram for D_{3h}: correlated equivalent methyl groups.

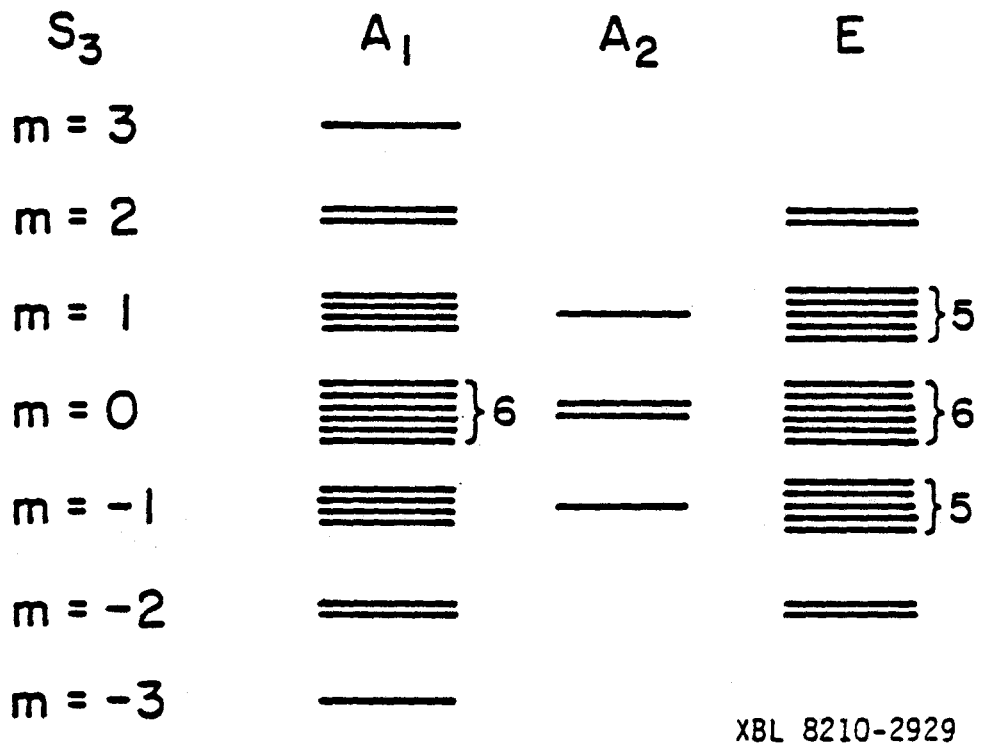

Figure 6.8 Energy level diagram for S_3: correlated, inequivalent methyl groups with the two C_3 axes and $\vec{H}_o$ contained in the same plane.

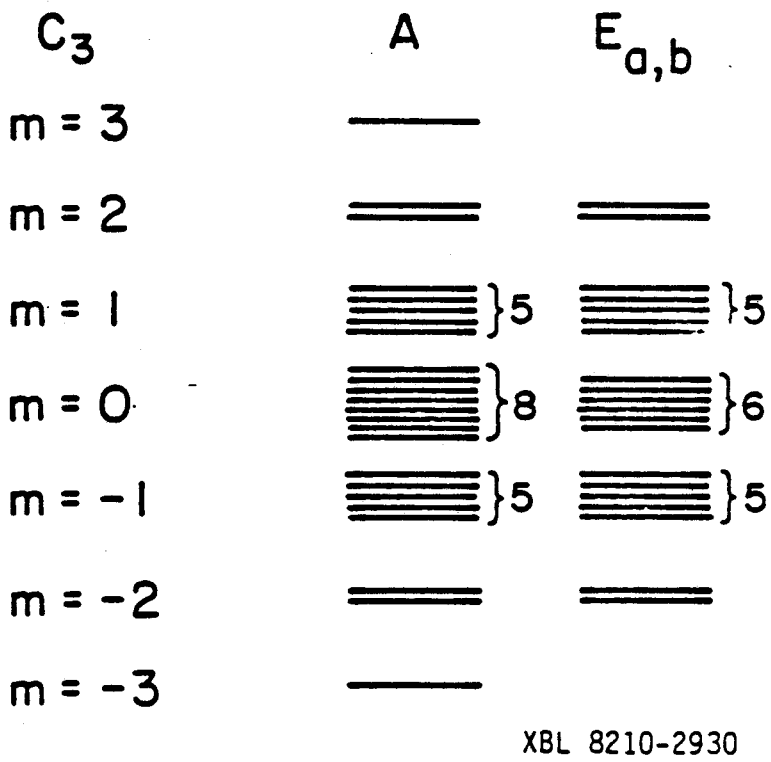

Figure 6.9 Energy level diagram for C_3: correlated inequivalent methyl groups at an arbitrary orientation.

representations into a linear combination of the irreducible representations of the lower group.

"Coalescence diagrams" describing the convergence and separation of representations in the transition region are shown in Figs. 6.10 - 6.12. Note that it is not possible to subduce or induce energy level diagrams between equivalent and inequivalent methyl groups. This is because equivalent methyl groups, whether uncorrelated or correlated, contain a C_2 type operation that is not present in inequivalent methyl groups, and complete correspondence between classes can never be achieved.

Coalescence diagrams can also be found between correlated methyl groups, and between uncorrelated methyl groups. Such diagrams show the change in the symmetry of the Hamiltonian with changes in the crystal orientation. These diagrams are in Figs. 6.13 - 6.16.

6.8 MQ SPECTRA

From the energy level diagram, one can count the number of transitions that occur for a given quantum order, excluding accidental degeneracy due to poor spectral resolution. Table 6.3 lists the number of transition lines for each quantum order and for each of the limiting cases. The NQ (6Q) order always contains one central line with no dipolar information (to first order) and is excluded from the table. The 5-quantum

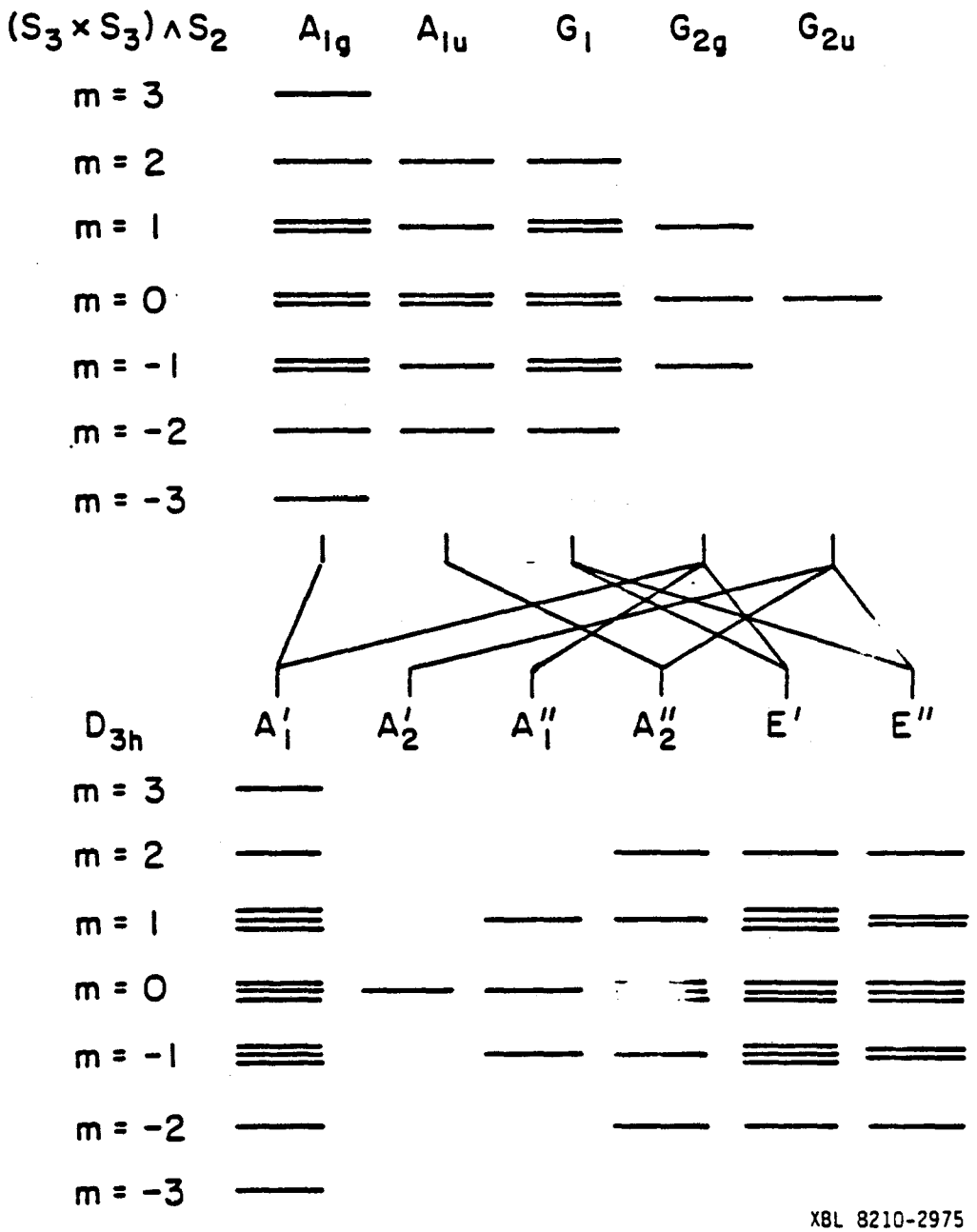

Figure 6.10 Coalescence diagram from uncorrelated, equivalent methyl groups $[(S_3 \times S_3)\hat{}S_2]$ to correlated equivalent methyl groups (D_{3h}).

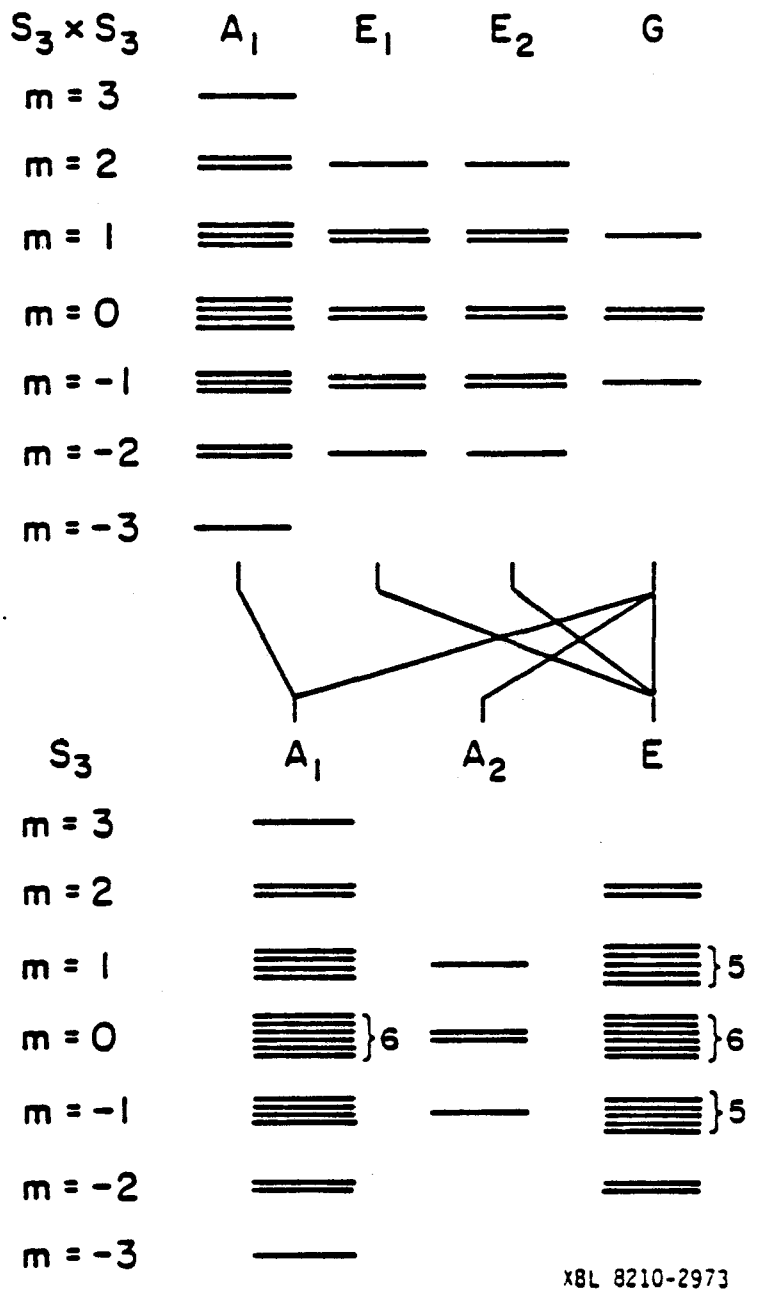

Figure 6.11 Coalescence diagram from uncorrelated inequivalent methyl groups ($S_3 \times S_3$) to correlated inequivalent methyl groups (S_3).

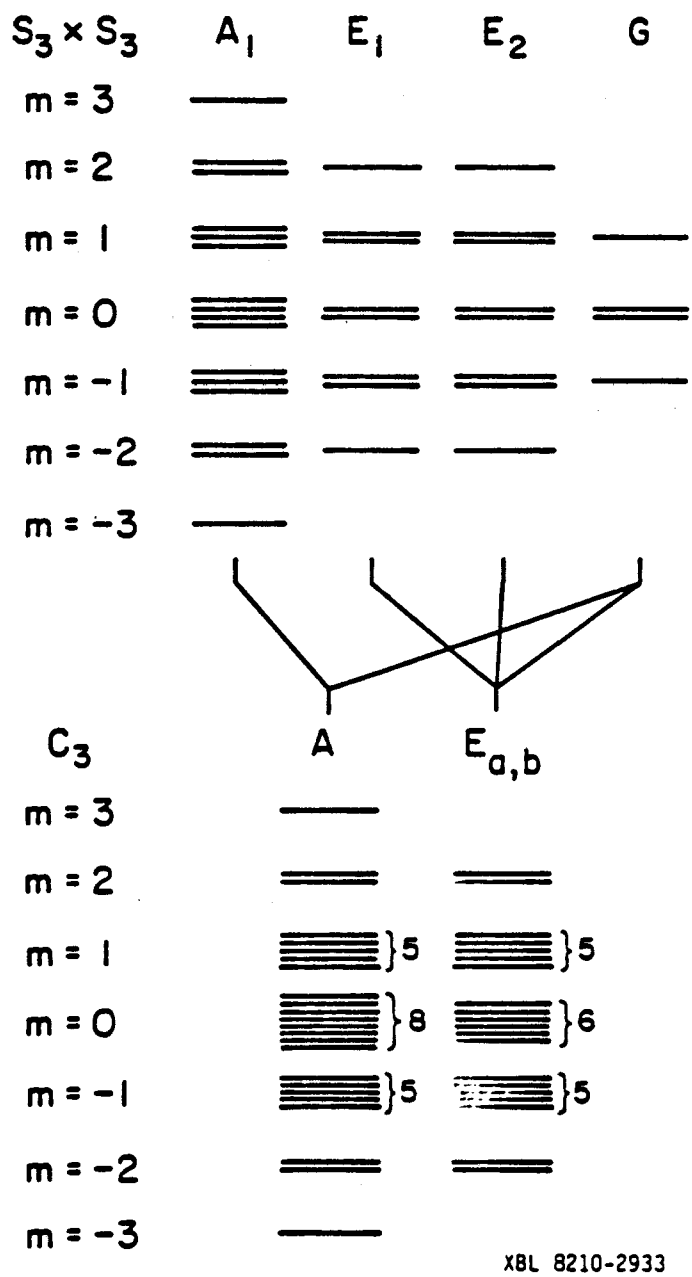

Figure 6.12 Coalescence diagram from uncorrelated inequivalent methyl groups ($S_3 \times S_3$) to correlated inequivalent methyl groups (C_3).

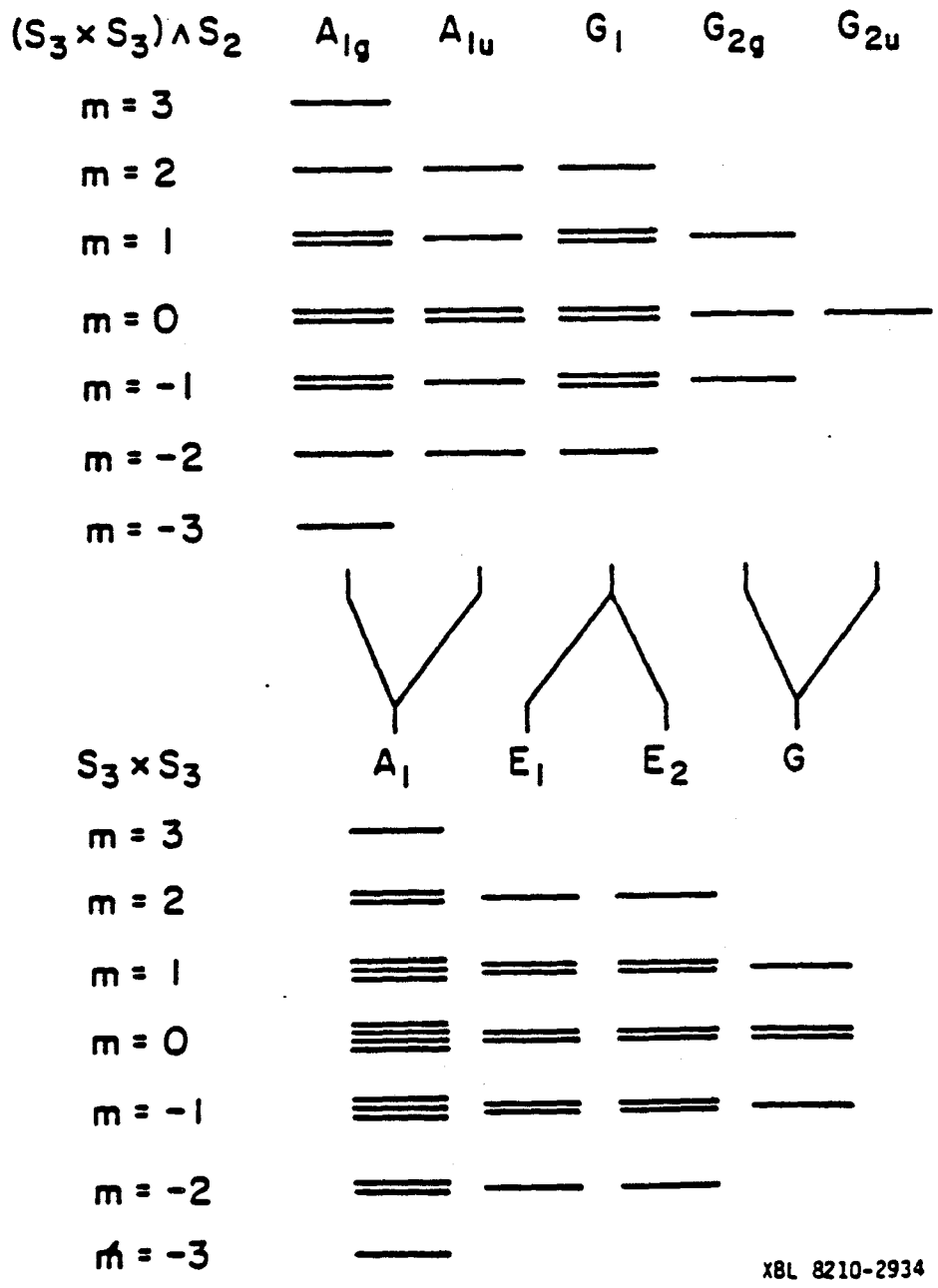

Figure 6.13 Coalescence diagram from equivalent uncorrelated methyl groups $[(S_3 \times S_3) \wedge S_2]$ to inequivalent uncorrelated methyl groups $(S_3 \times S_3)$.

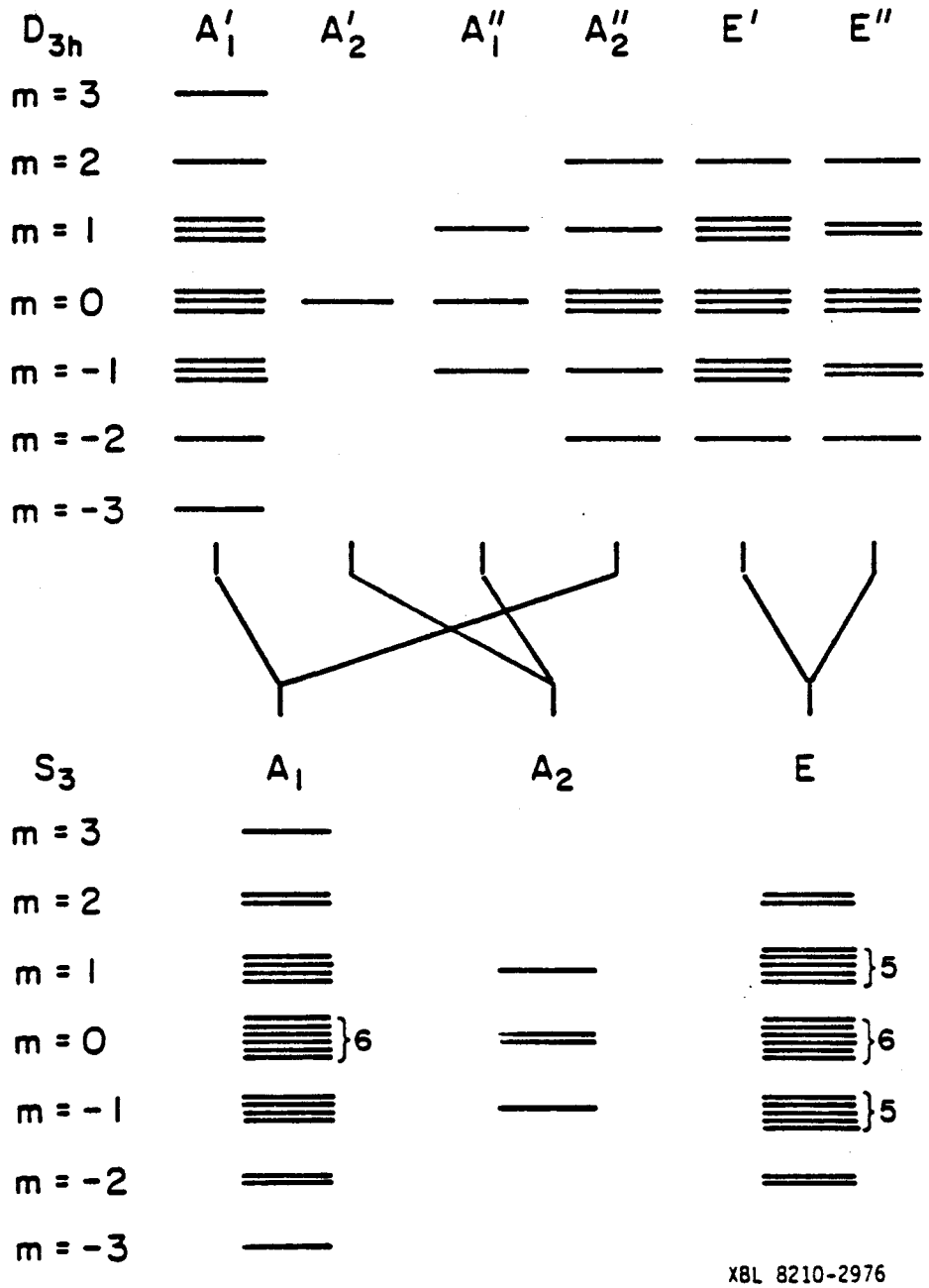

Figure 6.14 Coalescence diagram from equivalent correlated methyl groups (D_{3h}) to inequivalent correlated methyl groups (S_3).

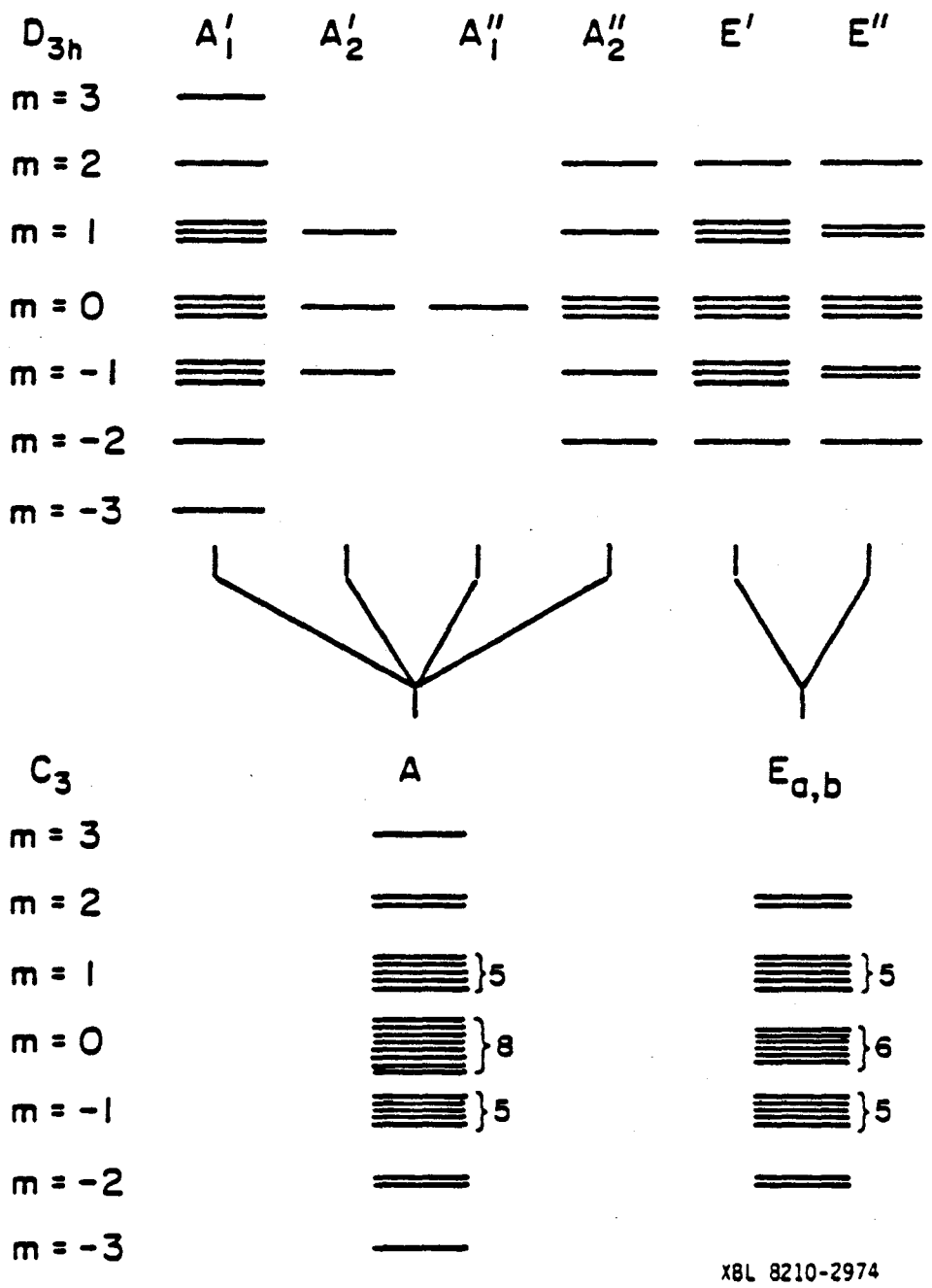

Figure 6.15 Coalescence diagram from equivalent correlated methyl groups (D_{3h}) to inequivalent correlated methyl groups (C_3).

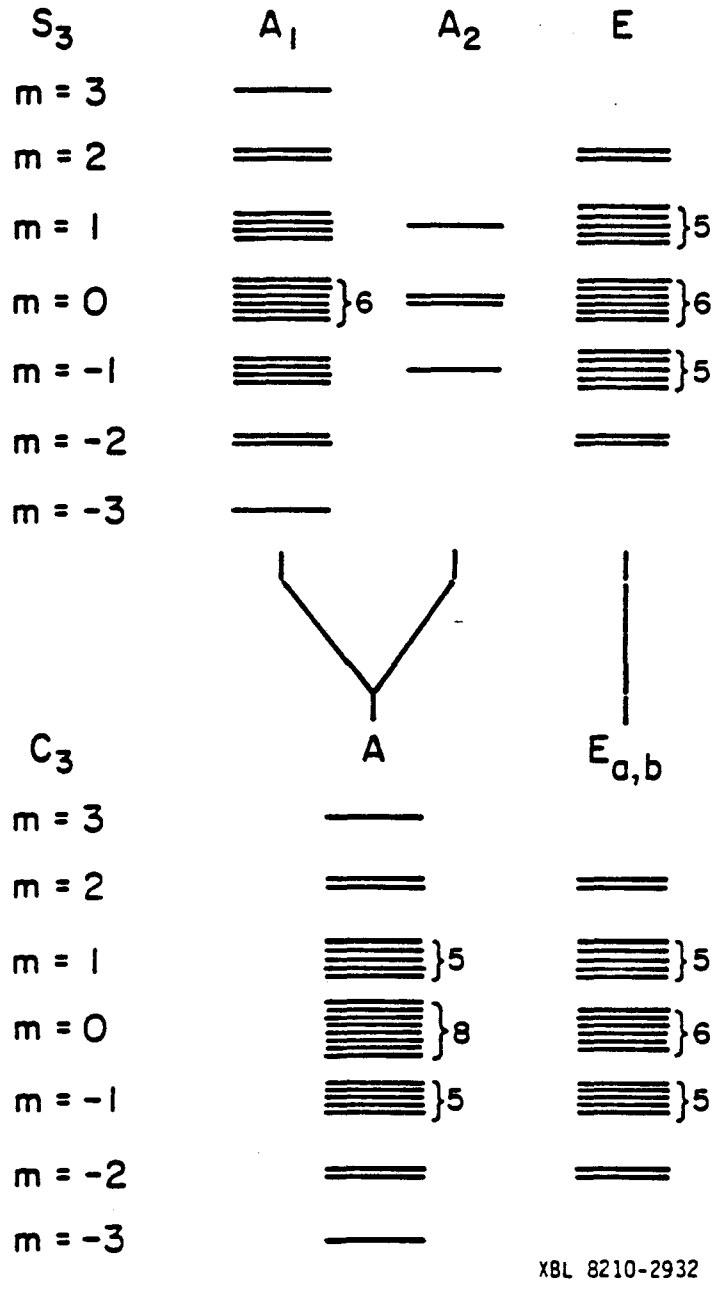

Figure. 6.16 Coalescence diagram between the groups S_3 and C_3, both of which correspond to correlated, inequivalent methyl groups but at different crystal orientation.

Table 6.3

Number of transitions in the MQ spectrum for each of the symmetry groups

	uncorrelated		correlated		
	$S_3 \times S_3 \hat{} S_2$	$S_3 \times S_3$	D_{3h}	S_3	C_3
5Q*	1	2	1	2	2
4Q*	2	4	3	6	7
3Q*	7	14	12	24	28
2Q*	13	20	22	36	53
1Q*	20	34	38	60	92
0Q†	6	15	19	36	65

* The entry corresponds to the number of doublets. The 4Q and 2Q orders have in addition a strong central line. Note that the nQ ($n \neq 0$) orders are symmetric about the order center.

† The entry corresponds to the number of lines. The 0Q order is not symmetric about the order center.

order offers no differentiation between correlated and uncorrelated motion. (It does tell however whether the methyl groups are equivalent.) The 4-quantum spectrum is sensitive to two-body correlations, and is able to distinguish the motions.

6.9 INTERMEDIATE REGION - EXCHANGE THEORY

Suppose we begin with a pair of correlated methyl groups at very low temperature. The methyl protons are undergoing fast torsional motions but always at a fixed relationship with one another. As the temperature increases, an occasional slippage of gears can occur, and the methyl groups change configurations. This slippage of gears can occur in either sense; i.e. one of the methyl gears can slip in the clockwise or counterclockwise direction (Fig. 6.17). This occasional slipppage in either sense can be envisioned as a hopping between three equivalent sites (configurations). Thus we can apply exchange theory to this process.

6.9.1 Exchange Operators

Let P represent a slippage of gears in one sense. Then its inverse P^{-1} must be the slippage in the opposite sense. Properties of the permutation operators P and P^{-1} are:

(1) $P^3 = P^{-3} = 1$,

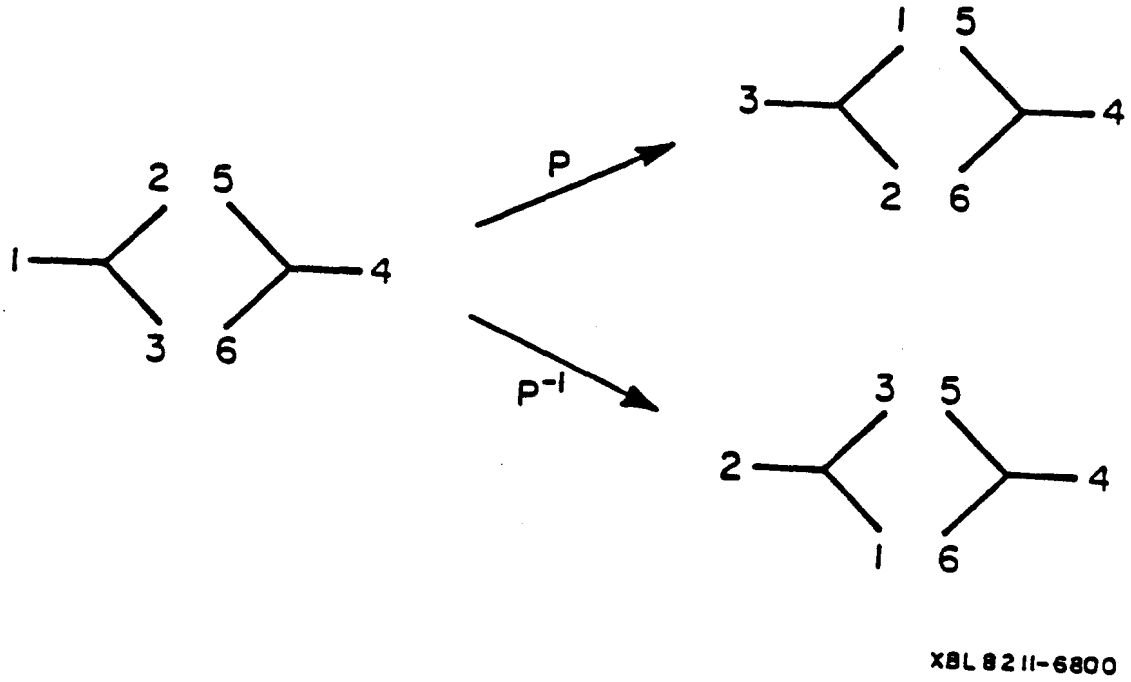

Figure 6.17 In becoming uncorrelated, one of the methyl groups can slip in a clockwise direction or in a counterclockwise direction.

(2) $P^2 = P^{-1}$,

(3) P, P^{-1} are real, nonsymmetric (non-Hermitian) and non-unitary,

(4) $(P + P^{-1})$ is real, symmetric (Hermitian) and non-unitary.

6.9.2 Master Equation with Exchange

Let ρ be the initial density operator. The form of the density operator after exchange P can be determined in the following manner. Let ψ be the wave function describing the initial state of the spin system. The density matrix ρ is defined as $\psi\psi^\dagger$, where here ψ is written as a column vector. The wavefunction after exchange by definition is $P\psi$. This implies that the density operator after exchange is $(P\psi)(P\psi)^\dagger = P\psi\psi^\dagger P^\dagger = P\rho P^\dagger$. The change in the density matrix as a result of exchange is then $P\rho P^\dagger - \rho$.

We assume that both senses of slippage are random independent processes with the same rate of occurrence characterized by τ_e^{-1}.[12] Because the exchanges are between equivalent sites, the Hamiltonians before and after exchange are the same. Neglecting all other relaxation effects, the master equation governing the evolution of the density matrix is:

$$\frac{d\rho}{dt} = i[\rho,H] + \frac{P\rho P^\dagger - \rho}{\tau_e} + \frac{P^{-1}\rho P^{-1\dagger} - \rho}{\tau_e}$$

In superoperator representation, this is written as:

$$\frac{d}{dt}\begin{bmatrix} \rho_{11} \\ \rho_{12} \\ \vdots \\ \rho_{kk} \end{bmatrix} = \begin{bmatrix} A_{11,11} & A_{11,12} & \cdots\cdots & A_{11,kk} \\ A_{12,11} & A_{12,12} & \cdots\cdots & A_{12,kk} \\ \vdots & \vdots & & \vdots \\ A_{kk,11} & A_{kk,12} & \cdots\cdots & A_{kk,kk} \end{bmatrix} \begin{bmatrix} \rho_{11} \\ \rho_{12} \\ \vdots \\ \rho_{kk} \end{bmatrix}$$

where here $k=2^N \times 2^N$. Compactly written, this is

$$\frac{d}{dt}\vec{\rho} = \hat{A}\vec{\rho}. \tag{2}$$

The superoperator $\hat{A}$ is composed of the Liouville operator $\hat{H}$ and an exchange superoperator $\hat{X}$:

$$\hat{A} = i\hat{H} + \hat{X}. \tag{3}$$

Equation (2) represents a set of $2^N \times 2^N$ simultaneous linear differential equations:

$$\frac{d}{dt}\rho_{\alpha\beta} = \sum_{\gamma,\delta}[i(H_{\delta\beta}\delta_{\gamma\alpha} - H_{\alpha\gamma}\delta_{\delta\beta}) + \frac{1}{\tau_e}(P_{\alpha\gamma}P^{\dagger}_{\delta\beta} + P^{-1}_{\alpha\gamma}P^{-1\dagger}_{\delta\beta})]\rho_{\gamma\delta} - \frac{2}{\tau_e}\rho_{\alpha\beta}.$$

where $(\alpha,\beta) = \{(1,1), (1,2), \ldots, (2,1), (2,2), \ldots, (k,k)\}$. The matrix elements of the superoperators can be related to those of the Heisenberg operators:

$$\hat{H}_{\alpha\beta,\gamma\delta} = H_{\delta\beta}\delta_{\gamma\alpha} - H_{\alpha\gamma}\delta_{\delta\beta},$$

$$\hat{X}_{\alpha\beta,\gamma\delta} = \frac{1}{\tau_e}[P_{\alpha\gamma}P^{\dagger}_{\delta\beta} + P^{-1}_{\alpha\gamma}P^{-1\dagger}_{\delta\beta} - 2\delta_{\alpha\beta,\gamma\delta}].$$

When solving for eigenvalues of the matrix A, properties of the superoperators to recognize are:

(1) $\hat{H}$ is Hermitian,

(2) $\hat{X}$ is real non-symmetric,

(3) Thus $\hat{A}$ is complex non-Hermitian.

A simplification results from the commutation of I_z with the exchange operators:

$$[P, I_z] = [P^{-1}, I_z] = 0.$$

This means that the Zeeman quantum number m is conserved under permutations (exchanges) P and P^{-1}. Alternatively stated, P and P^{-1} do not mix blocks of different m. Thus, each Zeeman manifold can be treated separately.

The exchange operators P and P^{-1} in general do mix states belonging to different irreducible representations. As evident from the coalescence diagrams of Figs. 6.10 - 6.12, this is to be expected since the states rearrange in the transition between the two energy level diagrams. However, some simplification do result and the symmetry-adapted-linear-combination[6] (SALC) basis will be adopted.

The solutions to the master equation are found by diagonalizing $\hat{A}$. The eigenvalues that result are

complex. Because the equations are linear, the solutions yield Lorentzian lineshapes with characteristic frequencies and linewidths. The imaginary part of the eigenvalue gives the frequency of transition, and the real part yields the exchange broadening $\Gamma = \pi/2$(full-width-half-maximum value). The phase of a transition is determined by the initial conditions, i.e. the phase factors of the prepared density matrix $\rho(t=0)$, where t refers to the evolution time.

Before performing a computer simulation, numerical values for the coupling constants are required. This takes us to the next section.

6.10 1,8-DIMETHYLNAPHTHALENE

The reasons for choosing 1,8-dimethylnaphthalene (1,8-DMN) for our studies are: (1) the methyl groups are sterically hindered, and (2) its crystallographic structure is known.[13] Presented below are some of the relevant structural information of this molecule in the single crystal form. Complete information is available from the structure parameters given in reference [13].

The crystal structure is monoclinic with four molecules per unit cell and lattice constants a=9.835Å, b=7.012Å, and c=16.114Å. The angles that a, b and c axes make with respect to one another are $\alpha=90°$,

β=124.35° and γ=90°. The crystallographic data presented in reference [13] are in fractional coordinates x, y, z as referred in this coordinate system. In order to determine an internuclear distance r_{ij}, the following formula should be used:

$$r_{ij}^2 = (x_i-x_j)^2a^2 + (y_i-y_j)^2b^2 + (z_i-z_j)^2c^2 + 2(x_i-x_j)(z_i-z_j)ab\cos\beta.$$

in Fig. 6.18 is the labeling scheme for 1,8-DMN molecule, consistent with reference [13]. In the minimum strain-energy configuration, the carbon skeleton of the 1,8-DMN molecule is planar. The methyl groups are in an eclipsed configuration where the outer methyl C-H bonds [C(11)-H(11C) and C(12)-H(12C)] lie roughly in the same plane as the aromatic frame. The amount of tilt of the outer C-H bonds out of the aromatic plane is 5° for the C(11)-H(11C) bond and -10.8° for the C(12)-H(12C) bond. Thus the two methyl groups are not quite mirror images.

The methyl C_3 axes are also slightly tilted out of this plane: the methyl(11) C_3 axis [C(1)-C(11) bond] deviates by 0.2°, and the methyl(12) C_3 axis [C(8)-(12) bond] deviates by -0.2°, which are negligible.

The methyl C_3 axes are not parallel; they are splayed outward to accomodate both methyl groups in such close proximity. Taking the C(9)-C(10) bond to be

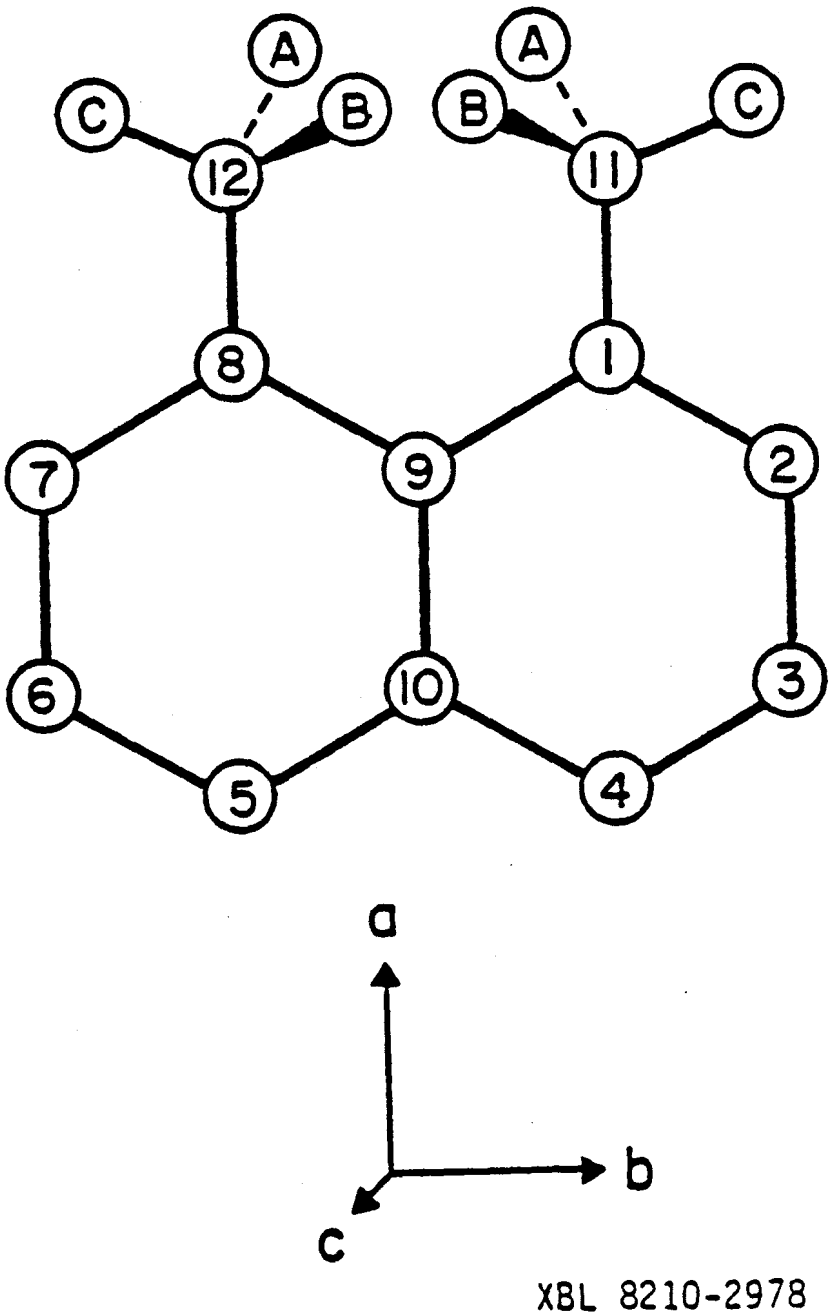

Figure 6.18 Molecular structure and the labeling scheme of 1,8-dimethylnaphthalene.

the axis of highest symmetry, the methyl(11) C_3 axis deviates by -7.4°, and the methyl(12) C_3 axis deviates by +7.4°.

In the equilibrium configuration, assuming the covalent radius of proton is 0.32Å, the clearance between the outer radii of the closest intermethyl protons is 1.32Å. The separation of the methyl C_3 axes are determined from the C(1)-C(8) distance (2.543Å) and the C(11)-C(12) distance (2.932Å). The effective activation barrier to methyl rotation for this molecule has been measured to be 3 kcal/mole.[14]

From Fig. 6.18, one observes that the aromatic protons H(2) and H(7) are significantly close to the methyl protons. The average distance of H(2) and H(7) with the methyl protons is 3.00Å. Another useful distance to know is the closest intermolecular proton-proton distance, which is 6.79Å. Both of these distances will be useful when estimating the rf power required for heteronuclear decoupling.

6.11 COMPUTER SIMULATION OF EXCHANGE PROCESS

We will choose one particular crystal orientation for discussion. The orientation chosen is where the methyl C_3 axes and H_o lie in the same plane and the polar angles of the C_3 axes with H_o are 78° and 92°. The methyl groups are inequivalent and the appropriate groups are $S_3 \times S_3$ if uncorrelated, and S_3 if

correlated. The dipolar coupling constants for this crystal orientation are:

$$u_1 = 10.858 \text{ kHz} \tag{4}$$

$$u_2 = 14.645 \text{ kHz}$$

uncorrelated: $v = 8.327$ kHz

correlated: $\begin{cases} v = 17.001 \text{ kHz} \\ w = 3.990 \text{ kHz.} \end{cases}$

The 5-quantum lines are unaffected by exchange. We will concern ourselves with the 4-quantum spectrum in the exchange process. The transitions of interest are between the $m=\pm 2$ to $m=\mp 2$ Zeeman manifolds, and $m=\pm 1$ to $m=\mp 3$ manifolds. We start with the correlated limit since it is easier to envision slippage of gears as an exchange process than the reverse situation.

The secular determinant can be constructed given the matrix elements of the Hamiltonian and the exchange operators in the SALC basis of the correlated symmetry group.

For simplicity we dictate that all coherences, or the elements of the prepared density matrix, assume the same initial phase and intensity. In the rotating frame and on resonance, only the dipolar Hamiltonian needs to be considered in the equation of motion [Eq. (2)].

6.11.1 Secular Determinant for $m=\pm 2$ to $m=\mp 2$ Manifolds

The $A_1(m=\pm 2)$ manifolds are unaffected by

exchange. These n=4 transitions remain sharp with no frequency shift.

The E manifold is affected by exchange. The secular determinant is 16×16 and will not be shown here. The actual construction was done trivially within a computer program, listed in appendix 6.A. The solutions to the secular determinant were derived from running a package computer program EIGCC from the IMSL library. EIGCC is an iterative routine for diagonalizing a general complex matrix.

6.11.2 Secular Determinant for m=±1 to m=∓3 Manifolds

Only the A_1 manifold is involved. In general, the manifolds corresponding to different irreducible representations are mixed by P and P^{-1}. Note that although the $A_2(m=\pm 1)$ is mixed with the $A_1(m=\pm 1)$ states, the secular determinant is not. This exception occurs when transitions involve the extreme states A_1 $(m=\pm 3)$. The origin of this exception arises from the invariance of the extreme states to exchange. Thus the secular determinant for the 4-quantum order is also block diagonal with respect to the irreducible representations of the group. For the A_1 transitions, it is:

$$\begin{vmatrix} a-\lambda & 0 & e & f \\ 0 & b-\lambda & e & f \\ e & e & c-\lambda & g \\ f & f & g & d-\lambda \end{vmatrix} = 0$$

where

$$a = -i(\tfrac{3}{2}u_1 + v + 2w)$$
$$b = -i(\tfrac{3}{4}u_2 + v + 2w)$$
$$c = -i(u_1 + u_2 + 2w) - \tfrac{2}{\tau}$$
$$d = -i[\tfrac{5}{4}(u_1+u_2) + v + w] - \tfrac{1}{\tau}$$
$$e = -i\tfrac{1}{2}w$$
$$f = -i\tfrac{\sqrt{2}}{4}(v + w)$$
$$g = -i\tfrac{\sqrt{2}}{4}(u_1 + u_2) + \tfrac{\sqrt{2}}{\tau}.$$

With the insertion of the coupling constants listed in Eq. (4) into the program EXCH2 listed in appendix 6.A for the E manifold and EXCH1 in appendix 6.B for the A_1 manifold, the results are shown in Table 6.4. The sharp transition $A_1(m=\pm 2)$ to $A_1(m=\mp 2)$ at 13.722 kHz is excluded from this table. Since the 4Q spectrum is symmetric, only half of it is tabulated. The frequencies are measured from the center of the 4Q order. The lines that are broadened near the center (at 0 kHz) are also excluded from the table.

The data in Table 6.4 and including the $A_1(m=\pm 2)$ transitions are illustrated in Fig. 6.19. At τ_e=1 sec, the lines are fairly sharp and correspond to correlated motion. The most action occurs in the 0.1 - 2 msec range. As the rate of exchange increases, the E transition at 7 kHz mixes with the central E transitions, broadens and is shifted in frequency

Table 6.4

The frequencies (ν) and exchange broadenings (Γ) for the 4-quantum order : E(m=±2) to E(m=∓2) and A_1(m=±2) to A_1(m=∓2) transitions.

τ(sec)	ν(kHz)		Γ(kHz)
1×10^{-7}	60.235	(A_1)	0.003
	44.758	(A_1)	0.0001
	36.805	(A_1)	0.0002
1×10^{-4}	61.545	(A_1)	1.157
	44.780	(A_1)	0.032
	36.814	(A_1)	0.025
2×10^{-4}	62.171	(A_1)	0.825
	44.802	(A_1)	0.032
	36.831	(A_1)	0.034
	26.777	(A_1)	14.109
	5.626	(E)	14.33
1×10^{-3}	62.485	(A_1)	0.188
	44.825	(A_1)	0.009
	36.871	(A_1)	0.017
	26.401	(A_1)	2.785
	6.91	(E)	2.08
2×10^{-3}	62.496	(A_1)	0.095
	44.825	(A_1)	0.005
	36.875	(A_1)	0.009
	26.386	(A_1)	1.392
	7.05	(E)	1.03
1	62.500	(A_1)	0.0002
	44.825	(A_1)	0.0
	36.876	(A_1)	0.0
	26.381	(A_1)	0.003
	7.099	(E)	0.002

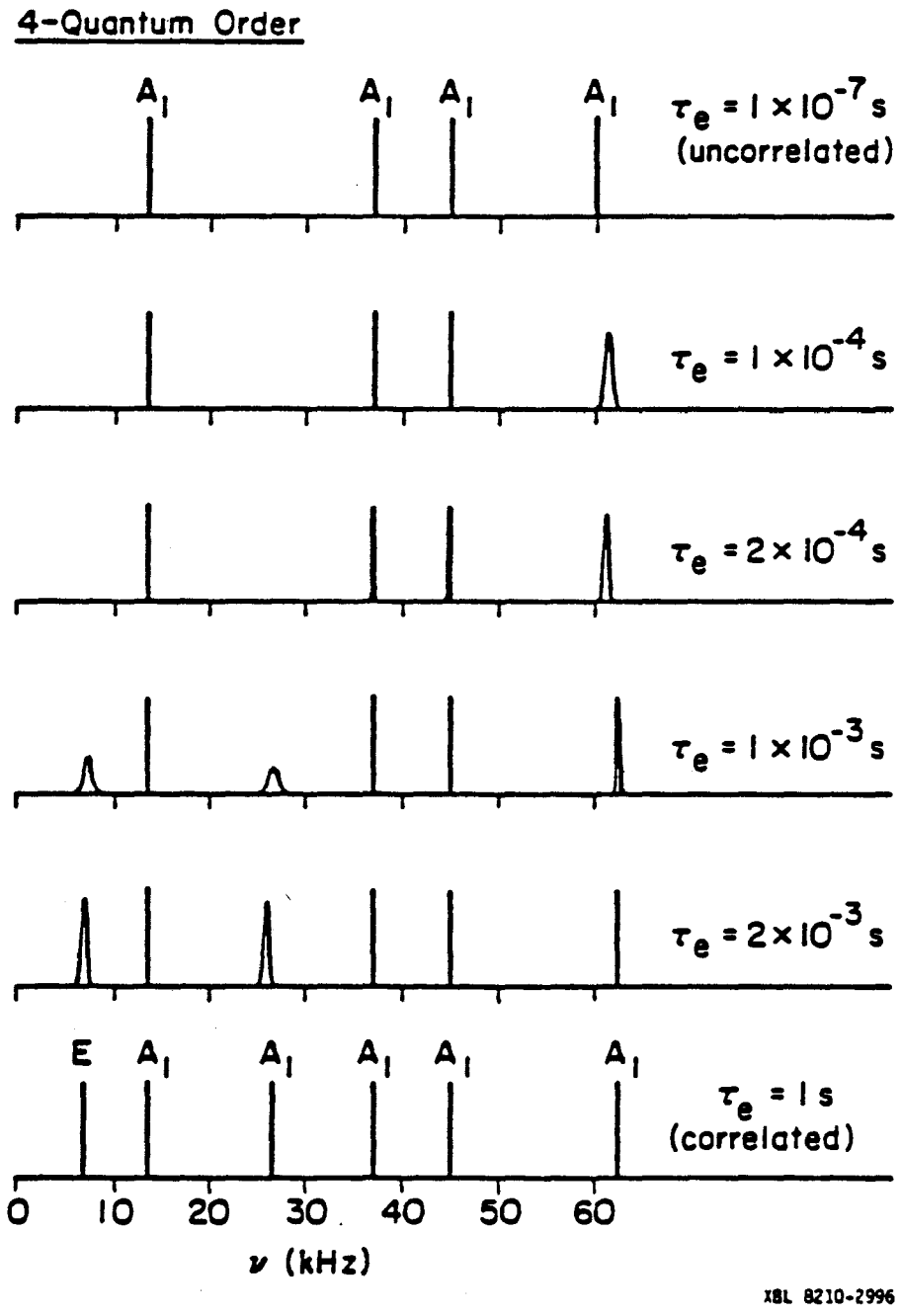

Figure 6.19 Computer simulation of one half of the 4-quantum region showing the broadening and merging of lines as correlation sets in.

toward the order center as it disappears. The outer four A_1 transitions are mixed and shifted in frequency toward each other as the transition line at 26 kHz broadens and disappears. At $\tau_e=10^{-7}$ sec, fast exchange is occuring and the spectrum corresponds to uncorrelated motion.

6.12 1,8-DIMETHYLNAPHTHALENE-D_6 IN A NEMATIC LIQUID CRYSTAL

A convenient method for molecular isolaton is the dissolution of the desired molecules in a nematic liquid crystal solvent. Its applicability is restricted to the narrow temperature range of the nematic phase. In the nematic phase, the long axis of the liquid crystal molecules have a defined direction when placed in a magnetic field. The translational freedom averages intermolecular couplings to zero and retains only intramolecular couplings. Molecular reorientation of the solute in the liquid crystal matrix does occur and scales down the intramolecular dipolar couplings. This scaling of coupling constants by restricted molecular reorientation is described by order parameters, the number of them depending on the structural symmetry of the solute molecule.

The MQ spectrum for 1,8-dimethylnaphthalene-d_6 (1,8-DMN-d_6) dissolved astman #15320 liquid crystal at room temperature is shown in Fig. 6.20. From this

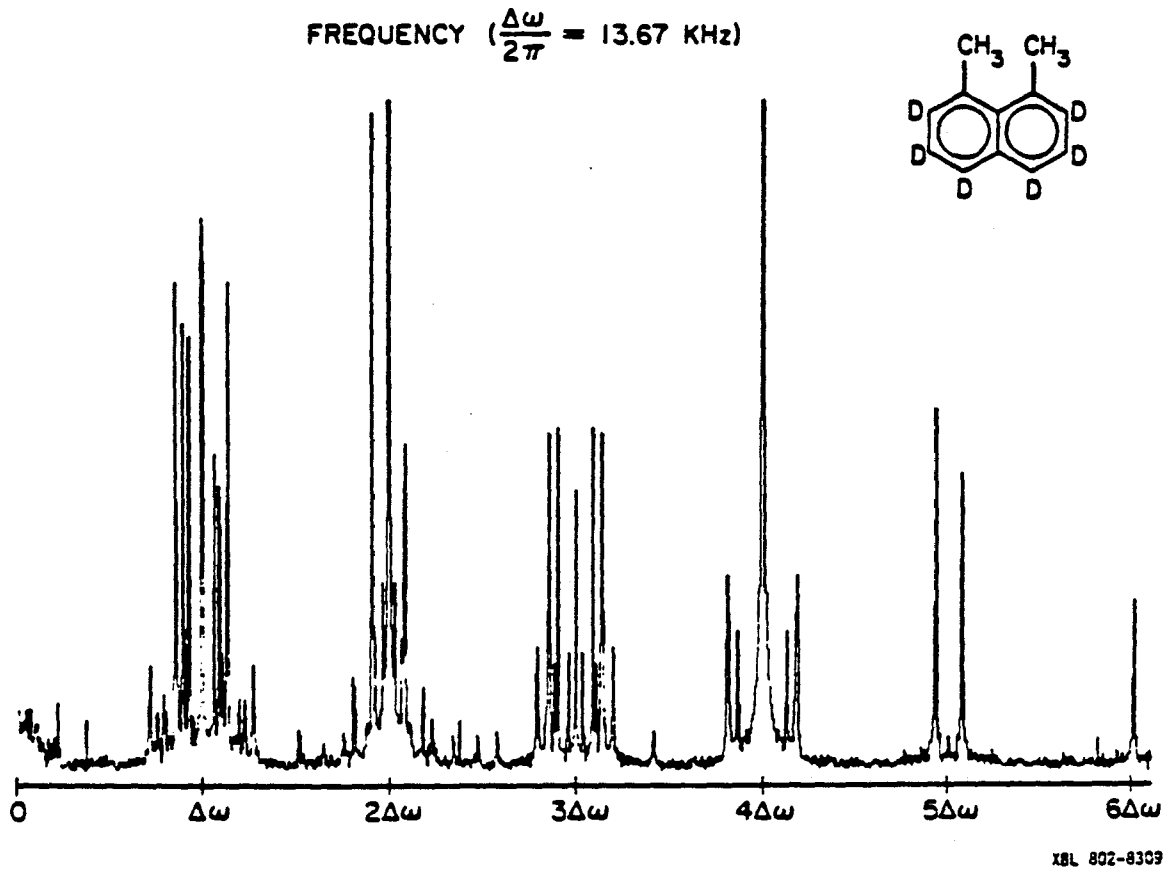

Figure 6.20 MQ spectrum of 1,8-dimethylnaphthalene-d_6 dissolved in a nematic liquid crystal at 25°C.

spectrum, we wish to determine whether the methyl groups are correlated in motion. It is not obvious a priori whether the methyl groups are equivalent. Their equivalency relies on the molecular reorientation that occurs in the liquid crystalline matrix. [See section 6.6.]

Figure 6.20 shows two doublets in the 4-quantum region. Referring to Table 6.3, we see immediately that this corresponds to the group $(S_3 \times S_3)\hat{}S_2$, implying equivalent and uncorrelated methyl groups.

Often the object is to obtain molecular structural information by iterating on the couplings and the order parameters. However in our case we know the molecular structure beforehand. We can use this extra piece of information to solve directly for the order parameters which informs us of the type of molecular reorientation occuring in the liquid crystal matrix.

To extract coupling constants from the 4- and 5-quantum orders, an iteration routine MQITER[9] is used. This routine requires as inputs the experimental transition frequencies and an initial guess of the coupling constants. The latter input requires specification of the type of motion that the methyl groups are experiencing. The resulting couplings from iterating on the 4- and 5-quantum orders are used to generate the 3-quantum order, which is then compared with the experimental 3-quantum spectrum. The best fit

for these orders corresponds to equivalent and uncorrelated methyl groups (as expected) with dipolar couplings (Fig. 6.21):

$$u = 1.196 \text{ kHz} \qquad (5)$$

$$v = -1.223 \text{ kHz}.$$

Here u and v are scaled by the order parameters.

For 1,8-DMN-d_6, the molecular point group is C_{2v}. For C_{2v} molecules, there are two order parameters:[15] S_{aa} and $S_{bb}-S_{cc}$, where a,b, and c are the axes of the molecular frame. The a-axis is taken to be the one of highest symmetry, the b-axis is defined here to lie also in the aromatic plane, and the c-axis is perpendicular to the aromatic plane (Fig. 6.18).

The motionally averaged dipolar Hamiltonian can be expressed as:

$$H_D = \sum_{i<j} \langle D_{ij} \rangle [I_{zi} I_{zj} - \frac{1}{4}(I_{+i} I_{-j} + I_{-i} I_{+j})]$$

where z refers to the direction of the external magnetic field. For molecules having more than one configuration, in the limit of fast conformational changes all configurations contribute to the observed coupling constants:

$$\langle D_{ij} \rangle = \frac{1}{n_\alpha} \sum_\alpha D_{ijzz}^{(\alpha)} \qquad (6)$$

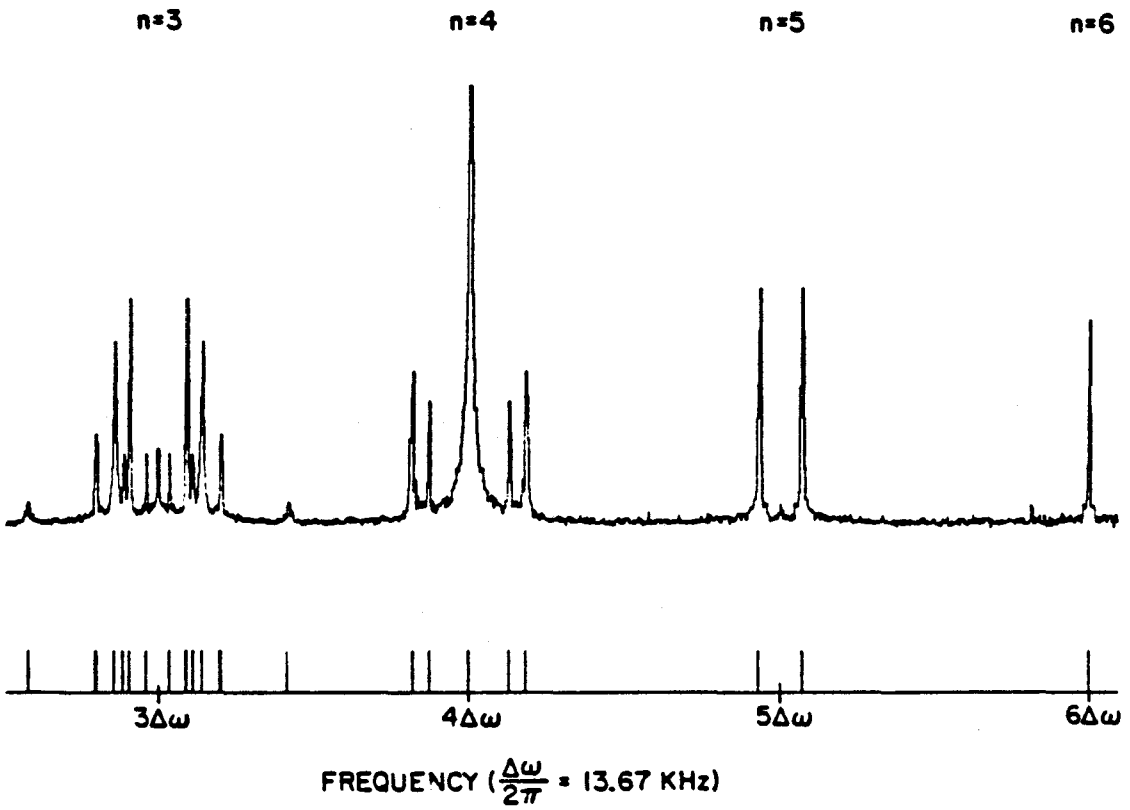

Figure 6.21 MQ spectrum of the 3- to 6-quantum region presented with the theoretical stick spectrum for uncorrelated equivalent methyl groups.

where n_α is the number of configurations. In general, each configuration may differ in symmetry and thus may have a different set of order parameters. In our case, the methyl reorientation about the C_3 axes does not affect the order parameters since they hop about equivalent positions. Hence each configuration must have the same order parameters, which can then be factored out of the summation. The spacial part of H_D is then:[15]

$$\langle D_{ij}\rangle = K\Big[\, S_{aa} \sum_\alpha \frac{(3\cos^2\theta_{ija}^{(\alpha)}-1)}{r_{ij}^3} + (S_{bb}-S_{cc}) \sum_\alpha \frac{(\cos^2\theta_{ijb}^{(\alpha)}-\cos^2\theta_{ijc}^{(\alpha)})}{r_{ij}^3} \Big] \qquad (7)$$

For the intramethyl coupling u there are six configurations to be averaged, and for the intermethyl coupling v there are nine. Inserting Eq. (7) into (6) given the observed coupling constants $\langle D_{ij}\rangle$ in Eq. (5), and calculating θ_{ij}'s from the crystallographic data result in an unique solution for the order parameters:

$$S_{aa} = 0.037$$

$$S_{bb}-S_{cc} = -0.291.$$

The relation $S_{aa} \ll S_{bb} - S_{cc}$ implies that the molecular reorientation in the liquid crystal solvent

is predominantly about an axis in the bc-plane. We deduce however that since 1,8-DMN is planar, the open volume required for a rotation about the c-axis is less than for about the b-axis (or about the a-axis). Thus we assert that the reorientation is predominantly about the c-axis. Also, this reorientation equalizes both methyl groups, which is consistent with the obtained MQ spectrum.

To summarize, the number of lines in the 4-quantum order allows us to determine that the methyl groups on 1,8-DMN at room temperature are uncorrelated and equivalent in the nematic liquid crystalline environment. Since 1,8-DMN is planar, to minimize steric hindrance between solute and solvent we can expect the aromatic plane to lie along the direction of the long axis of the liquid crystal. Considering the amount of free volume required, it can be argued that the molecular reorientation is predominantly about an axis perpendicular to the aromatic plane. The above affirmations are in agreement with the measured order parameters.

6.13 1,8-DIMETHYLNAPHTHALENE-D_{10}

The practical advantages and disadvantages of MQ spectroscopy on the molecule 1,8-DMN-d_6 can be compared with those of single-quantum (SQ) spectroscopy on 1,8-DMN-d_{10}. In both cases, an isolated molecular system

is simulated by diluting the desired guest molecule in a perdeuterated host which preserves the molecular and crystal structure. The power required for proton-deuteron decoupling is roughly the same for both cases. The advantages and disadvantages of MQ NMR on 1,8-DMN-d_6 is first discussed. The SQ spectroscopy of 1,8-DMN-d_{10} is analyzed and the significance of impurity concentration is examined.

For the MQ experiment, the wise choice for the guest molecule is 1,8-DMN-d_6 where the uninteresting aromatic positions are deuterated. The advantages are: (1) it requires a lower deuteration level, and (2) it has the capability of separating the desired signal from impurity signal. The previous sections have shown that the 4Q order is sensitive to correlation of motion. It is highly improbable that the perdeuterated host impurities will contribute to the 4Q spectrum - the probability of four or more impurity protons on the same molecule is extremely small. Thus the purity requirement of the host is not stringent. The impurities of the guest molecule <u>will</u> contribute to the 4Q region, but if the purity is reasonably high (>90%) the purity level again is not critical.

The disadvantage of a MQ experiment is that it is a two-dimensional experiment. Hence for a given data acquisition time, it is inherently a lower sensitivity experiment, with noise in t_1 as well as in t_2.[16] To

get the same amount of sensitivity as in an one-dimensional SQ experiment, perfect selective excitation of the desired quantum order and a full two-dimensional data acquisition are required.

For SQ spectroscopy to be feasible, a two-proton system with one proton on each methyl group (and the rest of the positions deuterated) is the most convenient choice. Single-quantum spectroscopy on this system can give information on the correlation of motion.

The advantage of SQ NMR is that it is a simple one-dimensional experiment, provided the magnet inhomogeneity is small compared to the dipolar broadening. The pulse sequence involves one pulse, or at best a two-pulse solid echo sequence.[17] (The solid echo experiment is preferred to minimize linear phase distortion and since most solids have a decay time comparable to the receiver deadtime.)

The major problem of SQ NMR is that the desired SQ signal will overlap with impurity signal. If the dilution level is high (which is desirable for better isolation of guest molecules), the impurities of the host contribute a significant amount of signal. The details of this matter will be discussed separately in section 6.13.2.

We make the case for preferring a powder sample to a single crystal.[18] The experimental problems

associated with a single crystal are: (1) a crystal may undergo crystal structural phase transitions as temperature is lowered, and (2) cracking of crystal may result if the cooling or heating of the sample occurs too quickly. In using a powder, it becomes unnecessary to know the crystal orientation, nor to know the number of molecules in the unit cell and their relative orientation in the unit cell. Though the S/N is lower for a powder per frequency bandwidth, the singularities (that occur at $\theta=90°$) in the powder spectrum should be sharp and the peak S/N should be substantial, excluding dominant impurity signal contributions.

6.13.1 Single-Quantum Spectrum

If the system is uncorrelated, we expect on the average one unique dipolar coupling constant. The nine configurations possible are shown in Fig. 6.22, where it is assumed that the methyl group can only hop between equilibrium orientations. The dipolar Hamiltonian for this case is just:

$$H_D = v[I_{z1}I_{z2} - \frac{1}{4}(I_{+1}I_{-2}+I_{-1}I_{+2})]$$
$$\equiv vV_{12}.$$

The extreme eigenstates $|++\rangle$ and $|--\rangle$ are shifted by $\frac{1}{4}v$, the symmetric eigenstate $\frac{1}{\sqrt{2}}(|+-\rangle + |-+\rangle)$ by $-\frac{1}{\sqrt{2}}v$, and the antisymmetric state $\frac{1}{\sqrt{2}}(|+-\rangle - |-+\rangle)$ is

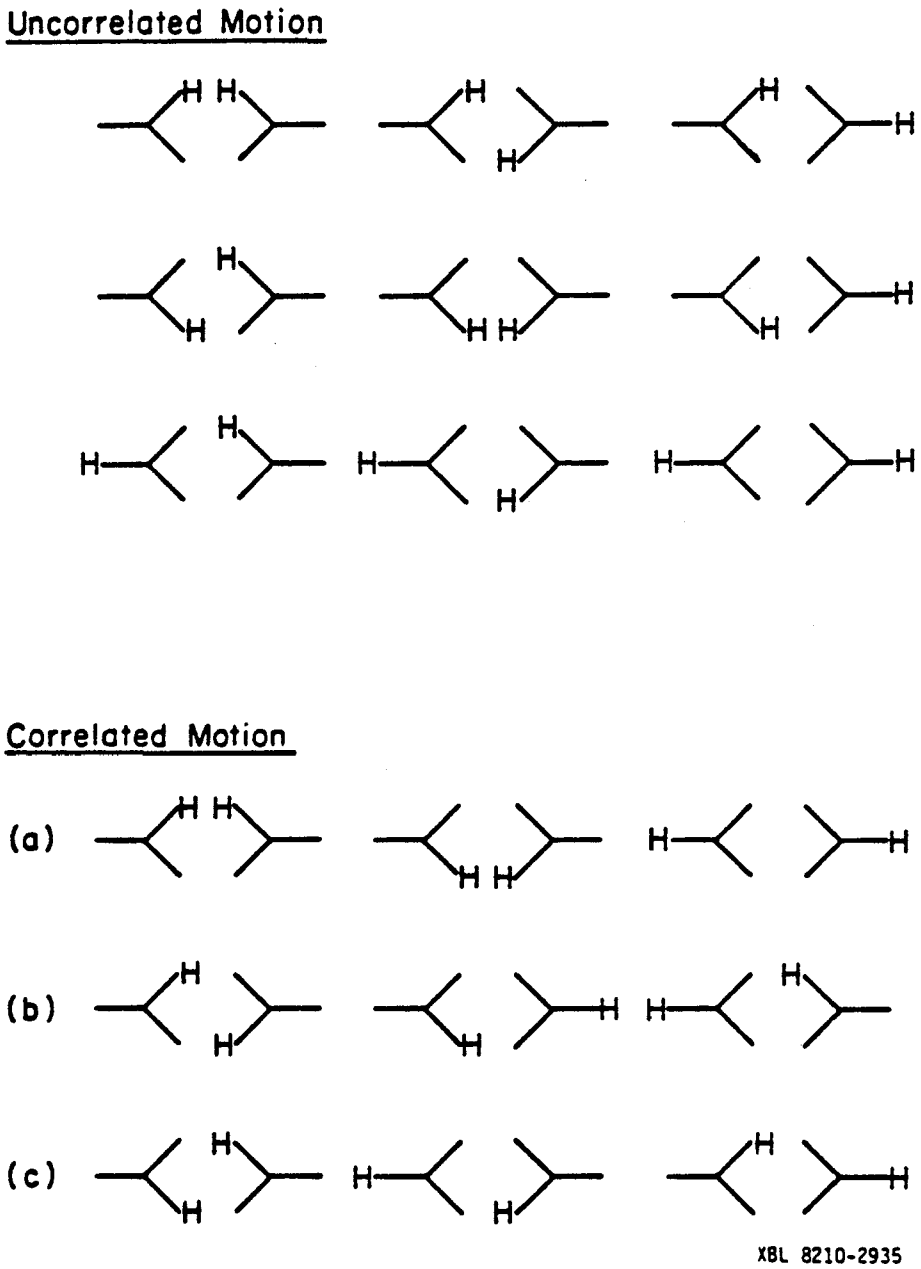

Figure 6.22 Assuming random hopping only between equilibrium positions, for uncorrelated motion the methyl groups have random relationship. For correlated motion there are only three possible initial conditions, and three possible configurations each. Note that configurations b and c are indistinguishable by NMR.

unshifted.

Assuming the methyl geometry is unaltered by deuteration, the coupling constant can be calculated. The coupling for $\theta=0°$, which is the maximum inherent value possible, is:

$$v_o = 5.784 \text{ kHz}.$$

The SQ spectrum for this molecule is then a doublet with a separation of $(\sqrt{2} + \frac{1}{2})v$, or 11.072 kHz for $\theta=0°$ [Fig. 6.23(a)].

If the system is correlated in motion, on the average there are two unique dipolar coupling constants. The two constants arise from the fact that there are two initial configurations possible [Fig. 6.22(b)]. (Actually there are three; however, two of them are NMR equivalent but are enantiomers.) The superimposed Hamiltonian is:

$$H_D = \frac{1}{3}vV_{12} + \frac{2}{3}wV_{12}.$$

The coupling constants for $\theta=0°$ are:

$$v_o = 10.535 \text{ kHz}$$
$$w_o = 3.408 \text{ kHz}$$

The SQ spectrum is a superposition of two doublets with separations $(\sqrt{2} + \frac{1}{2})v$ and $(\sqrt{2} + \frac{1}{2})w$, or 20.167 and

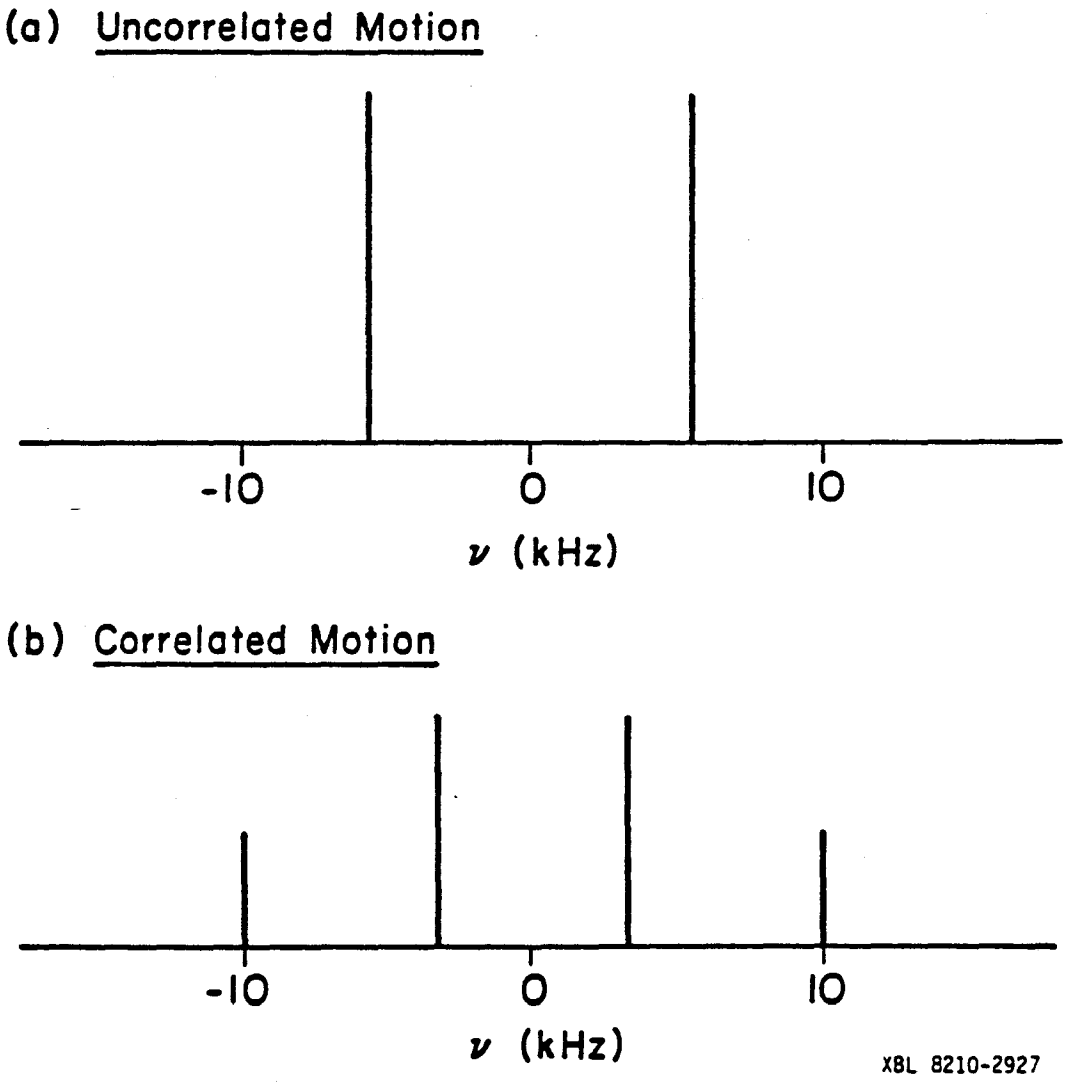

Figure 6.23 The single-quantum spectrum for 1,8-dimethylnapthalene-d_{10} molecule at orientation =90° undergoing (a) uncorrelated motion, resulting in a doublet, and (b) correlated motion, showing two doublets with one doublet having twice the intensity of the other.

6.524 kHz for $\theta=0°$ [Fig. 6.23(b)].

The dispersion function of a powder pattern is given by:[19]

$$f(\nu) = \left(\frac{2\nu}{d_o} + 1\right)^{-1/2}, \qquad -d_o<\nu<-\frac{1}{2}d_o$$

$$= \left(\frac{2\nu}{d_o} + 1\right)^{-1/2} + \left(\frac{2\nu}{d_o} + 1\right)^{-1/2}, \qquad -\frac{1}{2}d_o<\nu<\frac{1}{2}d_o$$

$$= \left(\frac{2\nu}{d_o} + 1\right)^{-1/2}, \qquad \frac{1}{2}d_o<\nu<d_o$$

where d_o corresponds to the appropriate coupling constant at $\theta=0°$. The singularities occur at $\pm d_o/2$, which corresponds to d at $\theta=90°$. Calculated dipolar powder patterns for uncorrelated and correlated motion of 1,8-DMN-d_{10} are shown in Fig. 6.24. Measurement of the splittings between singularities of a powder pattern yields the coupling constant at $\theta=0°$.

6.13.2 Impurity Content

The motivation for including this section stemmed from measurements made on 1,8-DMN-d_{10} showing impurity signal comparable to or larger than the desired signal, even at a high host purity level of 99.0% and at a 5% dilution. This came rather as a surprise at first. The arguments to be discussed below will clearly show why SQ spectroscopy requires high purity samples.

The level of sample purity can be estimated

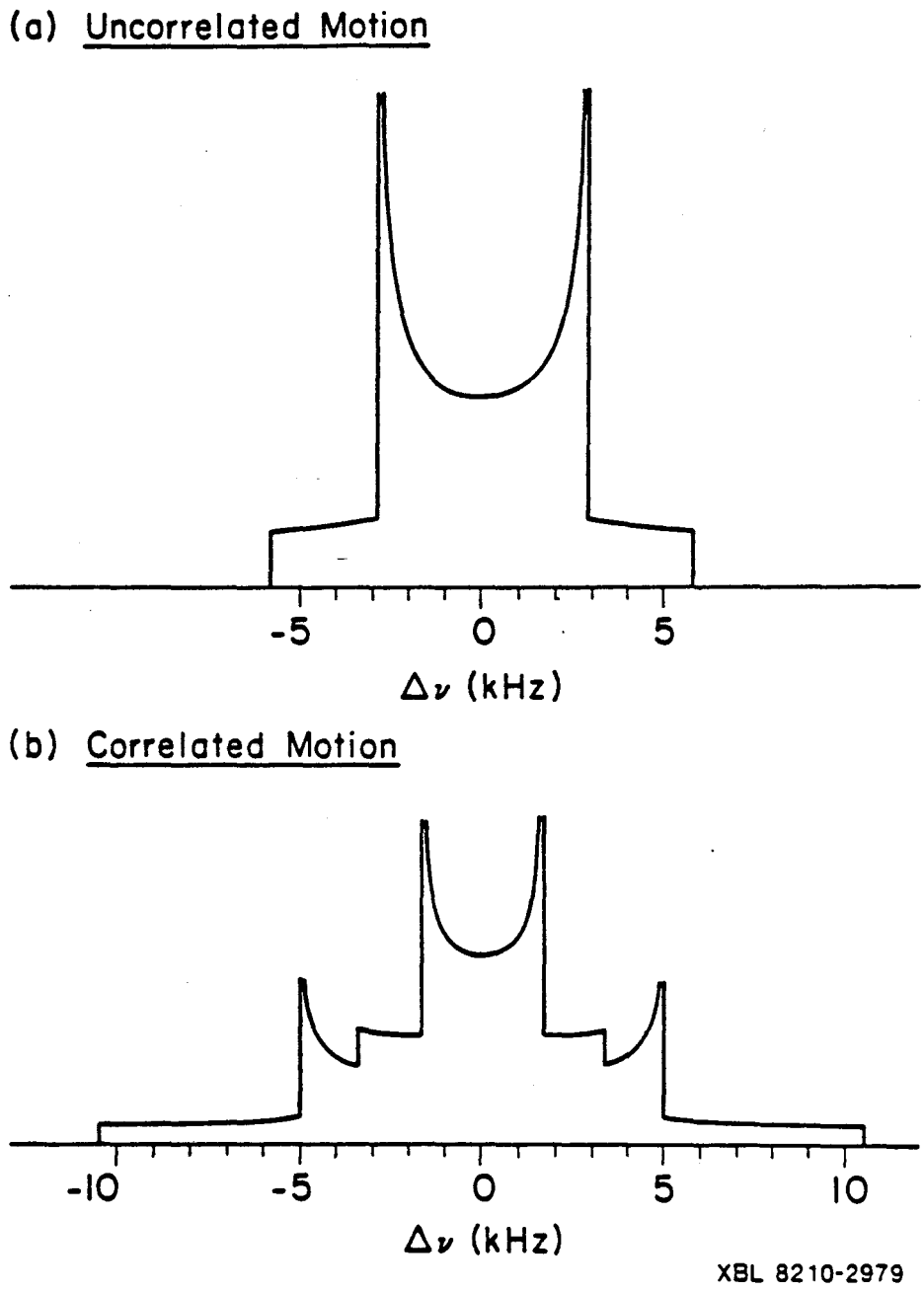

Figure 6.24 The single-quantum powder spectrum for 1,8-dimethylnaphthalene-d_{10} undergoing (a) uncorrelated motion, and (b) correlated motion, showing a superposition of two powder patterns.

assuming a statistical distribution of proton attachments. Generalizing, suppose there are N molecules with m sites each, totaling a number of mN sites. The question is: what is the probability that each molecule with m sites will have k impurities?

This can be abstracted to the following problem. Suppose there are a total of mN objects, where x of them are of one kind and y of them of another kind. What is the probability of picking m objects such that k of them are of the y type, assuming $k<y$ and $(m-k)<x$? Through combinatorial arguments, this probability is found to be:

$$P(m,k) = \frac{\binom{y}{k}\binom{x}{m-k}}{\binom{x+y}{m}}.$$

Listed in Table 6.5 are the probabilities for typical impurity levels. The percentage refers to the number of sites occupied by an impurity and not molar percent. The notation P(m,k) is interpreted as the probability of 1,8-DMN having k impurity protons. For 1,8-DMN, the number of sites is m=12. The tabulated values assume N=100 molecules, which is large enough to yield values close to those of $N\to\infty$.

Note that a portion of P(12,2) has protons in the desired location. This amount is $\binom{12}{2}^{-1}$ or 1/66, implying P(12,2) should be multiplied by 65/66 to give the correct impurity content.

Table 6.5

Probability P(m,k) of m sites being occupied by k impurities

impurity content	P(12,1)	P(12,2)	P(12,3)
10%	0.38	0.23	0.17
1%	0.11	0.006	2×10^{-4}
0.5%	0.06	0.001	1×10^{-5}

The calculation of impurity content of the starting guest material is more complicated. It depends on the selectivity of the deuteration procedure. Thus the proton attachment is no longer a statistical problem. Fortunately, the purity requirement is less stringent since the guest molecule will be in low abundance. For example, if the net effect of the selectivity and extraction procedure is 90% effective, then roughly >10% of the sites are occupied by mislocated protons and the desired signal is <90% of the expected value. (Compare this to a random deuteration composing of 38% single-proton impurity, 23% two-proton impurity and 17% three-proton impurity.) For the rough estimate that we want to make this modification can be neglected. Note that part of this reduction is counteracted by the perdeuterated host having the desired proton attachment.

Given Table 6.5, the comparison of the size of impurity signal from the host versus the desired guest signal can be made for a given guest dilution.

A 5% molar dilution is a reasonable amount for effecting isolation of guest molecules. (Considering cubic-closest-packing structure, 2% dilution is optimal. But if the nearest intermolecular distance is greater than the intramolecular distances, 5% dilution is tolerable.) When the dilution is high, the impurity of the guest compound can be neglected.

The total ^1H signal size is proportional to the number of proton occupied sites. At 5% dilution, 95% of the molecules are hosts. Assuming a host impurity level of 1%, the number of sites corresponding to single-proton host moleucles is (0.11)95% = 10%, to two-proton hosts is 2(0.06)95% = 1%, and to three-proton hosts is 3(0.016)95% = 0.05%. Compare this to the number of guest proton sites, which is at best (2)5% = 10%. The rest of the sites contribute to deuterium signal. Thus even at 5% molar dilution and with a 99% host purity level, the impurity signal is comparable to the desired signal.

To improve the above situation, one may either increase the amount of guest molecules (which may result in intermolecular broadening) or decrease the impurity content of the host. Let us consider the latter.

Suppose the host impurity level is ultra-low at 0.5%. At 5% dilution, the number of host impurity sites is 5% single-proton, 0.2% two-proton and negligible three-proton. The desired signal again derives from 10% of the sites. Thus at 0.5% host impurity level, the desired signal is twice as large as the impurity signal, which is tolerable.

It is worth mentioning that it is very difficult to get higher than 99.5% purity since most commercial starting materials (D_2O) are graded at 99.5%.

6.13.3 Conclusion

Provided the sample purity is high enough, it is feasible to perform SQ NMR spectroscopy on the selectively deuterated 1,8-DMN-d_{10} diluted in a perdeuterated matrix. The observation of correlation of motion of two methyl groups is then an one-pulse experiment with heteronuclear decoupling. A powder sample of 1,8-DMN-d_{10} is preferable to a single crystal for experimental ease and to remove the need to know the unit cell structure. In contrast to the single crystal spectrum, the powder spectrum is also unaffected by the fact that in the slow motional limit, the methyl groups can no longer be treated as an averaged specie.

A preliminary measurement on a powder sample of 5% dilution in a host of 99% purity resulted in a smearing out of the powder pattern by impurity signal. A simple calculation assuming statistical proton attachments reveals the importance of high purity requirement of the host compound.

APPENDIX 6.A

Computer listings of programs EXCH2 and HARDMAT

EXCH2 diagonalizes the superoperator A for the four-quantum transitions in the E manifold. The NMR permutation group S_3 and the dipolar couplings for the orientation specified in section 6.11 are assumed. It requires as inputs only the exchange times ("tau").

HARDMAT is called within EXCH2 to create a "hard copy" of the constructed 16x16 superoperator A. This subroutine was supplied by Jim Murdoch.

```
      program exch2
c
c     does the e-manifold superoperator
c
      complex s(16,16),w(16),z(16,16)
      dimension wk(40),h(4,4),p(4,4),pinv(4,4)
      character*50 title
c
      do 10 i=1,4
      do 10 j=1,4
      h(i,j)=0.0
10    p(i,j)=0.0
c
      h(1,1)=-1.223
      h(1,2)=-0.14823
      h(2,2)=-1.371
c
      p(1,1)=-0.5
      p(2,2)=1.0
      p(3,3)=-0.5
      p(4,4)=1.0
      p(1,3)=-1.0 / sqrt(2.0)
      p(3,1)=0.75 * sqrt(2.0)
c
c
      h(2,1)=h(1,2)
      do 15 i=1,2
      do 15 j=1,2
15    h(i+2,j+2)=h(i,j)
c
      do 22 i=1,4
      do 20 j=1,4
      if(i .eq. j) pinv(i,j)=p(i,j)
20    if(i .ne. j) pinv(i,j)=-p(i,j)
c
c
30    type 503
503   format(/,' enter a value for tau: ',$)
      accept *,tau
c
      do 40 i=1,16
      do 40 j=1,16
40    s(i,j)=0.0
c
      do 50 ia=1,4
      do 50 ib=1,4
      k=4*(ia-1) + ib
      do 60 ic=1,4
      do 60 id=1,4
      l=4*(ic-1) + id
      h1=0.0
      h2=0.0
      if(ia .eq. ic) h1=h(id,ib)
      if(ib .eq. id) h2=h(ia,ic)
      pp=( p(ia,ic)*p(ib,id) + pinv(ia,ic)*pinv(ib,id) ) / tau
      s(k,l)=cmplx(pp,h1-h2)
      if(k .eq. l) s(k,l)=s(k,l) - 2.0/tau
60    continue
50    continue
c
      title='E-MANIFOLD SUPEROPERATOR'
      call hardmat(s,title,tau)
c
```

```
      call eigcc(s,16,16,1,w,z,16,wk,ier)
c
      type 504, ier
504   format(/,5x,' ier = ',i5,/)
c
      print 510, tau
510   format(1h1,///,' TAU = ',e14.6)
      print 505
505   format(//,' eigervalues .. .. ',//)
      print 506, w
506   format(2e15.6)
c
      do 100 j=1,16
      sum=0.0
      do 90 i=1,16
90    sum=sum + z(i,j)*conjg(z(i,j))
      sqsum=sqrt(sum)
      do 95   i=1,16
95    z(i,j)=z(i,j) / sqsum
100   continue
c
      title='NORMALIZED EIGENVECTORS'
      call hardmat(z,title,tau)
c
      type 509
509   format(/,' do you want another tau ? (0=no,1=yes) ',$)
      accept *,itau
      if(itau .ne. 0) go to 30
c
      end
```

```
      subroutine hardmat(p,title,tau)
c
c     displays 16x16 complex matrices on one page
c
      complex p(256)
      dimension mag(16),iph(16),il(16),im(16)
      character*50 title
c
      indx(i,j)=(j-1)*nst + 1
c
      nst=16
c
      pi=4.0*atan(1.0)
      rad=180. / pi
c
      do 10 j=1,nst
      jj=j-1
      il(j)=jj/4 + 1
10    im(j)=mod(jj,4) + 1
c
      print 100, title,tau
100   format(1h1,//,5x,a,'  for tau = ',e14.6,//)
c
      print 110, (il(j),im(j),j=1,nst)
110   format(7x,16('  (',i1,',',i1,')'))
c
      print 111
111   format(1x,130(1h-))
c
      do 50 i=1,nst
      do 45 j=1,nst
      ij=indx(i,j)
      xx=real(p(ij))
      yy=aimag(p(ij))
      zz=cabs(p(ij))
      if(zz .lt. 0.2001) go to 35
      if(xx) 34,31,34
31    if(yy) 33,32,32
32    iph(j)=90
      go to 40
33    iph(j)=-90
      go to 40
34    ph=atan2(yy,xx) * rad
      iph(j)=ph + sign(0.5,ph)
      go to 40
35    iph(j)=0
40    mag(j)=1000. * zz + sign(0.5,zz)
45    mag(j)=min0(9999999,mag(j))
      print 112, il(i),im(i),(mag(j), j=1,nst)
112   format(1h0,'(',i1,',',i1,')  ',16i7)
      print 116, (iph(j), j=1,nst)
116   format(7x,16i7)
50    continue
c
      return
      end
```

APPENDIX 6.B

Computer listing for program EXCH1

EXCH1 diagonalizes the superoperator A for the four-quantum transitions involving the A_1 m=±1 and m=±3 manifolds. The NMR permutation group S_3 is assumed. The programs asks for the matrix elements of the Liouville operator H and the exchange times as inputs.

```
      program exch1
c
c     diagonalizing the al n-2 transitions
c
      complex a(4,4),w(4),z(4,4)
      dimension wx(12),aa(4,4)
c
      type 501
501   format(//,' enter the Imaginary elements of the superoperator a',
     1  ' .....',/)
      do 20 j=1,4
      do 22 i=1,j
      type 502, i,j
502   format(5x,'A(',i1,',',i1,'  :  ',$)
      accept *,aa(i,j)
20    continue
c
30    type 503
503   format(//,' enter a value for tau: ',$)
      accept *,tau
      do 40 j=1,4
      do 42 i=1,j
42    a(i,j)=cmplx(0.0,aa(i,j))
      a(3,3)=a(3,3) - 2.0/tau
      a(3,4)=a(3,4) - sqrt(2.0)/tau
      a(4,4)=a(4,4) - 1.0/tau
      do 50 j=2,4
      jm1=j-1
      do 52 i=1,jm1
52    a(j,i)=a(i,j)
c
      call eigrc(a,4,4,1,w,z,4,wx,ier)
c
      type 504, ier
504   format(/,5x,' ier = ',i5,/)
c
      print 510, tau
510   format(/,/,' tau = ',e11.3)
      print 525
525   format(//,' eigenvalues .....',/)
      print 526, w
526   format(2e12.6)
c
      do 70 j=1,4
      sum=0.0
      do 60 i=1,4
62    sum=sum + z(i,j)*conjg(z(i,j))
      sqsum=sqrt(sum)
      do 65 i=1,4
65    z(i,j)=z(i,j) / sqsum
70    continue
c
      print 507
507   format(//,' normalized eigenvectors .....',/)
      print 508, ((z(i,j), j=1,4), i=1,4)
508   format(4(2x,2f8.4))
c
      type 509
509   format(/,' do you want another tau ? (0=no,1=yes) ',$)
      accept *,itau
      if(itau .ne. 0) go to 30
c
      end
```

CHAPTER 6 REFERENCES

1. J couplings have been used to observe restricted rotations of methyl derivatives: M. Nakamura, M. Oki, H. Nakanishi, and O. Yamato, Bull. Chem. Soc. Japan 47, 2415 (1974); U. Berg and C. Roussel, J. Am. Chem. Soc. 102, 7848 (1980).
2. W.J. Orville-Thomas, Internal Rotations in Molecules, (John-Wiley & Sons, New York, 1974).
3. K. Balasubramanian, J. Chem. Phys. 74, 6824 (1981).
4. K. Balasubramanian, J. Chem. Phys. 72, 665 (1980).
5. An isomorphism is an one-to-one mapping of elements of one group to another such that the group operation is preserved. Alternatively stated, isomorphic groups are algebraically identical.
6. M. Tinkham, Group Theory and Quantum Mechanics, (McGraw-Hill, New York, 1971).
7. C.M. Woodman, Molec. Phys. 19, 753 (1970).
8. J. Serre, Int. J. Quant. Chem. I S, 713 (1967).
9. S.W.Sinton, Ph.D. thesis, University of California, Berkeley, 1981.
10. J. Serre, Int. J. Quant. Chem. II S, 107 (1968).
11. E.R. Andrews and R.A. Newing, Proc. Phys. Soc., London 72, 959 (1958).
12. When rotational polarization exists, it is

possible for the two rate of occurrences to differ.

13. D. Bright, I.E. Maxwell, and J. de Boer, J. Chem. Soc. Perkins II, 2101 (1973).

14. A. Saika, A. Kawamori, and R. Takagi, J. Magn. Reson. 7, 324 (1974).

15. J.W. Emsley and J.C. Lindon, NMR Spectroscopy Using Liquid Crystal Solvents, (Pergamon Press, New York, 1975).

16. D.P. Weitekamp, Advan. Magn. Reson., submitted for publication.

17. I. Solomon, Phys. Rev. 110, 61 (1958).

18. J. Tang, private communication, 1980.

19. A. Abragam, Principles of Nuclear Magnetism, (Oxford Press, London, 1961).